THE MULTIFUNCTIONAL KINASE BUB1 ACTS AS A SIGNALING HUB FOR THE SPINDLE CHECKPOINT

APPROVED BY SUPERVISORY COMMITTEE

Hongtao Yu, Ph.D., Supervisor

George DeMartino, Ph.D., Chairperson

Melanie Cobb, Ph.D.

Michael White, Ph.D.

THE MULTIFUNCTIONAL KINASE BUB1 ACTS AS A SIGNALING HUB FOR THE SPINDLE CHECKPOINT

By

LUYING JIA

DISSERTATION

Presented to the Faculty of the Graduate School of Biomedical Sciences

The University of Texas Southwestern Medical Center at Dallas

In Partial Fulfillment of the Requirements

For the Degree of

DOCTOR OF PHILOSOPHY

The University of Texas Southwestern Medical Center

Dallas, Texas

December, 2015

Acknowledgements

Looking back on the years in graduate school, I would like to first thank my mentor, Dr. Hongtao Yu, for his advices and encouragements. He has been very supportive and resourceful. As a scientist, he has really set a high standard for people in the lab. I also would like to thank my thesis committee members, Dr. George DeMartino, Dr. Melanie Cobb and Dr. Michael White. They are always trying to help and give me useful suggestions.

My great labmates are also one of the most important factors of my graduate student life. Everyone is so friendly and ready to help, I have never had the experience that when I need help but no one is there. I especially need to thank Bing, Laura, Hong, Soonjoung, and Ross, I learned a lot from them during these years in lab.

My friends and families have been very supportive and are the source of joy on my long road to the Ph.D. degree. I thank my friends, Ziying, Pei-Hsuan, Ruei-Jiun, Caroline, Hui and many others, for listening to my complaints, sharing their ideas and introducing me to a lot of new things. I will cherish those precious moments I had with my friends. I thank my parents for always encouraging me to try everything that interests me. They never try to put pressure on me. Instead, they always help me to release from the pressure I put on myself. Last but surely not least, I thank my husband, Chien-Der, for bringing to me a lot of happiness, and helping me to become a better self.

THE MULTIFUNCTIONAL KINASE BUB1 ACTS AS A SIGNALING HUB FOR THE SPINDLE CHECKPOINT

Luying Jia, Ph.D.

The University of Texas Southwestern Medical Center at Dallas, 2015

Supervising Professor: Hongtao Yu, Ph.D.

The spindle checkpoint is an essential mechanism to ensure accurate chromosome segregation during mitosis. The checkpoint signal originates from the kinetochore, which is a huge protein assembly on centromeric chromatin. Kinetochore is also the receptor for spindle microtubules, which enables it to translate microtubule attachment status into spindle checkpoint signal.

The separation of the sister chromatids and the progression from metaphase to anaphase requires the activation of an ubiquitin E3 ligase, anaphase-promoting complex or cyclosome

(APC/C). Cdc20 is the mitosis-specific APC/C activator. The spindle checkpoint prevents premature sister chromatids separation by preventing Cdc20 from activating APC/C.

Bub1 is a highly conserved spindle checkpoint protein that plays multiple roles in checkpoint signaling. On the kinetochore, Bub1 recruits other important checkpoint proteins like BubR1, Mad1 and Cdc20. We found phosphorylation on Bub1 serine 459 is essential for spindle checkpoint and for Bub1-Mad1 interaction. However, the majority of Mad1 still localize to the kinetochore in cells expressing Bub1-S459A mutant. These results suggest that the direct binding between Bub1 and Mad1 through Bub1-S459 may not be responsible for the localization of Mad1 to the kinetochore region. Instead, this interaction enables Mad1 to function in the checkpoint signaling pathway, possibly through regulating its interaction with Bub1-bound BubR1 and Cdc20.

Bub1 is also a serine/threonine kinase. The only two identified substrates are histone H2A and Cdc20. Bub1 phosphorylates histone H2A threonine 120, which is important in recruiting Sgo1 and Aurora B kinase to the kinetochore. Bub1 also phosphorylates Cdc20 serine 153. It was shown in vitro that phosphorylation by Bub1 can inhibit APC/C^{Cdc20}. However, mouse embryonic fibroblasts (MEFs) expressing Bub1 kinase dead mutant only display mild checkpoint defect due to abnormal Aurora B localization. In addition, over-expression of Bub1 kinase dead mutant in HeLa cells can rescue the checkpoint defect caused by Bub1 depletion using siRNA. These results challenged the importance of Cdc20 phosphorylation by Bub1 in the spindle checkpoint. Here I show that Bub1 binds another kinase Plk1, forming a kinase complex. Phosphorylation of Cdc20 by Bub1-Plk1 not only inhibits APC/C^{Cdc20} in vitro, but also is required for proper spindle checkpoint function in HeLa cells.

TABLE OF CONTENTS

PRIOR PUBLICATIONS

1. **Jia L**, Li B & Yu H. The Bub1–Plk1 kinase complex promotes spindle checkpoint signaling through Cdc20 phosphorylation**.** ***Nat Commun*****.** In revision.

2. Diaz-Martinez LA, Tian W, Li B, Warrington R, **Jia L**, Brautigam CA, Luo X, Yu H. (2015) The Cdc20-binding Phe box of the spindle checkpoint protein BubR1 maintains the mitotic checkpoint complex during mitosis. ***J Biol Chem.*** 290(4): 2431-43.

3. Lin Z*, **Jia L***, Tomchick DR, Luo X, Yu H. (2014) Substrate-specific activation of the mitotic kinase Bub1 through intramolecular autophosphorylation and kinetochore targeting. ***Structure.*** 22(11): 1616-27. (*: co-first authors)

4. Liu H, **Jia L**, Yu H. (2013) Phospho-H2A and cohesin specify distinct tension-regulated Sgo1 pools at kinetochores and inner centromeres. ***Curr Biol.*** 23(19): 1927-33.

5. **Jia L***, Kim S*, Yu H. (2013) Tracking spindle checkpoint signals from kinetochores to APC/C. ***Trends Biochem Sci.*** 38(6): 302-11. (*: co-first authors)

6. **Jia L**, Yu H. (2011) Cdh1 is a HECT of an activator. ***Mol Cell.*** 44(5): 681-3.

7. **Jia L***, Li B*, Warrington RT, Hao X, Wang S, Yu H. (2011) Defining pathways of spindle checkpoint silencing: functional redundancy between Cdc20 ubiquitination and $p31^{comet}$. ***Mol Biol Cell.*** 22(22): 4227-35. (*: co-first authors)

LIST OF FIGURES AND TABLES

CHAPTER 1.

CHAPTER 2.

CHAPTER 3.

LIST OF ABBREVIATIONS

APC/C	Anaphase-Promoting Complex or Cyclosome
Cdc20	Cell Division Cycle 20
Bub1	Budding Uninhibited by Benzimidazole 1
BubR1	Bub1 related protein
Mad1	Mitotic Arrest Deficient 1
Sgo1	Shugoshin-like 1
Plk1	Polo-like kinase 1
CENP-A	Histone H3-like centromeric protein A
CCAN	Centromere-associated network
Knl1	Kinetochore null protein 1
CPC	Chromosome Passenger Complex
INCENP	Inner centromere protein
Cdk1	Cyclin-dependent kinase 1
Mps1	Monopolar spindle 1
TPR	Tetratricopeptide repeat
CTD	C-terminal domain
PP1	Protein phosphatase 1
ATP	Adenosine Triphosphate
GLEBS	Gle2-binding sequence
MCC	Mitotic checkpoint complex
WT	Wild type
KD	Kinase-dead

CHAPTER ONE

INTRODUCTION

Accurate chromosome segregation during mitosis is critical for maintaining genomic stability. The kinetochore – a large protein assembly on centromeric chromatin – functions as the docking site for spindle microtubules and a signaling hub for the spindle checkpoint. At metaphase, spindle microtubules from opposing spindle poles capture each pair of sister kinetochores, exert pulling forces, and create tension across sister kinetochores. The spindle checkpoint detects improper kinetochore–microtubule attachments and translates these defects into biochemical activities that inhibit the anaphase-promoting complex or cyclosome (APC/C) throughout the cell to delay anaphase onset. A deficient spindle checkpoint leads to premature sister-chromatid separation and aneuploidy.

The Spindle Checkpoint

During the cell cycle, chromosomes are duplicated in S phase and the sister chromatids are held together through sister-chromatid cohesion. In mitosis, a large protein assembly at the centromeres, called the kinetochore, provides the docking site for spindle microtubules. Attachment of all sister kinetochores to microtubules from opposing spindle poles enables sister chromatids to align on the metaphase plate and generates tension across the sister kinetochores, a state referred to as bi-orientation. Dissolution of sister-chromatid cohesion then allows equal partition of sister chromatids to the two daughter cells. Premature sister-chromatid separation when even a single kinetochore has not achieved proper microtubule attachment can lead to chromosome missegregation and aneuploidy.

The spindle checkpoint is a cell-cycle surveillance system that senses the existence of kinetochores not attached to spindle microtubules or not under tension and delays cohesion dissolution and anaphase onset, thus preventing aneuploidy (Bharadwaj and Yu, 2004; Foley and Kapoor, 2013; Kim and Yu, 2011; Lara-Gonzalez et al., 2012; Musacchio and Salmon, 2007). A key molecular target of the spindle checkpoint is Cdc20, the mitotic activator of a multisubunit ubiquitin ligase called the anaphase-promoting complex or cyclosome (APC/C) (Peters, 2006; Yu, 2007). Inhibition of APC/C^{Cdc20} by the checkpoint stabilizes Securin and Cyclin B1, thereby delaying anaphase onset and mitotic exit.

Assembly and function of the kinetochore

The kinetochore serves both as the docking site for spindle microtubules and as a signaling hub for the spindle checkpoint (Cleveland et al., 2003). It has a layered morphology, including inner and outer plates, a middle layer, and the outermost fibrous corona (Cleveland et al., 2003). Proteomic analysis coupled to high-resolution fluorescence microscopy has begun to shed light on the molecular identities of each kinetochore layer.

The centromere is epigenetically marked by CENP-A, a centromere-specific histone H3 variant (Black and Cleveland, 2011). Synthetic CENP-A chromatin reconstituted from recombinant human histones is sufficient to assemble functional kinetochores in cell-free *Xenopus* egg extracts (Guse et al., 2011), supporting the key function of the CENP-A nucleosome in defining the centromere locus. In vertebrate cells, the CENP-A nucleosome interacts throughout the cell cycle with the constitutive centromere-associated network (CCAN) (Foltz et al., 2006; Okada et al., 2006; Takeuchi and Fukagawa, 2012), which contains CENP-C, -H, -I, -K, -L, -M, -N, -O, -P, -Q, -U, -R, -T, -W, -S, and -X (Figure 1). These CCAN

components form several functional subcomplexes, including CENP-T–W–S–X, CENP-H–I–K, CENP-L–M–N, and CENP-O–P–Q–U–R. CENP-C and CENP-N anchor CCAN to centromeric chromatin through direct interactions with the CENP-A nucleosome (Carroll et al., 2010; Carroll et al., 2009). The CENP-T–W–S–X subcomplex has folds related to core histones and can bind DNA, possibly to form a nucleosome-like structure (Nishino et al., 2012). Although this subcomplex does not directly bind to CENP-A, its deposition at centromeres is nonetheless dependent on CENP-A (Hori et al., 2008).

As its name suggests, CCAN constitutively localizes to centromeres. The protein levels of several CCAN components, including CENP-N, -T, -U, and -W, fluctuate during the cell cycle (Hellwig et al., 2011; Kang et al., 2006; Prendergast et al., 2011). Surprisingly, CENP-U (also known as PBIP1) is degraded in early mitosis, when the outer kinetochore begins to assemble (Kang et al., 2006). The functional significance and molecular mechanisms of the cell-cycle oscillations in the levels of these CENP proteins are unclear.

The outer kinetochore is assembled onto CCAN at late prophase, just before nuclear envelope breakdown. With astounding speed and accuracy, more than 100 proteins are recruited and pieced together in a hierarchical fashion to form the mature, functional kinetochore. Although much remains to be learned about this fascinating process, recent progress has delineated the molecular pathways that install the core microtubule receptor, the KMN network, at kinetochores (Figure 1). The KMN network consists of Knl1 (also known as blinkin), the Mis12 complex (Mis12C, which contains Mis12, Nsl1, Nnf1, and Dsn1), and the Ndc80 complex (Ndc80C, which contains Ndc80, Nuf2, Spc24, and Spc25) (Cheeseman et al., 2006). Both Knl1 and Ndc80C have microtubule-binding activities. Mis12C interacts with both Knl1 and Ndc80C,

and nucleates the formation of the intact KMN (Petrovic et al., 2010), which allows cooperative microtubule binding by Knl1 and Ndc80C.

Artificial targeting of CENP-C and CENP-T to an ectopic chromatin locus is sufficient to recruit KMN and specify a functional kinetochore (Gascoigne et al., 2011), suggesting that the kinetochore assembly pathway has two branches (Figure 1). In one branch, the conserved N-terminal motif of CENP-C interacts with Mis12C and recruits it to the kinetochore (Kim and Yu, 2015; Przewloka et al., 2011; Screpanti et al., 2011). In the other branch, CENP-T functions as a direct kinetochore receptor for Ndc80C (Bock et al., 2012; Schleiffer et al., 2012). Thus, CENP-C and CENP-T connect KMN to CCAN.

Unlike CCAN, KMN does not localize constitutively to centromeres, and only assembles onto kinetochores during prophase. Two recent studies have shown that mitosis-specific, Cdk1-dependent phosphorylation of the conserved Ndc80C-binding motif of CENP-T increases the affinity of the Ndc80C–CENP-T interaction, and is required for proper Ndc80C targeting to kinetochores during mitosis (Malvezzi et al., 2013; Nishino et al., 2013).

It has become increasingly clear that the CENP-A nucleosome nucleates the formation of a large protein assembly called CCAN at the inner kinetochore, which serves as the foundation for mitosis-specific maturation of the outer kinetochore. This maturation mechanism requires further investigation and likely involves post-translational modifications and possibly selective degradation or stabilization of CCAN and outer kinetochore components. An important task of outer kinetochores is to recruit spindle checkpoint proteins and promote their activation during mitosis.

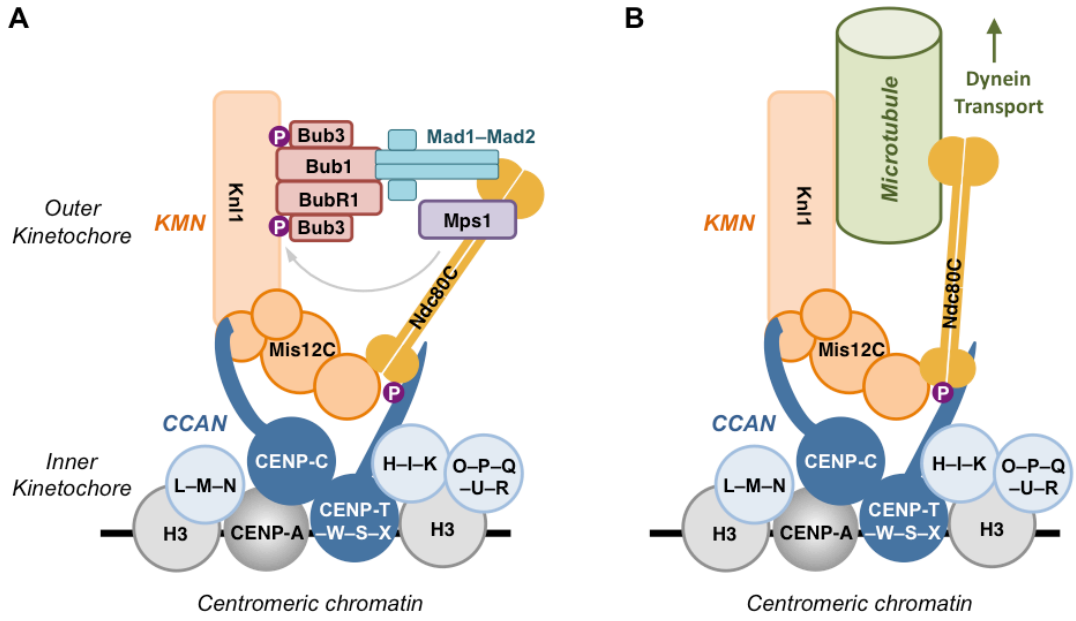

Figure 1. Kinetochore targeting of spindle checkpoint proteins and microtubule binding by the KMN network. (A) The centromere protein A (CENP-A) nucleosome is the key determinant of centromeric chromatin. The constitutive centromere-associated network (CCAN, dark blue and light blue) associates with the CENP-A nucleosome throughout the cell cycle. In mitosis, CCAN subunits CENP-C and CENP-T recruit the KMN network consisting of Knl1, the Mis12 complex (Mis12C), and the Ndc80 complex (Ndc80C). Mitosis-specific binding of KMN to CCAN is possibly regulated by Cdk1-dependent phosphorylation of CENP-T. KMN serves as an important binding platform for the spindle checkpoint proteins, including Mps1, Bub1–Bub3, BubR1–Bub3, and Mad1–Mad2. Phosphorylation of Knl1 by Mps1 enhances Bub1–Bub3 binding to Knl1. Mad1 has an extensive kinetochore-binding interface, and its C-terminal domain may interact with Bub1. **(B)** KMN is a key kinetochore receptor of spindle microtubules. It has two microtubule-binding interfaces: the N-terminal region of Knl1 and the head domains of Ndc80 and Nuf2. Microtubule binding to KMN may displace spindle checkpoint proteins. The checkpoint proteins can also be depleted from attached kinetochores through dynein-dependent, poleward transport along microtubules.

Kinetochore recruitment and activation of spindle checkpoint proteins

First identified in budding yeast, the molecular components of the spindle checkpoint were later shown to be evolutionarily conserved from yeast to man. The kinases Aurora B and Mps1 lie at or near the top of the checkpoint pathway, and appear to mutually regulate each other (Heinrich et al., 2012; Saurin et al., 2011; van der Waal et al., 2012). The centromere and kinetochore targeting of these two kinases has been linked to activation of their kinase activities (Jelluma et al., 2010; Kang et al., 2007; Kelly et al., 2007). The downstream spindle checkpoint proteins Bub1, BubR1, Bub3, Mad1, and Mad2 form three constitutive binary complexes: Bub1–Bub3, BubR1–Bub3, and Mad1–Mad2. These are recruited to kinetochores during mitosis in a KMN-dependent manner (Figure 1A). At kinetochores, these proteins undergo enzymatic or conformational activation. Activated checkpoint proteins then collaborate to inhibit APC/C^{Cdc20}. A key APC/C inhibitor is the mitotic checkpoint complex (MCC) consisting of BubR1–Bub3, Cdc20, and Mad2 (Figure 2).

Kinetochore localization of key checkpoint proteins is required for proper checkpoint signaling. Dissection of the kinetochore recruitment mechanisms of these checkpoint proteins thus holds the key to understanding the generation and propagation of checkpoint signals. The KMN network not only serves as the kinetochore receptor for microtubules, but also interacts directly or indirectly with most spindle checkpoint proteins (Figure 1). KMN thus couples spindle checkpoint signaling to microtubule binding.

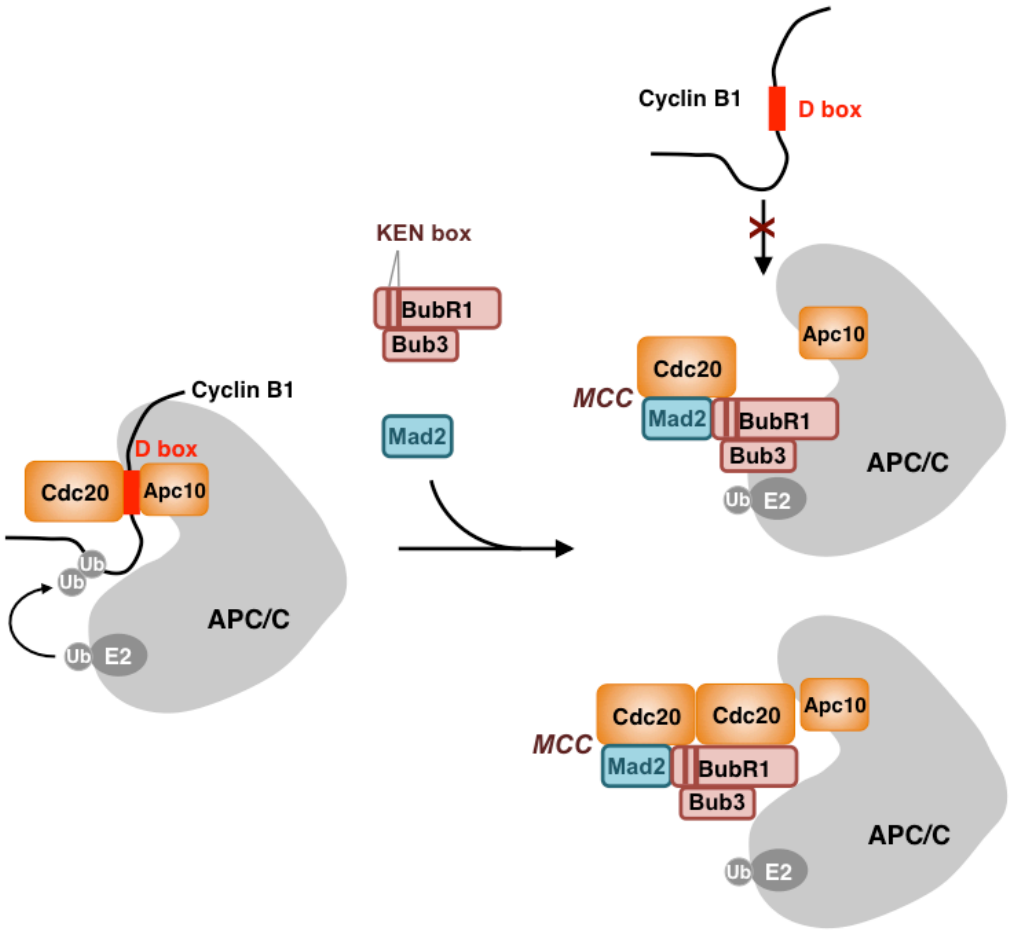

Figure 2. Model of APC/C inhibition by MCC. It has been proposed that MCC inhibits APC/C in two ways. First, BubR1/Mad3 contains KEN boxes and other motifs commonly found in APC/C substrates, but is not efficiently ubiquitylated by APC/C. It serves as a direct competitive inhibitor of substrate binding to APC/C. Second, binding of BubR1/Mad3 and of Mad2 to Cdc20 anchors Cdc20 away from Apc10, preventing D-box binding at the Cdc20–Apc10 interface. In addition, after forming MCC, the C-terminal KEN box of BubR1 can bind free or APC/C bound Cdc20, preventing it from activating APC/C with an unknown mechanism.

Recruitment and checkpoint functions of Aurora B and Mps1

Aurora B is a conserved serine/threonine kinase and a component of the chromosome passenger complex (CPC), which also contains INCENP, survivin, and borealin (Ruchaud et al., 2007). Aurora B has important functions in multiple mitotic processes, including sister chromatid

cohesion, spindle assembly, the spindle checkpoint, chromosome bi-orientation, and cytokinesis. Aurora B localizes to inner centromeres in early mitosis. Its centromeric localization is mediated by fellow CPC components INCENP and survivin. The localization of INCENP and survivin to centromeres is in turn driven by specific histone marks. In mitosis, the checkpoint kinase Bub1 phosphorylates histone H2A (T120 in humans) at kinetochores (Kawashima et al., 2010). Phospho-H2A-T120 serves as a chromatin mark to recruit the shugoshin proteins, which interact with INCENP (Kawashima et al., 2010; Yamagishi et al., 2010). Another mitotic kinase, haspin, phosphorylates histone H3-T3 at centromeres (Kelly et al., 2010; Wang et al., 2010; Yamagishi et al., 2010). Phospho-H3-T3 directly binds to survivin. The combined actions of shugoshin–INCENP and survivin–phospho-H3-T3 interactions then drive centromeric localization of CPC and contribute to activation of Aurora B. Mps1 and the master mitotic kinase Cdk1 also promote Aurora B activation through phosphorylation of borealin and survivin, respectively (Jelluma et al., 2008; Tsukahara et al., 2010).

When localizing at inner centromeres, Aurora B promotes sister-chromatid bi-orientation by phosphorylating multiple KMN components at outer kinetochores and breaking improper kinetochore–microtubule attachments (Cheeseman et al., 2006; Welburn et al., 2010). For example, Aurora-B-mediated phosphorylation of Ndc80 and Knl1 introduces unfavorable negative charges onto the microtubule-binding surface of KMN and reduces its microtubule-binding affinity. The phosphorylation level of an Aurora B target is inversely correlated with its physical distance from Aurora B (Figure 3A) (Liu et al., 2009; Wang et al., 2011), which suggests a mechanism by which Aurora B can promote bi-orientation of sister chromatids and suppress erroneous attachments. When a pair of sister kinetochores is captured by microtubules from the same spindle pole, this pair of sister kinetochores is not under tension, and the distance

between Aurora B and its KMN substrates is small. Aurora B then efficiently phosphorylates KMN and disrupts this type of improper microtubule attachment. When a pair of kinetochores is captured by microtubules from opposing spindle poles, the microtubule-pulling force generates tension across the kinetochores and physically separates Aurora B at the inner centromeres from KMN at the outer kinetochores. It has been proposed that this spatial separation between Aurora B and its substrates decreases phosphorylation of Ndc80 and Knl1, preserving the correct mode of kinetochore–microtubule attachment (Lampson and Cheeseman, 2011).

Unlike other spindle checkpoint proteins, Aurora B is only required for the checkpoint activation and mitotic arrest induced by the microtubule-stabilizing drug taxol, but not for the mitotic arrest induced by the microtubule-destabilizing drug nocodazole (Ruchaud et al., 2007). Because of this unique feature, it has been argued that Aurora B is indirectly involved in the spindle checkpoint by breaking unstable kinetochore–microtubule attachment in the presence of taxol and transiently producing unattached kinetochores to facilitate the activation of other checkpoint proteins (Pinsky et al., 2006). Two studies have shown that Aurora B is critical for the nocodazole-induced mitotic arrest in human cells depleted of Ndc80 or with partial inhibition of their Mps1 activity (Santaguida et al., 2011; Saurin et al., 2011). These studies confirmed earlier findings (Vanoosthuyse and Hardwick, 2009) and established a microtubule-independent role of Aurora B in the spindle checkpoint. It was further shown that Aurora B phosphorylates Dsn1 in Mis12C (Kim and Yu, 2015), which contributes to the installment of KMN on the kinetochore and therefore recruitment of downstream checkpoint signaling proteins.

Mps1 is a master regulator of checkpoint signaling. Its kinase activity is required for the kinetochore recruitment of all the other checkpoint proteins (Abrieu et al., 2001; Heinrich et al., 2012; Tighe et al., 2008; Weiss and Winey, 1996). Mps1 localizes to the kinetochore depending

on Ndc80C in KMN network (Martin-Lluesma et al., 2002; Stucke et al., 2004). It has two motifs that independently bind two different subunits in Ndc80C (Ji et al., 2015). One of the two interactions is enhanced by Aurora B phosphorylation on Ndc80, which explains previous findings that Aurora B helps Mps1 recruitment and activation (Nijenhuis et al., 2013; Saurin et al., 2011; Zhu et al., 2013). The checkpoint kinases Mps1, Bub1 and Aurora B constitute a feed-forward checkpoint signaling loop. Aurora B phosphorylates Ndc80C to weaken microtubule binding and enhance Mps1 localization. Activated Mps1 recruits Bub1, which phosphorylates histone H2A. Phospho-H2A then further promotes centromeric accumulation of Aurora B.

The attachment of spindle microtubule to the kinetochore directly regulates Mps1 in order to control spindle checkpoint signaling. The binding between Mps1 and Ndc80C involves the microtubule binding sites of Ndc80C (Ji et al., 2015). Mps1 and microtubule compete to bind Ndc80C, coupling microtubule-kinetochore attachment status to spindle checkpoint switch.

Kinetochore recruitment of Bub1 and BubR1

The spindle checkpoint proteins are recruited to unattached or tensionless kinetochores, where they undergo enzymatic or conformational activation to produce diffusible APC/C inhibitors. Bub1 and BubR1 share extensive sequence similarity and both contain a kinase domain. Both also form a constitutive complex with Bub3. BubR1 is a component of MCC and directly participates in APC/C^{Cdc20} inhibition. Bub1 phosphorylates histone H2A to recruit shugoshin to kinetochores. Bub1 also phosphorylates Cdc20 and contributes to APC/C^{Cdc20} inhibition (Kang et al., 2008; Tang et al., 2004). Finally, independently of its kinase activity, Bub1 acts as a scaffold to recruit downstream checkpoint components, including BubR1 and Mad1, to kinetochores.

Several recent studies have refined our understanding of the kinetochore targeting of Bub1 and BubR1.

Bub1 contains an N-terminal tetratricopeptide repeat (TPR) domain, a Phe box and a KEN box that interact with Cdc20, and a GLEBS motif that binds to Bub3. The kinetochore localization of Bub1 is strictly dependent on the KMN component Knl1 (Kiyomitsu et al., 2007). The TPR domain of Bub1 binds to a conserved motif in the N-terminal region of Knl1 (Kiyomitsu et al., 2011; Kiyomitsu et al., 2007). This interaction, however, has a marginal role in the kinetochore localization of Bub1 (Krenn et al., 2012). Instead, Bub3 binding is critical for kinetochore targeting of Bub1, because mutations of the Bub1 GLEBS motif abolish its kinetochore localization.

Bub3 mediates Bub1 kinetochore targeting through binding with Knl1. Mps1 phosphorylates Knl1 on multiple conserved Met-Glu-Leu-Thr (MELT) motifs and promotes kinetochore targeting of Bub1 in both yeast and human cells (London et al., 2012; Shepperd et al., 2012; Yamagishi et al., 2012). In yeast cells without Mps1 activity, a phospho-mimicking mutant of Knl1 supports kinetochore targeting of Bub1, which is, however, abolished by Bub3 deletion. Crystal structure of Bub3 binding to the phosphorylated MELT motif was later determined (Primorac et al., 2013). A loop region preceding the Bub3-binding domain of Bub1 also facilitates the interaction between Bub3 and MELT motif, and is therefore required for Bub1 localization (Overlack et al., 2015). Mutating Bub3 residues on the interaction interface disrupts kinetochore localization of Bub1-Bub3 and causes spindle checkpoint defect (Figure 1A). These results confirmed a direct role of Bub3 in Bub1 localization to the kinetochore.

A similar mechanism governs kinetochore targeting of the Bub1 homolog BubR1. The N-terminal TPR domain of BubR1 binds to a conserved motif in Knl1 that is adjacent to and shares

sequence similarity with the Bub1-binding motif of Knl1 (Bolanos-Garcia et al., 2011). Like Bub1, this interaction is largely dispensable for kinetochore localization of BubR1 (Krenn et al., 2012), and the BubR1–Bub3 interaction is instead required for kinetochore targeting of BubR1 (Elowe et al., 2010). However, unlike Bub1, Bub3 is not sufficient to bring BubR1 to the kinetochore. The loop region in BubR1 cannot facilitate Bub3 binding to MELT motif like in Bub1 (Overlack et al., 2015). This is consistent with previous observation that BubR1 localization not only depends on Bub3 but also requires Bub1 (Figure 1A). Ectopic targeting of Bub1 to the telomere is sufficient to recruit BubR1 to that location (Rischitor et al., 2007). Expression of the phospho-mimicking Knl1 recruits BubR1 to kinetochores in the absence of Mps1 kinase activity, but this recruitment is dependent on Bub1 (Yamagishi et al., 2012). Bub1 facilitates BubR1 localization through direct binding, which does not require Bub3 (Overlack et al., 2015). How Bub3 is involved in BubR1 localization is not clear. Because the ectopic recruitment of BubR1 using Bub1 requires Bub3 binding but is independent of kinetochore, it is possible that Bub3 facilitate BubR1-Bub1 interaction without involving Knl1 (Overlack et al., 2015).

Kinetochore recruitment of Mad1

Throughout the cell cycle, Mad1 and Mad2 form a constitutive heterotetramer referred to as the Mad1–Mad2 core complex (Luo et al., 2002; Sironi et al., 2002). When the spindle checkpoint is active, the Mad1–Mad2 core complex localizes to kinetochores and recruits another copy of Mad2 from the cytosol to catalyze its conformational activation (Luo and Yu, 2008; Mapelli and Musacchio, 2007). Kinetochore targeting of the Mad1–Mad2 core complex is dependent on

Ndc80C, Mps1, and Bub1. Recent studies have shed more light on the kinetochore-targeting mechanisms of Mad1–Mad2 (Kim et al., 2012; London and Biggins, 2014).

Mad1 has an unusually extensive kinetochore-binding interface, and non-overlapping Mad1 fragments retain partial kinetochore localization in human cells (Kim et al., 2012). The crystal structure of the conserved C-terminal domain (CTD) of human Mad1 reveals unexpected structural similarity between Mad1 CTD and the kinetochore-binding domain of Spc25 (an Ndc80C component), suggesting that Mad1 CTD might be involved in kinetochore binding. Indeed, a conserved RLK motif within Mad1 CTD contributes to the kinetochore targeting of Mad1. In yeast, this RLK motif of Mad1 is required for its mitosis-specific interaction with Bub1 (Brady and Hardwick, 2000). In human cells, Bub1 is required for proper kinetochore localization of Mad1 (Figure 1A). The Bub1-Mad1 interaction depends on Bub1 phosphorylation by Mps1 (London and Biggins, 2014). The phosphorylation on Bub1 associates with the conserved basic patch RLK in Mad1 CTD, contributing to Mad1 localization. CTD is, however, not the only region of Mad1 that mediates kinetochore binding. The N-terminal coiled-coil region of *Xenopus* or human Mad1 alone also retains partial kinetochore targeting (Chung and Chen, 2002; Kim et al., 2012). The kinetochore receptors of the Mad1 N-terminal region have not been identified. Because kinetochore recruitment of Mad1 also requires Ndc80C and Mps1 (Abrieu et al., 2001; Martin-Lluesma et al., 2002), we speculate that the Mad1 N-terminal region likely binds to Ndc80C or Mps1 or both.

The metazoan-specific RZZ complex consisting of Rod, Zwilch, and Zw10 is also required for Mad1 kinetochore localization (Karess, 2005). In *Caenorhabditis elegans*, the RZZ-binding protein spindly interacts with Mad1 and regulates Mad1 kinetochore localization (Yamamoto et al., 2008). The spindly–RZZ complex likely contributes to Mad1 kinetochore

targeting in metazoans. However, spindly–RZZ also serves as a kinetochore receptor for the microtubule-based motor dynein–dynactin, which strips spindle checkpoint proteins and spindly from microtubule-attached kinetochores (Barisic et al., 2010; Gassmann et al., 2010; Howell et al., 2001). This is an important mechanism for checkpoint silencing (discussed later). Thus, it is possible that RZZ and spindly regulate Mad1 kinetochore localization indirectly by blocking untimely dynein-mediated stripping of Mad1 from kinetochores.

Interestingly, mutation of the dynein-binding motif of spindly causes accumulation of Mad1–Mad2 at microtubule-bound kinetochores, delaying anaphase onset (Gassmann et al., 2010). Extending this finding further, a recent study has directly investigated the consequences of forced kinetochore targeting of Mad1 (Maldonado and Kapoor, 2011). Covalent tethering of Mad1 to the KMN component Mis12 prevents the timely removal of this fusion protein from kinetochores and causes a prolonged mitotic arrest. Surprisingly, this arrest is dependent on upstream checkpoint components, such as Aurora B and Mps1. Thus, Mad1 kinetochore localization by itself is insufficient to sustain the spindle checkpoint, but it may prolong the activation or prevent the inactivation of upstream checkpoint components through a yet uncharacterized feedback mechanism.

Taken together, recent findings strengthen the overall theme of hierarchical and interdependent targeting of checkpoint proteins to outer kinetochores. Enrichment of checkpoint proteins at these sites promotes their efficient crosstalk and enables their enzymatic and conformational activation.

Checkpoint inhibition of APC/C

An important output of kinetochore recruitment and activation of checkpoint proteins is the assembly of the mitotic checkpoint complex (MCC) consisting of BubR1–Bub3, Cdc20, and Mad2. In yeast, forced formation of MCC or MCC sub-complexes by covalently tethering Mad2 to Mad3 (the yeast ortholog of BubR1) or tethering Mad2 to Cdc20 is sufficient to arrest cells in mitosis, even without functional kinetochores or checkpoint signaling (Lau and Murray, 2012). Thus, MCC is a critical checkpoint inhibitor of APC/C. Its assembly and disassembly are key events in the regulation of APC/C by the checkpoint.

When not incorporated into MCC, free Cdc20 activates APC/C by contributing to the recognition of two common motifs in APC/C substrates: the KEN box and the destruction box (D box) (Yu, 2007). Cdc20 has a C-terminal WD40 domain that folds into a β propeller. The KEN box binds at the narrow face of the propeller, whereas the D box binds at the interface between the core APC/C subunit Apc10 and the side of the Cdc20 propeller (Buschhorn et al., 2011; Chao et al., 2012; da Fonseca et al., 2011; Tian et al., 2012). In light of the APC/C-activating mechanism of free Cdc20, two complementary mechanisms have been proposed to explain APC/C inhibition by MCC (Figure 2). First, BubR1 and Mad3 serve as pseudo-substrates to block substrate recruitment by Cdc20. Second, Mad2 and BubR1/Mad3 alter the mode and site of Cdc20 binding to APC/C. In addition, the MCC can function as an inhibitor for another molecule of Cdc20. But the detailed mechanism how the inhibition works is not clearly understood.

Similar to APC/C substrates, the budding yeast Mad3 has two KEN boxes and a D box, all of which are required to compete with substrates for binding to Cdc20 and for spindle checkpoint signaling (Burton and Solomon, 2007; King et al., 2007). BubR1 also has two KEN boxes, which are critical for the spindle checkpoint in human cells, suggesting a conserved

Cdc20-binding mechanism (Lara-Gonzalez et al., 2011). The N-terminal KEN box of BubR1 mediates its interaction with Cdc20 and Mad2 and the assembly of MCC, whereas the C-terminal KEN box of BubR1 has been shown to block D-box-dependent substrate binding to APC/C (Lara-Gonzalez et al., 2011). Furthermore, the C-terminal KEN box can bind another copy of Cdc20, making MCC an inhibitor for free Cdc20 that is bound to APC/C (Izawa and Pines, 2015). Even though BubR1 and Mad3 contain APC/C degradation motifs, they are not efficiently ubiquitylated by APC/C. BubR1 is protected from ubiquitylation by acetylation at K250 by the p300/CBP-associate factor (PCAF), which occurs during prometaphase (Choi et al., 2009). Therefore, BubR1 and Mad3 act as pseudo-substrates to block substrate recruitment to APC/C^{Cdc20}. Intriguingly, BubR1 K250 can also be sumoylated following prolonged mitotic arrest (Yang et al., 2012). Future experiments are necessary to sort out the roles of the competing modifications (acetylation and sumoylation) at the same lysine of BubR1 in mitotic progression.

The crystal structures of the fission yeast MCC and human Cdc20 reveal that the N-terminal KEN box of Mad3 or BubR1 occupies the conserved KEN-box-binding site of Cdc20 and promotes MCC assembly through establishing multiple interactions with both Mad2 and Cdc20 (Chao et al., 2012; Tian et al., 2012). Mad2 exists in two native conformers, N1/open-Mad2 (O-Mad2) and N2/closed Mad2 (C-Mad2). The Mad1/Cdc20-bound Mad2 adopts the C-Mad2 conformation. Consistent with two recent biochemical studies (Mariani et al., 2012; Tipton et al., 2011), the structure of MCC shows that the dimerization helix (αC) of C-Mad2 interacts with Mad3 in MCC. It has been proposed that cytosolic C-Mad2 bound to Cdc20 can further recruit and activate another copy of O-Mad2, thus propagating checkpoint signals (De Antoni et al., 2005). Because the αC helix of C-Mad2 is a major binding determinant for O-Mad2, C-Mad2 in MCC cannot further recruit and activate O-Mad2 in the cytosol. The structures, however, do

not explain how the C-terminal KEN box of Mad3 or BubR1 inhibit APC/C^{Cdc20}. Future studies on Cdc20 bound to larger fragments of Mad3 or BubR1 are needed to address this important issue.

Several lines of evidence indicate that BubR1 and Mad2 alter the mode of Cdc20 binding to APC/C and hinder its ability to activate APC/C. First, electron microscopy (EM) studies revealed that Cdc20 binds to different sites on APC/C, depending on whether it is functioning as an activator or as part of MCC (Herzog et al., 2009). Docking the crystal structure of yeast MCC into the EM structure of human APC/C–MCC further suggests that Cdc20 is displaced away from Apc10 while part of MCC, so that Cdc20 and Apc10 cannot form a co-receptor for the D box of substrates (Chao et al., 2012). Second, depending on whether the checkpoint is on or off, different APC/C subunits are differentially required for Cdc20 binding (Izawa and Pines, 2011). Third, Cdc20 contains several conserved motifs, including an N-terminal conserved motif with the consensus DRYIP termed the C box and the IR motif at its extreme C-terminal tail with the characteristic Ile-Arg dipeptide. Both the C box and the IR motif are required for Cdc20 to bind APC/C as an activator when the spindle checkpoint is off, but they are not required for APC/C binding during prometaphase when the checkpoint is on (Izawa and Pines, 2012). Finally, the Mad2-interacting motif (MIM) of Cdc20 is required for Cdc20 to bind to and activate APC/C (Izawa and Pines, 2012). When Cdc20 is bound to either Mad2 alone or in the context of MCC, this motif is no longer available for APC/C binding. The APC/C-binding modes of free Cdc20 and Mad2-bound Cdc20 must therefore be different.

In summary, tremendous progress has been made towards understanding APC/C inhibition by the checkpoint. Central to this inhibition is the sequestration of the APC/C activator Cdc20 into MCC, which can further inhibit free and APC/C bound Cdc20. However, there are

still unresolved questions in this area. Although MCC is a more potent inhibitor of APC/C, its sub-complexes, such as Mad2–Cdc20 and BubR1–Cdc20, are also capable of preventing Cdc20 from activating APC/C (Tang et al., 2001). The mechanism by which Mad2 alone inhibits APC/C is likely related to its ability to alter Cdc20 binding to APC/C, as discussed earlier. Two studies have suggested that Mad2 merely primes BubR1 binding to Cdc20, and BubR1 alone is the ultimate inhibitor of APC/C (Kulukian et al., 2009; Nilsson et al., 2008). In the absence of Mad2, the middle region of BubR1 is critical for Cdc20 binding and APC/CCdc20 inhibition in vitro (Tang et al., 2001). Two Cdc20-binding motifs were identified in this region (Di Fiore et al., 2015) (Diaz-Martinez et al., 2015), which contribute to maintain MCC level in cells with active spindle checkpoint. Yet, this region does not appear to be required for the checkpoint function of BubR1 in mammalian cells (Diaz-Martinez et al., 2015). The function of APC/CCdc20 inhibition by BubR1 alone needs to be further clarified.(Lara-Gonzalez et al., 2011; Malureanu et al., 2009)

MCC is a stoichiometric inhibitor of APC/C. Because of the high sensitivity of the checkpoint, it is possible that there are additional mechanisms that inhibit APC/C catalytically. Cdc20 phosphorylation by Bub1 has been implicated as such a mechanism (Tang et al., 2004). The kinase activity of Bub1 is not, however, strictly required for the spindle checkpoint (Klebig et al., 2009). The role of Cdc20 phosphorylation by Bub1 and the connection between this APC/C-inhibitory mechanism and MCC need to be further investigated.

Silencing the spindle checkpoint

A few unattached kinetochores in a mammalian cell are sufficient to activate the spindle checkpoint (Collin et al., 2013; Rieder et al., 1995). It takes only approximately 20 min from the

capturing of these unattached kinetochores by the mitotic spindle to checkpoint silencing and chromosome segregation. The highly dynamic nature of MCC assembly and disassembly is a key feature that enables rapid checkpoint silencing. When the checkpoint is on, Cdc20 is recruited to unattached kinetochores and sequestered in MCC. MCC is released into the cytosol and associates with APC/C. Cdc20 in the APC/C–MCC complex undergoes autoubiquitylation and degradation, leading to MCC disassembly. Dynamic MCC assembly and disassembly ensure that the concentrations of MCC and active APC/C^{Cdc20} both remain low and are highly responsive to the status of kinetochore attachment. We discuss the checkpoint silencing process in two separable aspects: (I) turning off MCC production at kinetochores, and (Nishino et al.) dismantling the existing MCC in the cytosol.

Turning off the kinetochore checkpoint signal

When the kinetochores are properly attached by microtubules from the two opposite spindle poles and are under tension, the checkpoint signal from the kinetochores needs to be extinguished. Multiple mechanisms have been described to explain the connection between the establishment of microtubule attachment and kinetochore tension and the termination of the spindle checkpoint signal.

Establishment of the kinetochore–microtubule attachment leads to transport of checkpoint proteins from kinetochores to spindle poles through the dynein motor along microtubules (Figure 1) (Gassmann et al., 2010; Howell et al., 2001). In addition, because the KMN network serves as the kinetochore receptor for both microtubules and spindle checkpoint proteins, microtubule binding to KMN may displace checkpoint proteins independently of dynein. Recent studies have provided evidence of the involvement of microtubule binding by

KMN in checkpoint silencing (Espeut et al., 2012) (Ji et al., 2015). As discussed previously, KMN has two microtubule-binding interfaces: the N-terminal region of Knl1 and the head domains of Ndc80 and Nuf2. In *C. elegans*, microtubule binding by the N-terminal domain of KNL-1 is dispensable for load-bearing kinetochore–microtubule attachment and for the kinetochore recruitment of dynein, but facilitates spindle checkpoint silencing. Thus, the KNL-1–microtubule interaction contributes to checkpoint silencing in a dynein-independent way, although how microtubule binding by KNL-1 inactivates the checkpoint still needs further investigation. On the other hand, Mps1 competes with microtubule as they bind to the same domain on Nuf2. Microtubule binding to Ndc80 releases Mps1 from the kinetochore, silencing the checkpoint signaling.

Another mechanism that helps to shut off the checkpoint signal at kinetochores is capping of the Mad1–Mad2 core complex by the Mad2 inhibitor $p31^{comet}$. $p31^{comet}$ interacts with C-Mad2 in the Mad1–Mad2 core complex and prevents recruitment and conformational activation of O-Mad2 (De Antoni et al., 2005; Fava et al., 2011; Mapelli et al., 2006; Xia et al., 2004; Yang et al., 2007). Binding of $p31^{comet}$ to Mad1–Mad2 is not completely blocked during mitosis, and a pool of $p31^{comet}$ localizes to kinetochores (Hagan et al., 2011). In this way, $p31^{comet}$ attenuates Mad2 activation and MCC formation at the kinetochores.

Finally, the protein phosphatase PP1 promotes checkpoint silencing by antagonizing checkpoint kinases at the centromeres and kinetochores. PP1 directly antagonizes Aurora B by dephosphorylating phospho-H3-T3 (Qian et al., 2011), a histone mark that helps to recruit the Aurora-B-containing CPC to inner centromeres. Conversely, Aurora-B-mediated phosphorylation of several PP1-binding proteins at the outer kinetochores, including Knl1, prevents their interaction with PP1 (Liu et al., 2010; Rosenberg et al., 2011). When sister

kinetochores are under tension, these Aurora B substrates on the outer kinetochores are spatially separated from Aurora B, leading to their decreased phosphorylation and enhanced PP1 binding (Figure 3A). Recruitment of PP1 to kinetochores leads to further dephosphorylation of substrates of Aurora B and other kinases. For example, phosphorylation of Knl1 by Mps1 and the resulting enhanced Bub1 binding to Knl1 can be reversed by PP1 (London et al., 2012; Shepperd et al., 2012). Therefore, PP1 is a key contributor to checkpoint silencing at the kinetochores.

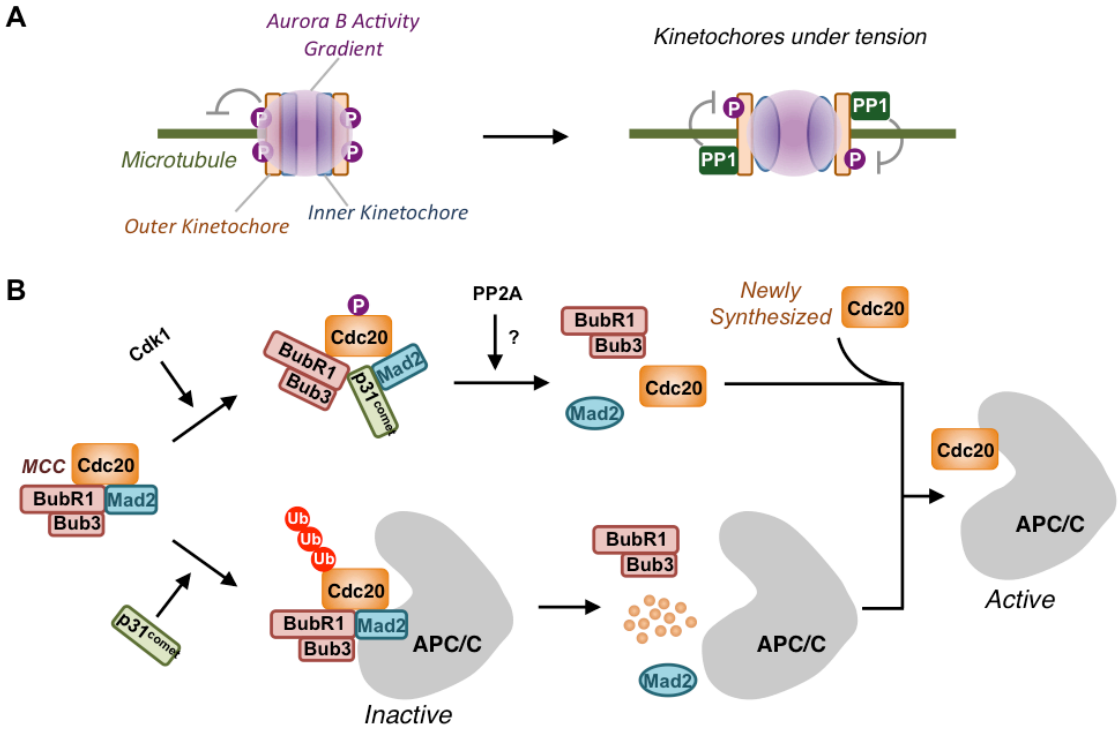

Figure 3. Models of spindle checkpoint silencing at kinetochores and in the cytosol. (A) Incomplete or improper kinetochore–microtubule attachments do not create tension across sister kinetochores. The outer kinetochore is exposed to the activity gradient of Aurora B, which resides at centromeres. Aurora B-dependent phosphorylation of certain KMN components disrupts improper attachments. Proper microtubule attachment at kinetochores generates tension and physically separates Aurora B and its substrates at outer kinetochores. Diminished phosphorylation of these substrates allows PP1 binding, which further dephosphorylates key substrates of Aurora B and other proteins and promotes checkpoint silencing. **(B)** When the kinetochore checkpoint signal is turned off, MCC is disassembled in Cdc20 ubiquitylation-

dependent (bottom) and -independent (top) pathways. In the ubiquitylation-independent pathway, p31^{comet} directly competes with BubR1 for Mad2 binding and disrupts MCC. Cdc20 phosphorylation by Cdk1 might also contribute to MCC disassembly in this pathway through an unknown mechanism. In the ubiquitylation-dependent pathway, p31^{comet} promotes autoubiquitylation and degradation of Cdc20 as part of MCC. The newly synthesized Cdc20 and Cdc20 released in the ubiquitylation-independent pathway bind to and activate APC/C.

MCC disassembly and APC/C activation in the cytosol

The APC/C–MCC complex does not efficiently ubiquitylate APC/C substrates, including cyclin B1 and securin. It does, however, autoubiquitylate Cdc20 within MCC, triggering its dissociation from Mad2 and BubR1 and proteasomal degradation (Figure 3B). A newly identified APC/C subunit, Apc15, is specifically required for Cdc20 autoubiquitylation and degradation (Foster and Morgan, 2012; Mansfeld et al., 2011; Uzunova et al., 2012). p31^{comet} can also promote Cdc20 autoubiquitylation and degradation and MCC disassembly (Nilsson et al., 2008; Reddy et al., 2007; Varetti et al., 2011; Westhorpe et al., 2011). MCCs containing non-ubiquitylatable Cdc20 mutants are, however, still disassembled in human cells (Jia et al., 2011; Nilsson et al., 2008). Interestingly, p31^{comet} depletion still delayed disassembly of MCC containing a non-ubiquitylatable Cdc20 mutant, indicating that p31^{comet} can promote MCC disassembly independently of Cdc20 ubiquitylation (Jia et al., 2011). Thus, Cdc20 ubiquitylation and p31^{comet} act in somewhat redundant pathways to promote MCC disassembly in the cytosol. In addition to p31^{comet}, the CUE-domain-containing protein CUEDC2 also contributes to MCC disassembly by binding to Cdc20 and disrupting the Mad2–Cdc20 interaction (Gao et al., 2011).

Cells use a two-pronged strategy to turn off the spindle checkpoint when all sister kinetochores reach bi-orientation, namely switching off signal production at the kinetochores and promoting the turnover of existing APC/C-inhibitory complexes in the cytosol. Intriguingly,

active MCC disassembly occurs even when the spindle checkpoint is on. It remains to be established whether this process is constitutive or accelerated during checkpoint silencing. The mechanism by which $p31^{comet}$ promotes MCC disassembly independently of Cdc20 ubiquitylation is also not understood. $p31^{comet}$ may do so directly by competing with BubR1 for binding to the dimerization helix of Mad2 and thus destabilizing MCC (Figure 3B) (Chao et al., 2012). In addition, this process may involve $p31^{comet}$-stimulated, Cdk-dependent phosphorylation of Cdc20 (Miniowitz-Shemtov et al., 2012).

Concluding remarks

The spindle checkpoint is in essence an intracellular signal transduction system. Checkpoint signals originate at unattached or tensionless kinetochores and are propagated through the combined actions of kinase activation and a regulated conformational change in Mad2. The end point of this signaling system is sequestration of Cdc20 and inhibition of APC/C. Future studies are needed to deepen our understanding of this fascinating system.

References

Abrieu, A., Magnaghi-Jaulin, L., Kahana, J.A., Peter, M., Castro, A., Vigneron, S., Lorca, T., Cleveland, D.W., and Labbe, J.C. (2001). Mps1 is a kinetochore-associated kinase essential for the vertebrate mitotic checkpoint. Cell *106*, 83-93.

Barisic, M., Sohm, B., Mikolcevic, P., Wandke, C., Rauch, V., Ringer, T., Hess, M., Bonn, G., and Geley, S. (2010). Spindly/CCDC99 is required for efficient chromosome congression and mitotic checkpoint regulation. Molecular biology of the cell *21*, 1968-1981.

Bharadwaj, R., and Yu, H. (2004). The spindle checkpoint, aneuploidy, and cancer. Oncogene *23*, 2016-2027.

Black, B.E., and Cleveland, D.W. (2011). Epigenetic centromere propagation and the nature of CENP-a nucleosomes. Cell *144*, 471-479.

Bock, L.J., Pagliuca, C., Kobayashi, N., Grove, R.A., Oku, Y., Shrestha, K., Alfieri, C., Golfieri, C., Oldani, A., Dal Maschio, M.*, et al.* (2012). Cnn1 inhibits the interactions between the KMN complexes of the yeast kinetochore. Nature cell biology *14*, 614-624.

Bolanos-Garcia, V.M., Lischetti, T., Matak-Vinkovic, D., Cota, E., Simpson, P.J., Chirgadze, D.Y., Spring, D.R., Robinson, C.V., Nilsson, J., and Blundell, T.L. (2011). Structure of a Blinkin-BUBR1 complex reveals an interaction crucial for kinetochore-mitotic checkpoint regulation via an unanticipated binding Site. Structure (London, England : 1993) *19*, 1691-1700.

Brady, D.M., and Hardwick, K.G. (2000). Complex formation between Mad1p, Bub1p and Bub3p is crucial for spindle checkpoint function. Current biology : CB *10*, 675-678.

Burton, J.L., and Solomon, M.J. (2007). Mad3p, a pseudosubstrate inhibitor of APCCdc20 in the spindle assembly checkpoint. Genes & development *21*, 655-667.

Buschhorn, B.A., Petzold, G., Galova, M., Dube, P., Kraft, C., Herzog, F., Stark, H., and Peters, J.M. (2011). Substrate binding on the APC/C occurs between the coactivator Cdh1 and the processivity factor Doc1. Nature structural & molecular biology *18*, 6-13.

Carroll, C.W., Milks, K.J., and Straight, A.F. (2010). Dual recognition of CENP-A nucleosomes is required for centromere assembly. The Journal of cell biology *189*, 1143-1155.

Carroll, C.W., Silva, M.C., Godek, K.M., Jansen, L.E., and Straight, A.F. (2009). Centromere assembly requires the direct recognition of CENP-A nucleosomes by CENP-N. Nature cell biology *11*, 896-902.

Chao, W.C., Kulkarni, K., Zhang, Z., Kong, E.H., and Barford, D. (2012). Structure of the mitotic checkpoint complex. Nature *484*, 208-213.

Cheeseman, I.M., Chappie, J.S., Wilson-Kubalek, E.M., and Desai, A. (2006). The conserved KMN network constitutes the core microtubule-binding site of the kinetochore. Cell *127*, 983-997.

Choi, E., Choe, H., Min, J., Choi, J.Y., Kim, J., and Lee, H. (2009). BubR1 acetylation at prometaphase is required for modulating APC/C activity and timing of mitosis. The EMBO journal *28*, 2077-2089.

Chung, E., and Chen, R.H. (2002). Spindle checkpoint requires Mad1-bound and Mad1-free Mad2. Molecular biology of the cell *13*, 1501-1511.

Cleveland, D.W., Mao, Y., and Sullivan, K.F. (2003). Centromeres and kinetochores: from epigenetics to mitotic checkpoint signaling. Cell *112*, 407-421.

Collin, P., Nashchekina, O., Walker, R., and Pines, J. (2013). The spindle assembly checkpoint works like a rheostat rather than a toggle switch. Nature cell biology *15*, 1378-1385.

da Fonseca, P.C., Kong, E.H., Zhang, Z., Schreiber, A., Williams, M.A., Morris, E.P., and Barford, D. (2011). Structures of APC/C(Cdh1) with substrates identify Cdh1 and Apc10 as the D-box co-receptor. Nature *470*, 274-278.

De Antoni, A., Pearson, C.G., Cimini, D., Canman, J.C., Sala, V., Nezi, L., Mapelli, M., Sironi, L., Faretta, M., Salmon, E.D.*, et al.* (2005). The Mad1/Mad2 complex as a template for Mad2 activation in the spindle assembly checkpoint. Current biology : CB *15*, 214-225.

Di Fiore, B., Davey, N.E., Hagting, A., Izawa, D., Mansfeld, J., Gibson, T.J., and Pines, J. (2015). The ABBA motif binds APC/C activators and is shared by APC/C substrates and regulators. Developmental cell *32*, 358-372.

Diaz-Martinez, L.A., Tian, W., Li, B., Warrington, R., Jia, L., Brautigam, C.A., Luo, X., and Yu, H. (2015). The Cdc20-binding Phe box of the spindle checkpoint protein BubR1 maintains the mitotic checkpoint complex during mitosis. The Journal of biological chemistry *290*, 2431-2443.

Elowe, S., Dulla, K., Uldschmid, A., Li, X., Dou, Z., and Nigg, E.A. (2010). Uncoupling of the spindle-checkpoint and chromosome-congression functions of BubR1. Journal of cell science *123*, 84-94.

Espeut, J., Cheerambathur, D.K., Krenning, L., Oegema, K., and Desai, A. (2012). Microtubule binding by KNL-1 contributes to spindle checkpoint silencing at the kinetochore. The Journal of cell biology *196*, 469-482.

Fava, L.L., Kaulich, M., Nigg, E.A., and Santamaria, A. (2011). Probing the in vivo function of Mad1:C-Mad2 in the spindle assembly checkpoint. The EMBO journal *30*, 3322-3336.

Foley, E.A., and Kapoor, T.M. (2013). Microtubule attachment and spindle assembly checkpoint signalling at the kinetochore. Nat Rev Mol Cell Biol *14*, 25-37.

Foltz, D.R., Jansen, L.E., Black, B.E., Bailey, A.O., Yates, J.R., 3rd, and Cleveland, D.W. (2006). The human CENP-A centromeric nucleosome-associated complex. Nature cell biology *8*, 458-469.

Foster, S.A., and Morgan, D.O. (2012). The APC/C subunit Mnd2/Apc15 promotes Cdc20 autoubiquitination and spindle assembly checkpoint inactivation. Molecular cell *47*, 921-932.

Gao, Y.F., Li, T., Chang, Y., Wang, Y.B., Zhang, W.N., Li, W.H., He, K., Mu, R., Zhen, C., Man, J.H.*, et al.* (2011). Cdk1-phosphorylated CUEDC2 promotes spindle checkpoint inactivation and chromosomal instability. Nature cell biology *13*, 924-933.

Gascoigne, K.E., Takeuchi, K., Suzuki, A., Hori, T., Fukagawa, T., and Cheeseman, I.M. (2011). Induced ectopic kinetochore assembly bypasses the requirement for CENP-A nucleosomes. Cell *145*, 410-422.

Gassmann, R., Holland, A.J., Varma, D., Wan, X., Civril, F., Cleveland, D.W., Oegema, K., Salmon, E.D., and Desai, A. (2010). Removal of Spindly from microtubule-attached kinetochores controls spindle checkpoint silencing in human cells. Genes & development *24*, 957-971.

Guse, A., Carroll, C.W., Moree, B., Fuller, C.J., and Straight, A.F. (2011). In vitro centromere and kinetochore assembly on defined chromatin templates. Nature *477*, 354-358.

Hagan, R.S., Manak, M.S., Buch, H.K., Meier, M.G., Meraldi, P., Shah, J.V., and Sorger, P.K. (2011). p31(comet) acts to ensure timely spindle checkpoint silencing subsequent to kinetochore attachment. Molecular biology of the cell *22*, 4236-4246.

Heinrich, S., Windecker, H., Hustedt, N., and Hauf, S. (2012). Mph1 kinetochore localization is crucial and upstream in the hierarchy of spindle assembly checkpoint protein recruitment to kinetochores. Journal of cell science *125*, 4720-4727.

Hellwig, D., Emmerth, S., Ulbricht, T., Doring, V., Hoischen, C., Martin, R., Samora, C.P., McAinsh, A.D., Carroll, C.W., Straight, A.F.*, et al.* (2011). Dynamics of CENP-N kinetochore binding during the cell cycle. Journal of cell science *124*, 3871-3883.

Herzog, F., Primorac, I., Dube, P., Lenart, P., Sander, B., Mechtler, K., Stark, H., and Peters, J.M. (2009). Structure of the anaphase-promoting complex/cyclosome interacting with a mitotic checkpoint complex. Science (New York, N.Y.) *323*, 1477-1481.

Hori, T., Amano, M., Suzuki, A., Backer, C.B., Welburn, J.P., Dong, Y., McEwen, B.F., Shang, W.H., Suzuki, E., Okawa, K.*, et al.* (2008). CCAN makes multiple contacts with centromeric DNA to provide distinct pathways to the outer kinetochore. Cell *135*, 1039-1052.

Howell, B.J., McEwen, B.F., Canman, J.C., Hoffman, D.B., Farrar, E.M., Rieder, C.L., and Salmon, E.D. (2001). Cytoplasmic dynein/dynactin drives kinetochore protein transport to the spindle poles and has a role in mitotic spindle checkpoint inactivation. The Journal of cell biology *155*, 1159-1172.

Izawa, D., and Pines, J. (2011). How APC/C-Cdc20 changes its substrate specificity in mitosis. Nature cell biology *13*, 223-233.

Izawa, D., and Pines, J. (2012). Mad2 and the APC/C compete for the same site on Cdc20 to ensure proper chromosome segregation. The Journal of cell biology *199*, 27-37.

Izawa, D., and Pines, J. (2015). The mitotic checkpoint complex binds a second CDC20 to inhibit active APC/C. Nature *517*, 631-634.

Jelluma, N., Brenkman, A.B., van den Broek, N.J., Cruijsen, C.W., van Osch, M.H., Lens, S.M., Medema, R.H., and Kops, G.J. (2008). Mps1 phosphorylates Borealin to control Aurora B activity and chromosome alignment. Cell *132*, 233-246.

Jelluma, N., Dansen, T.B., Sliedrecht, T., Kwiatkowski, N.P., and Kops, G.J. (2010). Release of Mps1 from kinetochores is crucial for timely anaphase onset. The Journal of cell biology *191*, 281-290.

Ji, Z., Gao, H., and Yu, H. (2015). CELL DIVISION CYCLE. Kinetochore attachment sensed by competitive Mps1 and microtubule binding to Ndc80C. Science (New York, N.Y.) *348*, 1260-1264.

Jia, L., Li, B., Warrington, R.T., Hao, X., Wang, S., and Yu, H. (2011). Defining pathways of spindle checkpoint silencing: functional redundancy between Cdc20 ubiquitination and p31(comet). Molecular biology of the cell *22*, 4227-4235.

Kang, J., Chen, Y., Zhao, Y., and Yu, H. (2007). Autophosphorylation-dependent activation of human Mps1 is required for the spindle checkpoint. Proceedings of the National Academy of Sciences of the United States of America *104*, 20232-20237.

Kang, J., Yang, M., Li, B., Qi, W., Zhang, C., Shokat, K.M., Tomchick, D.R., Machius, M., and Yu, H. (2008). Structure and substrate recruitment of the human spindle checkpoint kinase Bub1. Molecular cell *32*, 394-405.

Kang, Y.H., Park, J.E., Yu, L.R., Soung, N.K., Yun, S.M., Bang, J.K., Seong, Y.S., Yu, H., Garfield, S., Veenstra, T.D.*, et al.* (2006). Self-regulated Plk1 recruitment to kinetochores by the Plk1-PBIP1 interaction is critical for proper chromosome segregation. Molecular cell *24*, 409-422.

Karess, R. (2005). Rod-Zw10-Zwilch: a key player in the spindle checkpoint. Trends in cell biology *15*, 386-392.

Kawashima, S.A., Yamagishi, Y., Honda, T., Ishiguro, K., and Watanabe, Y. (2010). Phosphorylation of H2A by Bub1 prevents chromosomal instability through localizing shugoshin. Science (New York, N.Y.) *327*, 172-177.

Kelly, A.E., Ghenoiu, C., Xue, J.Z., Zierhut, C., Kimura, H., and Funabiki, H. (2010). Survivin reads phosphorylated histone H3 threonine 3 to activate the mitotic kinase Aurora B. Science (New York, N.Y.) *330*, 235-239.

Kelly, A.E., Sampath, S.C., Maniar, T.A., Woo, E.M., Chait, B.T., and Funabiki, H. (2007). Chromosomal enrichment and activation of the Aurora B pathway are coupled to spatially regulate spindle assembly. Developmental cell *12*, 31-43.

Kim, S., Sun, H., Tomchick, D.R., Yu, H., and Luo, X. (2012). Structure of human Mad1 C-terminal domain reveals its involvement in kinetochore targeting. Proceedings of the National Academy of Sciences of the United States of America *109*, 6549-6554.

Kim, S., and Yu, H. (2011). Mutual regulation between the spindle checkpoint and APC/C. Semin Cell Dev Biol *22*, 551-558.

Kim, S., and Yu, H. (2015). Multiple assembly mechanisms anchor the KMN spindle checkpoint platform at human mitotic kinetochores. The Journal of cell biology *208*, 181-196.

King, E.M., van der Sar, S.J., and Hardwick, K.G. (2007). Mad3 KEN boxes mediate both Cdc20 and Mad3 turnover, and are critical for the spindle checkpoint. PloS one *2*, e342.

Kiyomitsu, T., Murakami, H., and Yanagida, M. (2011). Protein interaction domain mapping of human kinetochore protein Blinkin reveals a consensus motif for binding of spindle assembly checkpoint proteins Bub1 and BubR1. Molecular and cellular biology *31*, 998-1011.

Kiyomitsu, T., Obuse, C., and Yanagida, M. (2007). Human Blinkin/AF15q14 is required for chromosome alignment and the mitotic checkpoint through direct interaction with Bub1 and BubR1. Developmental cell *13*, 663-676.

Klebig, C., Korinth, D., and Meraldi, P. (2009). Bub1 regulates chromosome segregation in a kinetochore-independent manner. The Journal of cell biology *185*, 841-858.

Krenn, V., Wehenkel, A., Li, X., Santaguida, S., and Musacchio, A. (2012). Structural analysis reveals features of the spindle checkpoint kinase Bub1-kinetochore subunit Knl1 interaction. The Journal of cell biology *196*, 451-467.

Kulukian, A., Han, J.S., and Cleveland, D.W. (2009). Unattached kinetochores catalyze production of an anaphase inhibitor that requires a Mad2 template to prime Cdc20 for BubR1 binding. Developmental cell *16*, 105-117.

Lampson, M.A., and Cheeseman, I.M. (2011). Sensing centromere tension: Aurora B and the regulation of kinetochore function. Trends in cell biology *21*, 133-140.

Lara-Gonzalez, P., Scott, M.I., Diez, M., Sen, O., and Taylor, S.S. (2011). BubR1 blocks substrate recruitment to the APC/C in a KEN-box-dependent manner. Journal of cell science *124*, 4332-4345.

Lara-Gonzalez, P., Westhorpe, F.G., and Taylor, S.S. (2012). The spindle assembly checkpoint. Current biology : CB *22*, R966-980.

Lau, D.T., and Murray, A.W. (2012). Mad2 and Mad3 cooperate to arrest budding yeast in mitosis. Current biology : CB *22*, 180-190.

Liu, D., Vader, G., Vromans, M.J., Lampson, M.A., and Lens, S.M. (2009). Sensing chromosome bi-orientation by spatial separation of Aurora B kinase from kinetochore substrates. Science (New York, N.Y.) *323*, 1350-1353.

Liu, D., Vleugel, M., Backer, C.B., Hori, T., Fukagawa, T., Cheeseman, I.M., and Lampson, M.A. (2010). Regulated targeting of protein phosphatase 1 to the outer kinetochore by KNL1 opposes Aurora B kinase. The Journal of cell biology *188*, 809-820.

London, N., and Biggins, S. (2014). Mad1 kinetochore recruitment by Mps1-mediated phosphorylation of Bub1 signals the spindle checkpoint. Genes & development *28*, 140-152.

London, N., Ceto, S., Ranish, J.A., and Biggins, S. (2012). Phosphoregulation of Spc105 by Mps1 and PP1 regulates Bub1 localization to kinetochores. Current biology : CB *22*, 900-906.

Luo, X., Tang, Z., Rizo, J., and Yu, H. (2002). The Mad2 spindle checkpoint protein undergoes similar major conformational changes upon binding to either Mad1 or Cdc20. Molecular cell *9*, 59-71.

Luo, X., and Yu, H. (2008). Protein metamorphosis: the two-state behavior of Mad2. Structure (London, England : 1993) *16*, 1616-1625.

Maldonado, M., and Kapoor, T.M. (2011). Constitutive Mad1 targeting to kinetochores uncouples checkpoint signalling from chromosome biorientation. Nature cell biology *13*, 475-482.

Malureanu, L.A., Jeganathan, K.B., Hamada, M., Wasilewski, L., Davenport, J., and van Deursen, J.M. (2009). BubR1 N terminus acts as a soluble inhibitor of cyclin B degradation by APC/C(Cdc20) in interphase. Developmental cell *16*, 118-131.

Malvezzi, F., Litos, G., Schleiffer, A., Heuck, A., Mechtler, K., Clausen, T., and Westermann, S. (2013). A structural basis for kinetochore recruitment of the Ndc80 complex via two distinct centromere receptors. The EMBO journal *32*, 409-423.

Mansfeld, J., Collin, P., Collins, M.O., Choudhary, J.S., and Pines, J. (2011). APC15 drives the turnover of MCC-CDC20 to make the spindle assembly checkpoint responsive to kinetochore attachment. Nature cell biology *13*, 1234-1243.

Mapelli, M., Filipp, F.V., Rancati, G., Massimiliano, L., Nezi, L., Stier, G., Hagan, R.S., Confalonieri, S., Piatti, S., Sattler, M.*, et al.* (2006). Determinants of conformational dimerization of Mad2 and its inhibition by p31comet. The EMBO journal *25*, 1273-1284.

Mapelli, M., and Musacchio, A. (2007). MAD contortions: conformational dimerization boosts spindle checkpoint signaling. Current opinion in structural biology *17*, 716-725.

Mariani, L., Chiroli, E., Nezi, L., Muller, H., Piatti, S., Musacchio, A., and Ciliberto, A. (2012). Role of the Mad2 dimerization interface in the spindle assembly checkpoint independent of kinetochores. Current biology : CB *22*, 1900-1908.

Martin-Lluesma, S., Stucke, V.M., and Nigg, E.A. (2002). Role of Hec1 in spindle checkpoint signaling and kinetochore recruitment of Mad1/Mad2. Science (New York, N.Y.) *297*, 2267-2270.

Miniowitz-Shemtov, S., Eytan, E., Ganoth, D., Sitry-Shevah, D., Dumin, E., and Hershko, A. (2012). Role of phosphorylation of Cdc20 in p31(comet)-stimulated disassembly of the mitotic checkpoint complex. Proceedings of the National Academy of Sciences of the United States of America *109*, 8056-8060.

Musacchio, A., and Salmon, E.D. (2007). The spindle-assembly checkpoint in space and time. Nat Rev Mol Cell Biol *8*, 379-393.

Nijenhuis, W., von Castelmur, E., Littler, D., De Marco, V., Tromer, E., Vleugel, M., van Osch, M.H., Snel, B., Perrakis, A., and Kops, G.J. (2013). A TPR domain-containing N-terminal module of MPS1 is required for its kinetochore localization by Aurora B. The Journal of cell biology *201*, 217-231.

Nilsson, J., Yekezare, M., Minshull, J., and Pines, J. (2008). The APC/C maintains the spindle assembly checkpoint by targeting Cdc20 for destruction. Nature cell biology *10*, 1411-1420.

Nishino, T., Rago, F., Hori, T., Tomii, K., Cheeseman, I.M., and Fukagawa, T. (2013). CENP-T provides a structural platform for outer kinetochore assembly. The EMBO journal *32*, 424-436.

Nishino, T., Takeuchi, K., Gascoigne, K.E., Suzuki, A., Hori, T., Oyama, T., Morikawa, K., Cheeseman, I.M., and Fukagawa, T. (2012). CENP-T-W-S-X forms a unique centromeric chromatin structure with a histone-like fold. Cell *148*, 487-501.

Okada, M., Cheeseman, I.M., Hori, T., Okawa, K., McLeod, I.X., Yates, J.R., 3rd, Desai, A., and Fukagawa, T. (2006). The CENP-H-I complex is required for the efficient incorporation of newly synthesized CENP-A into centromeres. Nature cell biology *8*, 446-457.

Overlack, K., Primorac, I., Vleugel, M., Krenn, V., Maffini, S., Hoffmann, I., Kops, G.J., and Musacchio, A. (2015). A molecular basis for the differential roles of Bub1 and BubR1 in the spindle assembly checkpoint. eLife *4*, e05269.

Peters, J.M. (2006). The anaphase promoting complex/cyclosome: a machine designed to destroy. Nat Rev Mol Cell Biol *7*, 644-656.

Petrovic, A., Pasqualato, S., Dube, P., Krenn, V., Santaguida, S., Cittaro, D., Monzani, S., Massimiliano, L., Keller, J., Tarricone, A.*, et al.* (2010). The MIS12 complex is a protein interaction hub for outer kinetochore assembly. The Journal of cell biology *190*, 835-852.

Pinsky, B.A., Kung, C., Shokat, K.M., and Biggins, S. (2006). The Ipl1-Aurora protein kinase activates the spindle checkpoint by creating unattached kinetochores. Nature cell biology *8*, 78-83.

Prendergast, L., van Vuuren, C., Kaczmarczyk, A., Doering, V., Hellwig, D., Quinn, N., Hoischen, C., Diekmann, S., and Sullivan, K.F. (2011). Premitotic assembly of human CENPs -T and -W switches centromeric chromatin to a mitotic state. PLoS biology *9*, e1001082.

Primorac, I., Weir, J.R., Chiroli, E., Gross, F., Hoffmann, I., van Gerwen, S., Ciliberto, A., and Musacchio, A. (2013). Bub3 reads phosphorylated MELT repeats to promote spindle assembly checkpoint signaling. eLife *2*, e01030.

Przewloka, M.R., Venkei, Z., Bolanos-Garcia, V.M., Debski, J., Dadlez, M., and Glover, D.M. (2011). CENP-C is a structural platform for kinetochore assembly. Current biology : CB *21*, 399-405.

Qian, J., Lesage, B., Beullens, M., Van Eynde, A., and Bollen, M. (2011). PP1/Repo-man dephosphorylates mitotic histone H3 at T3 and regulates chromosomal Aurora B targeting. Current biology : CB *21*, 766-773.

Reddy, S.K., Rape, M., Margansky, W.A., and Kirschner, M.W. (2007). Ubiquitination by the anaphase-promoting complex drives spindle checkpoint inactivation. Nature *446*, 921-925.

Rieder, C.L., Cole, R.W., Khodjakov, A., and Sluder, G. (1995). The checkpoint delaying anaphase in response to chromosome monoorientation is mediated by an inhibitory signal produced by unattached kinetochores. The Journal of cell biology *130*, 941-948.

Rischitor, P.E., May, K.M., and Hardwick, K.G. (2007). Bub1 is a fission yeast kinetochore scaffold protein, and is sufficient to recruit other spindle checkpoint proteins to ectopic sites on chromosomes. PloS one *2*, e1342.

Rosenberg, J.S., Cross, F.R., and Funabiki, H. (2011). KNL1/Spc105 recruits PP1 to silence the spindle assembly checkpoint. Current biology : CB *21*, 942-947.

Ruchaud, S., Carmena, M., and Earnshaw, W.C. (2007). Chromosomal passengers: conducting cell division. Nat Rev Mol Cell Biol *8*, 798-812.

Santaguida, S., Vernieri, C., Villa, F., Ciliberto, A., and Musacchio, A. (2011). Evidence that Aurora B is implicated in spindle checkpoint signalling independently of error correction. The EMBO journal *30*, 1508-1519.

Saurin, A.T., van der Waal, M.S., Medema, R.H., Lens, S.M., and Kops, G.J. (2011). Aurora B potentiates Mps1 activation to ensure rapid checkpoint establishment at the onset of mitosis. Nature communications *2*, 316.

Schleiffer, A., Maier, M., Litos, G., Lampert, F., Hornung, P., Mechtler, K., and Westermann, S. (2012). CENP-T proteins are conserved centromere receptors of the Ndc80 complex. Nature cell biology *14*, 604-613.

Screpanti, E., De Antoni, A., Alushin, G.M., Petrovic, A., Melis, T., Nogales, E., and Musacchio, A. (2011). Direct binding of Cenp-C to the Mis12 complex joins the inner and outer kinetochore. Current biology : CB *21*, 391-398.

Shepperd, L.A., Meadows, J.C., Sochaj, A.M., Lancaster, T.C., Zou, J., Buttrick, G.J., Rappsilber, J., Hardwick, K.G., and Millar, J.B. (2012). Phosphodependent recruitment of Bub1 and Bub3 to Spc7/KNL1 by Mph1 kinase maintains the spindle checkpoint. Current biology : CB *22*, 891-899.

Sironi, L., Mapelli, M., Knapp, S., De Antoni, A., Jeang, K.T., and Musacchio, A. (2002). Crystal structure of the tetrameric Mad1-Mad2 core complex: implications of a 'safety belt' binding mechanism for the spindle checkpoint. The EMBO journal *21*, 2496-2506.

Stucke, V.M., Baumann, C., and Nigg, E.A. (2004). Kinetochore localization and microtubule interaction of the human spindle checkpoint kinase Mps1. Chromosoma *113*, 1-15.

Takeuchi, K., and Fukagawa, T. (2012). Molecular architecture of vertebrate kinetochores. Experimental cell research *318*, 1367-1374.

Tang, Z., Bharadwaj, R., Li, B., and Yu, H. (2001). Mad2-Independent inhibition of APCCdc20 by the mitotic checkpoint protein BubR1. Developmental cell *1*, 227-237.

Tang, Z., Shu, H., Oncel, D., Chen, S., and Yu, H. (2004). Phosphorylation of Cdc20 by Bub1 provides a catalytic mechanism for APC/C inhibition by the spindle checkpoint. Molecular cell *16*, 387-397.

Tian, W., Li, B., Warrington, R., Tomchick, D.R., Yu, H., and Luo, X. (2012). Structural analysis of human Cdc20 supports multisite degron recognition by APC/C. Proceedings of the National Academy of Sciences of the United States of America *109*, 18419-18424.

Tighe, A., Staples, O., and Taylor, S. (2008). Mps1 kinase activity restrains anaphase during an unperturbed mitosis and targets Mad2 to kinetochores. The Journal of cell biology *181*, 893-901.

Tipton, A.R., Wang, K., Link, L., Bellizzi, J.J., Huang, H., Yen, T., and Liu, S.T. (2011). BUBR1 and closed MAD2 (C-MAD2) interact directly to assemble a functional mitotic checkpoint complex. The Journal of biological chemistry *286*, 21173-21179.

Tsukahara, T., Tanno, Y., and Watanabe, Y. (2010). Phosphorylation of the CPC by Cdk1 promotes chromosome bi-orientation. Nature *467*, 719-723.

Uzunova, K., Dye, B.T., Schutz, H., Ladurner, R., Petzold, G., Toyoda, Y., Jarvis, M.A., Brown, N.G., Poser, I., Novatchkova, M.*, et al.* (2012). APC15 mediates CDC20 autoubiquitylation by APC/C(MCC) and disassembly of the mitotic checkpoint complex. Nature structural & molecular biology *19*, 1116-1123.

van der Waal, M.S., Saurin, A.T., Vromans, M.J., Vleugel, M., Wurzenberger, C., Gerlich, D.W., Medema, R.H., Kops, G.J., and Lens, S.M. (2012). Mps1 promotes rapid centromere accumulation of Aurora B. EMBO reports *13*, 847-854.

Vanoosthuyse, V., and Hardwick, K.G. (2009). A novel protein phosphatase 1-dependent spindle checkpoint silencing mechanism. Current biology : CB *19*, 1176-1181.

Varetti, G., Guida, C., Santaguida, S., Chiroli, E., and Musacchio, A. (2011). Homeostatic control of mitotic arrest. Molecular cell *44*, 710-720.

Wang, E., Ballister, E.R., and Lampson, M.A. (2011). Aurora B dynamics at centromeres create a diffusion-based phosphorylation gradient. The Journal of cell biology *194*, 539-549.

Wang, F., Dai, J., Daum, J.R., Niedzialkowska, E., Banerjee, B., Stukenberg, P.T., Gorbsky, G.J., and Higgins, J.M. (2010). Histone H3 Thr-3 phosphorylation by Haspin positions Aurora B at centromeres in mitosis. Science (New York, N.Y.) *330*, 231-235.

Weiss, E., and Winey, M. (1996). The Saccharomyces cerevisiae spindle pole body duplication gene MPS1 is part of a mitotic checkpoint. The Journal of cell biology *132*, 111-123.

Welburn, J.P., Vleugel, M., Liu, D., Yates, J.R., 3rd, Lampson, M.A., Fukagawa, T., and Cheeseman, I.M. (2010). Aurora B phosphorylates spatially distinct targets to differentially regulate the kinetochore-microtubule interface. Molecular cell *38*, 383-392.

Westhorpe, F.G., Tighe, A., Lara-Gonzalez, P., and Taylor, S.S. (2011). p31comet-mediated extraction of Mad2 from the MCC promotes efficient mitotic exit. Journal of cell science *124*, 3905-3916.

Xia, G., Luo, X., Habu, T., Rizo, J., Matsumoto, T., and Yu, H. (2004). Conformation-specific binding of p31(comet) antagonizes the function of Mad2 in the spindle checkpoint. The EMBO journal *23*, 3133-3143.

Yamagishi, Y., Honda, T., Tanno, Y., and Watanabe, Y. (2010). Two histone marks establish the inner centromere and chromosome bi-orientation. Science (New York, N.Y.) *330*, 239-243.

Yamagishi, Y., Yang, C.H., Tanno, Y., and Watanabe, Y. (2012). MPS1/Mph1 phosphorylates the kinetochore protein KNL1/Spc7 to recruit SAC components. Nature cell biology *14*, 746-752.

Yamamoto, T.G., Watanabe, S., Essex, A., and Kitagawa, R. (2008). SPDL-1 functions as a kinetochore receptor for MDF-1 in Caenorhabditis elegans. The Journal of cell biology *183*, 187-194.

Yang, F., Hu, L., Chen, C., Yu, J., O'Connell, C.B., Khodjakov, A., Pagano, M., and Dai, W. (2012). BubR1 is modified by sumoylation during mitotic progression. The Journal of biological chemistry *287*, 4875-4882.

Yang, M., Li, B., Tomchick, D.R., Machius, M., Rizo, J., Yu, H., and Luo, X. (2007). p31comet blocks Mad2 activation through structural mimicry. Cell *131*, 744-755.

Yu, H. (2007). Cdc20: a WD40 activator for a cell cycle degradation machine. Molecular cell *27*, 3-16.

Zhu, T., Dou, Z., Qin, B., Jin, C., Wang, X., Xu, L., Wang, Z., Zhu, L., Liu, F., Gao, X.*, et al.* (2013). Phosphorylation of microtubule-binding protein Hec1 by mitotic kinase Aurora B specifies spindle checkpoint kinase Mps1 signaling at the kinetochore. The Journal of biological chemistry *288*, 36149-36159.

CHAPTER TWO

BUB1 FUNCTION IN THE SPINDLE CHECKPOINT IS REGULATED BY PHOSPHORYLATION

Summary

The spindle checkpoint is a cellular surveillance mechanism that senses unattached kinetochore in mitosis and prevents premature sister chromatids separation. Bub1 is one of the first spindle checkpoint proteins recruited to the kinetochore in early prophase. Ablation of Bub1 leads to loss of the spindle checkpoint. However, it is not clearly understood how Bub1 can be regulated during mitosis by post-translational modifications. Bub1 becomes highly phosphorylated during mitosis, suggesting potential regulation by phosphorylation. We have identified mitotic phosphorylation sites of Bub1 using mass spectrometry, one of which is essential for functional checkpoint. In the phosphorylation site mutant, the kinase activity of Bub1 is not affected. The kinetochore recruitment of downstream checkpoint proteins like Mad1 and BubR1 are also normal. However, the interaction between Bub1 and Mad1 is abolished. We concluded that the Bub1-Mad1 binding is a key event in the spindle checkpoint, and it is regulated by phosphorylation on Bub1.

Introduction

Failure to accurately separate duplicated chromosomes in eukaryotic cell division leads to abnormal chromosome number in daughter cells (aneuploidy). Aneuploidy has a complicated role in tumorigenesis, but can drive tumor formation under certain circumstances (Bharadwaj and Yu, 2004; Torres et al., 2008). Defects in the spindle checkpoint contribute to aneuploidy

development. During mitosis, sister chromatids need to be attached to microtubules from the two spindle poles before separation. The spindle checkpoint delays anaphase onset until all chromosomes are correctly attached. To initiate anaphase, an E3 ubiquitin ligase APC/C (the anaphase-promoting complex or cyclosome) needs to be activated by its cofactor Cdc20, which targets cyclin B and securin for degradation (Peters, 2006; Yu, 2007). Checkpoint proteins on the unattached kinetochores signal to inhibit APC/C^{Cdc20} (Jia et al., 2013). Mad1 form a constitutive tetramer with Mad2 in a 2:2 ratio (Luo et al., 2002; Sironi et al., 2002). When localized on the kinetochore, this Mad1-Mad2 core complex can activate soluble Mad2 by facilitating its conformational change, and the activated Mad2 inhibits Cdc20. Tethering the wild type Mad1, but not the Mad2-binding deficient mutant, to the kinetochore arrests cells in metaphase, indicating the recruitment of Mad1-Mad2 core complex to the kinetochore is a key event in the checkpoint signaling (Maldonado and Kapoor, 2011).

A huge protein complex called KMN network consisting of Knl1, Mis12 complex (Mis12C) and Ndc80 complex (Ndc80C) is assembled on the kinetochores at late anaphase as a platform for checkpoint proteins and microtubule binding (Cheeseman et al., 2006; Martin-Lluesma et al., 2002; McCleland et al., 2003; Pagliuca et al., 2009). Mps1 kinase lies at the top of checkpoint signaling cascade (Heinrich et al., 2012). It localizes to the kinetochore by binding to Ndc80C (Ji et al., 2015) and phosphorylates Knl1 to recruit Bub1 (London et al., 2012; Shepperd et al., 2012; Yamagishi et al., 2012). Both Mps1 and Bub1 are essential to recruit the Mad1-Mad2 complex (Heinrich et al., 2012; Kim et al., 2012; Rischitor et al., 2007; Tighe et al., 2008). It was shown in yeast that Mps1 phosphorylates Bub1 in the middle region, which enables Bub1 to directly interact with Mad1-Mad2 and bring the complex to the kinetochore (London and Biggins, 2014). However, the Bub1-Mad1 interaction has not been shown in human cells.

We identified mitotic Bub1 phosphorylation sites using mass spectrometry. These phosphorylation sites were further characterized by examining whether the exogenously expressed mutants can rescue Bub1 depletion using siRNA. With this complementation assay, we found one phosphorylation site, Bub1 serine 459, is important for the proper spindle checkpoint function of Bub1. Mutation of this single site to alanine leads to escape from mitosis in the presence of spindle poison. The recruitment of BubR1 and Mad1 are not affected in Bub1-S459A mutant stable cell line. But the interaction between Bub1 and Mad1 in the presence of Mps1 is disrupted as shown by in vitro binding assay. The results suggest that the direct binding between Bub1 and Mad1 requires phosphorylation on S459. However, this binding is not required for Mad1 localization to the kinetochore region. There may be other pathways that can recruit Mad1. Instead, the Bub1-Mad1 binding is essential for Mad1 to be fully functional in the spindle checkpoint signaling pathway.

Results

Bub1 serine 459 is essential for the spindle checkpoint

Bub1 is an important player in the spindle checkpoint. It is heavily phosphorylated during mitosis. We identified multiple phosphorylation sites using immunoprecipitated Bub1 from mitotic cells (Figure 1A). Three short stretches of Bub1 were highly phosphorylated, including amino acids 432-463, 585-614, 651-680, with the first two stretches being also highly conserved. These features indicate that these phosphorylation events may be functionally important. We mutated these serine and threonine residues to alanine in different combinations, and used these mutants to rescue checkpoint defect caused by Bub1 siRNA in a complementation assay. Any mutant with serine 459 mutated to alanine was unable to be arrested in mitosis in the presence of

taxol (Figure 1B), suggesting that phosphorylation on S459 is important for the checkpoint function of Bub1. We further confirmed this result in stable cell lines expressing Bub1 wild type (WT) or S459A mutant (Figure 1C and 1D). In the complementation assay in stable cell lines, the Bub1 S459A mutant was also defective in rescuing Bub1 siRNA. The Bub1$^{\Delta Kinase}$ fragment was also used in this experiment, because this fragment can be expressed at a higher level in cells, and it can rescue Bub1 siRNA when over-expressed. The Bub1$^{\Delta Kinase}$ and the Bub1$^{\Delta Kinase}$ S459A mutant showed similar phenotype as the Bub1 WT and S459A mutant, respectively (Figure 1C and 1D).

To analyze the phenotype of S459A mutant in more detail, I used live cell imaging to look at the mitotic progression in both log phase and after taxol treatment. I quantified the time each cell spent in mitosis using both the Bub1$^{\Delta Kinase}$ and the Bub1$^{\Delta Kinase}$ S459A lines in log phase (Figure 1E), each dot represents one cell. The cells expressing Bub1$^{\Delta Kinase}$ S459A progressed through mitosis much faster, which is consistent with the checkpoint defect observed before in taxol treatment. I also quantified the mitotic timing of cell lines expressing Bub1 WT, Bub1$^{\Delta Kinase}$ and Bub1$^{\Delta Kinase}$ S459A when treated with taxol (Figure 1F-I). Figure 1F shows the percentage of cells in mitosis at different time points. The Bub1 WT and Bub1$^{\Delta Kinase}$ lines were arrested in mitosis for similar length of time before cells escaped from mitosis or died. On the contrary, Bub1$^{\Delta Kinase}$ S459A mutant had a much weaker checkpoint, and escaped much faster. Figure G-I shows the final destiny for each cell filmed. The Bub1 WT and Bub1$^{\Delta Kinase}$ lines showed similar profile, with many cells died after long time arrest in mitosis. Comparing to the Bub1$^{\Delta Kinase}$ S459A mutant, where most cells escaped from mitosis after a brief arrest.

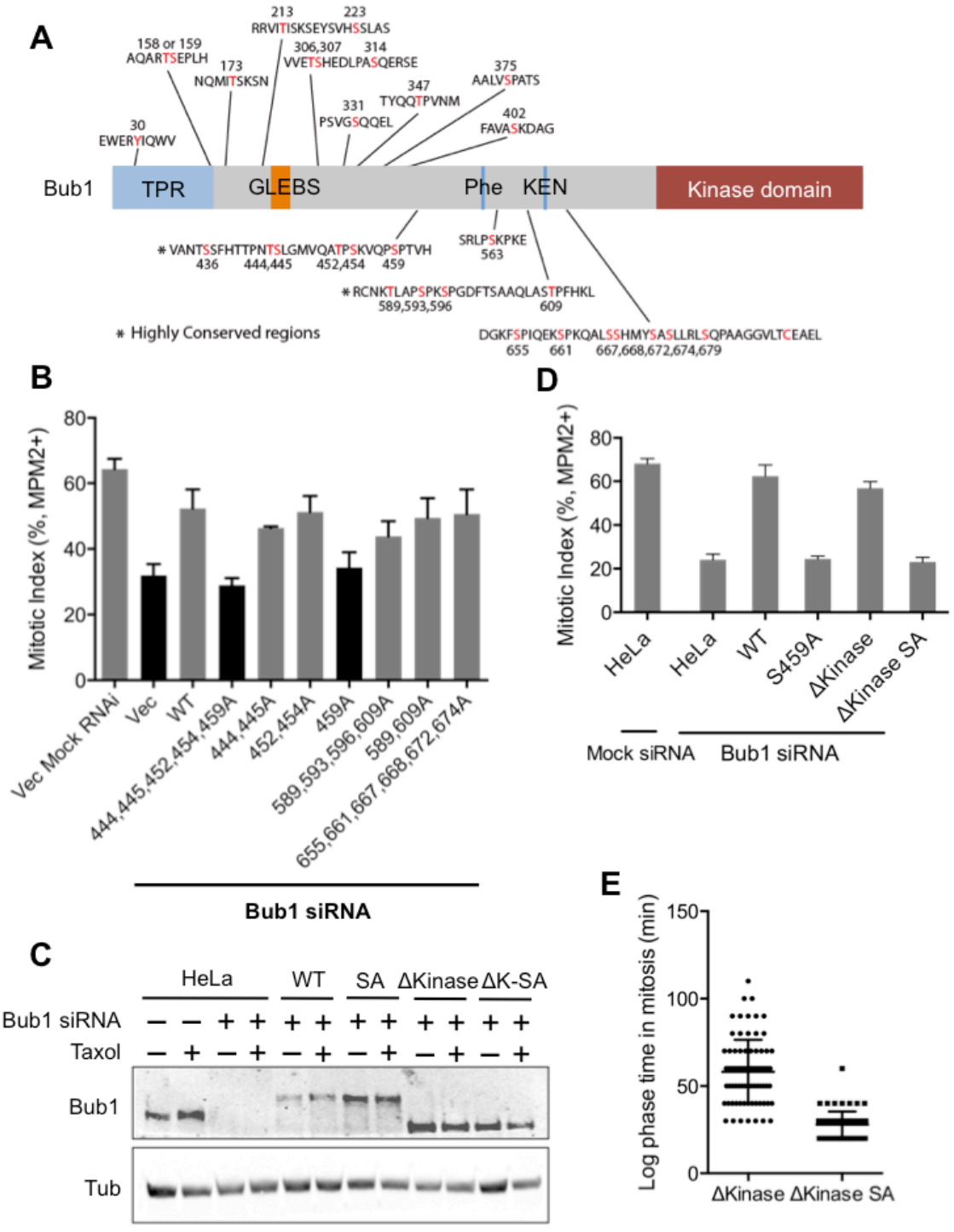
A
213
223
RRVITISKSEYSVHSSLAS
158 or 159
AQARTSEPLH
306,307
314
VVETSHEDLPASQERSE
173
NQMITSKSN
375
AALVSPATS
347
TYQQTPVNM
331
PSVGSQQEL
30
EWERYIQWV
402
FAVASKDAG
Bub1
TPR
GLEBS
Phe
KEN
Kinase domain
* VANTSSFHTTPNTSLGMVQATPSKVQPSPTVH
436
444,445
452,454
459
SRLPSKPKE
563
* RCNKTLAPSPKSPGDFTSAAQLASTPFHKL
589,593,596
609
* Highly Conserved regions
DGKFSPIQEKSPKQALSSHMYSASLLRLSQPAAGGVLTCEAEL
655
661
667,668,672,674,679
B
Mitotic Index (%, MPM2+)
80
60
40
20
0
Vec Mock RNAi
Vec
WT
444,445,452,454,459A
444,445A
452,454A
459A
589,593,596,609A
589,609A
655,661,667,668,672,674A
Bub1 siRNA
D
Mitotic Index (%, MPM2+)
80
60
40
20
0
HeLa
HeLa
WT
S459A
ΔKinase
ΔKinase SA
Mock siRNA
Bub1 siRNA
C
HeLa
WT
SA
ΔKinase
ΔK-SA
Bub1 siRNA
Taxol
Bub1
Tub
E
Log phase time in mitosis (min)
150
100
50
0
ΔKinase
ΔKinase SA

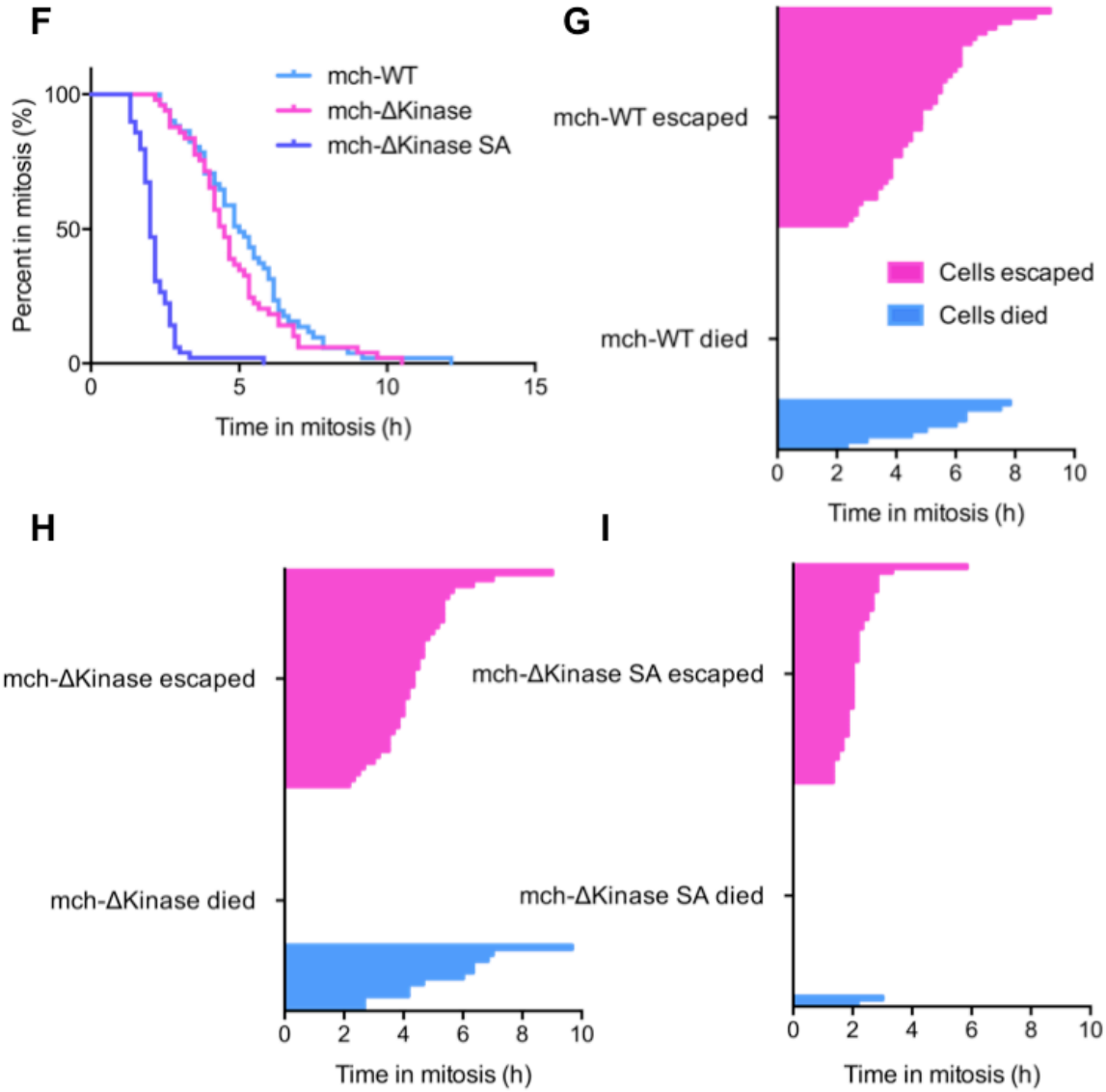

Figure 1. Bub1 S459A mutant is defective in spindle checkpoint signaling. (A) Schematic view of Bub1 showing the functional motifs and the mitotic phosphorylation sites identified in this study. TPR, tetratricopeptide repeat; GLEBS, Gle2-binding sequence; Phe, phenylalanine-containing box (Phe box); KEN, Lys-Glu-Asn box (KEN box). The C-terminal is a kinase domain. **(B)** HeLa Tet-on cells were treated with Bub1 siRNA and vectors expressing Bub1 WT and different mutants. The mitotic indexes (the percentage of cells in mitosis as defined by MPM2 antibody staining) in the presence of 100 nM taxol were recorded. Vec, vector without Bub1 gene. **(C)** HeLa Tet-on parental cell line (HeLa) and stable cell lines expressing Bub1 WT

(WT), Bub1 S459A (SA), Bub1$^{\Delta Kinase}$ (ΔKinase), and Bub1$^{\Delta Kinase}$ S459A (ΔK-SA) were treated as indicated. Cell lysates were blotted with indicated antibodies. **(D)** Quantification of the mitotic index of HeLa Tet-on and stable cell lines treated with indicated siRNAs and 100 nM taxol. **(E)** Quantification of the time Bub1$^{\Delta Kinase}$ (ΔKinase) and Bub1$^{\Delta Kinase}$ S459A (ΔKinase SA) spend in mitosis when in log phase. Each dot represents one cell. For Bub1$^{\Delta Kinase}$, 79 cells were quantified. For Bub1$^{\Delta Kinase}$ S459A, 66 cells were quantified. **(F)** Quantification of the time indicated stable cell lines spend in mitosis when treated with 100 nM taxol. mch-WT: cell line stably expressing mcherry tagged Bub1 WT. mch-ΔKinase: cell line stably expressing mcherry tagged Bub1$^{\Delta Kinase}$. mch-ΔKinase SA: cell line stably expressing mcherry tagged Bub1$^{\Delta Kinase}$ S459A. For mch-WT, 51 cells were quantified. For mch-ΔKinase, 49 cells were quantified. For mch-ΔKinase SA, 49 cells were quantified. **(G-I)** Waterfall plot for data in **(F)**, indicating the destiny for each cell in cell lines as indicated, whether they escaped from mitosis or died. (Figure 1B is from Jungseog Kang)

Bub1 S459 phosphorylation is responsive to the spindle checkpoint

To further study the regulation of Bub1 by S459 phosphorylation, I tried to identify the kinase that phosphorylates this site. A phospho-specific antibody was made to recognize phosphorylation on Bub1 S459 (Bub1-pS459). Purified Bub1$^{\Delta Kinase}$ protein was used as substrate in in vitro kinase assays (Figure 2A and 2B). Cdk1 was found to phosphorylate Bub1 S459. It was shown in yeast that Bub1 could be phosphorylated by Mps1 (London and Biggins, 2014), but S459 was not phosphorylated by Mps1 in vitro (Figure 2B).

Cdk1 is not inactivated immediately after spindle checkpoint silencing. It is the checkpoint silencing that leads to progressive Cdk1 inactivation. Previous experiments showed that loss of Bub1-pS459 leads to checkpoint inactivation, I tried to examine whether the reverse is also true (Figure 2C and 2D). Bub1$^{\Delta Kinase}$ and Bub1$^{\Delta Kinase}$ S459A lines were arrested in mitosis using taxol, and were treated with Aurora B inhibitor ZM447439 together with proteasome

inhibitor MG132 to inactivate the checkpoint while keeping cells in mitosis (Jia et al., 2011). The mitotic index was determined by flow cytometry and labeled below each sample. Aurora B phosphorylates histone H3-S10, so the H3-pS10 in cell lysate was blotted to confirm the effect of Aurora B inhibitor. Over-expressed Bub1$^{\Delta Kinase}$ and Bub1$^{\Delta Kinase}$ S459A were immunoprecipitated and blotted with Bub1-pS459 antibody (Figure 2C). After normalized to Bub1 signal (Figure 2D), Bub1-pS459 signal showed a significant decrease even though Cdk1 was still active under this condition. The results suggest that Bub1-pS459 is tightly regulated by the spindle checkpoint signal, possibly through phophatase.

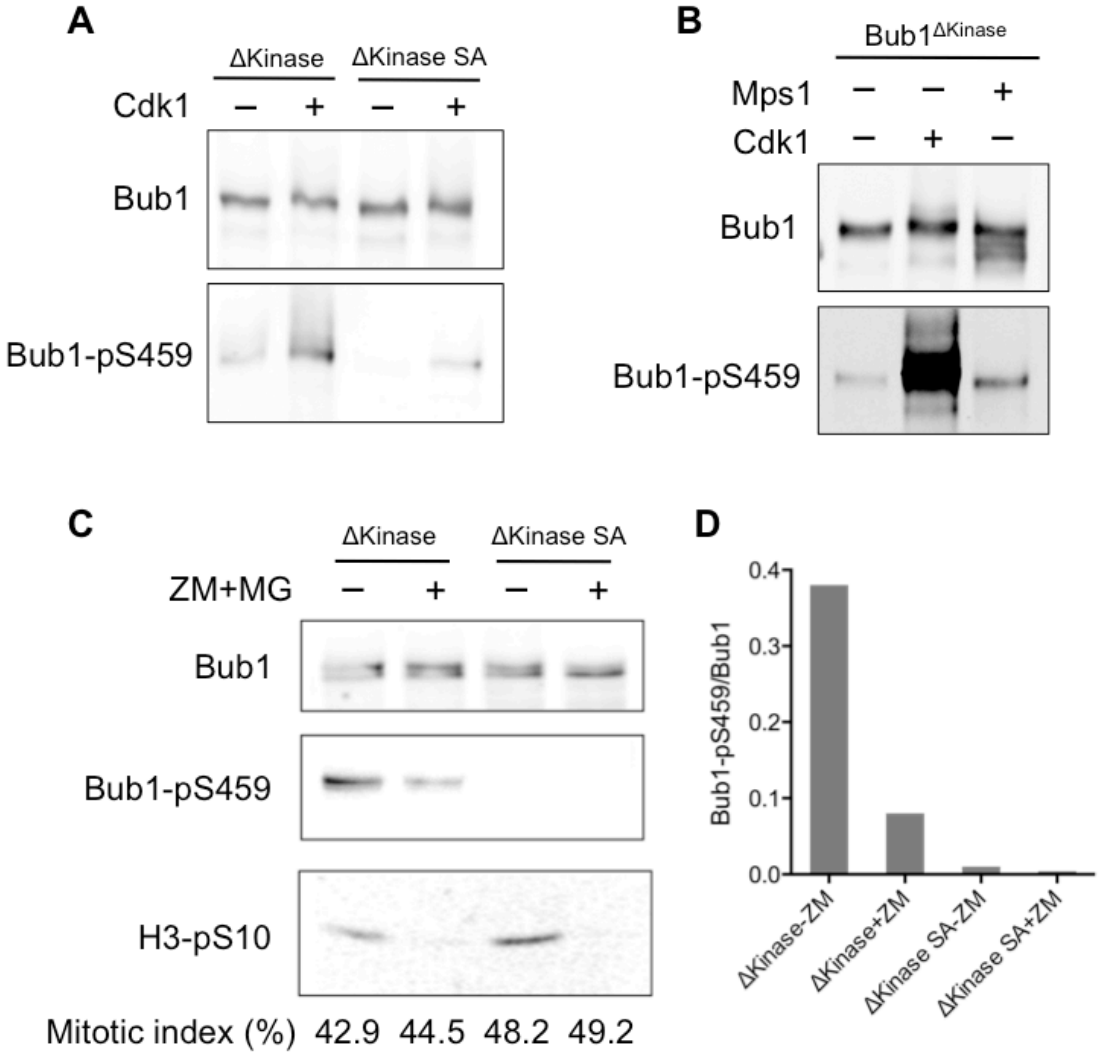

Figure 2. Bub1 S459 is phosphorylated by Cdk1 and is regulated by the checkpoint signal. **(A)** Purified Bub1$^{\Delta Kinase}$ (ΔKinase) and Bub1$^{\Delta Kinase}$ S459A (ΔKinase SA) protein were incubated with or without Cdk1 kinase before being blotted with indicated antibodies. **(B)** Purified Bub1$^{\Delta Kinase}$ was incubated with indicated kinase and was blotted with indicated antibody to analyze S459 phosphorylation. **(C)** Stable cell lines expressing Bub1$^{\Delta Kinase}$ or Bub1$^{\Delta Kinase}$ S459A were arrested in mitosis using 100 nM taxol and were treated with or without Aurora B inhibitor ZM447439 (ZM) and proteasome inhibitor MG132 (MG). Endogenous Bub1 was depleted using siRNA, and exogenous Bub1 was immunoprecipitated and blotted with Bub1 and Bub1-pS459 antibodies. The cell lysate was blotted with H3-pS10 antibody to show the effect of ZM447439. The mitotic index of each sample is labeled below the blots. **(D)** Quantification of Bub1-pS459 signal in **(C)** normalized to Bub1 signal.

The Bub1 kinase activity is not affected by the S459A mutation

To determine why the Bub1 S459A mutant is defective in spindle checkpoint signaling, I tried to examine the known checkpoint functions of Bub1 in the S459A mutant. Bub1 was shown to phosphorylate Cdc20, which leads to APC/C^{Cdc20} inhibition in vitro (Tang et al., 2004). I examined Cdc20 phosphorylation by Bub1 with both in vitro kinase assay (Figure 3A) and immunoprecipitation from cell lysate (Figure 3B). Cdc20-S153 is a major Bub1 site (Kang et al., 2008). Cdc20-pS153 signal was used as an indicator for Bub1 kinase activity. In the kinase assay, increasing amount of Bub1 WT or Bub1 S459A mutant was used to phosphorylate purified Cdc20. Both the WT and the S459A mutant showed similar trend of increasing Cdc20 phosphorylation with increasing amount of kinase (Figure 3A). Cdc20 immunoprecipitated from Bub1 S459A mutant line was phosphorylated as well as that from Bub1 WT line. The phosphorylation level correlated with exogenous Bub1 expression level. When endogenous Bub1 was depleted from the Bub1$^{\Delta Kinase}$ line using siRNA, Cdc20-pS153 signal was diminished,

further confirming that Cdc20 S153 is phosphorylated by Bub1. These results clearly show that Bub1 kinase function is normal in Bub1 S459A mutant.

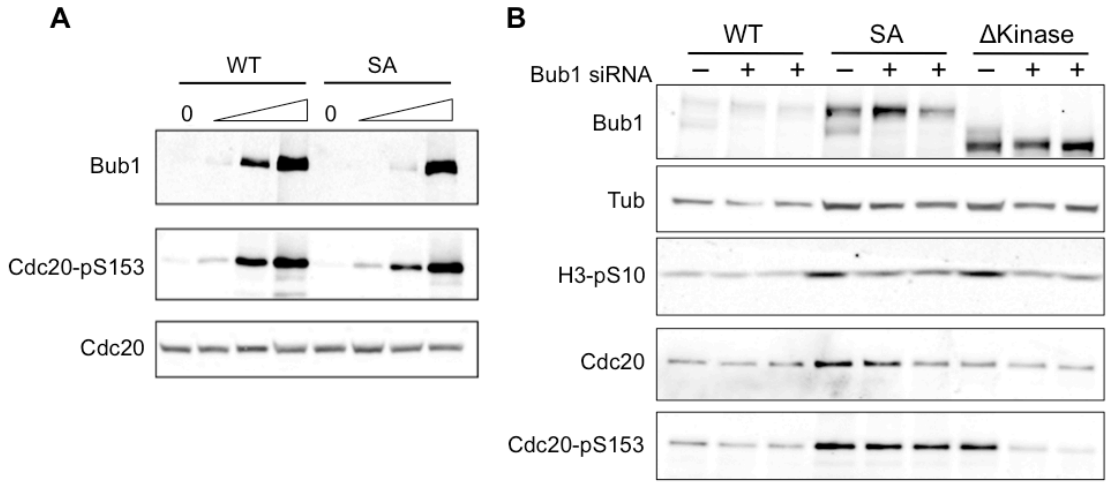

Figure 3. Bub1 S459A mutant is not defective in phosphorylating Cdc20. (A) Purified Cdc20 was incubated with different amount of Bub1 WT (WT) or Bub1 S459A (SA) proteins. Phophorylation on Cdc20 by Bub1 was analyzed using Cdc20-pS153 antibody. The amount of Bub1 and Cdc20 proteins was shown by immunoblots using indicated antibodies. **(B)** Cdc20 was immunoprecipitated from mitotic cells. Cell lines stably expressing Bub1 WT (WT), Bub1 S459A (SA) and Bub1$^{\Delta Kinase}$ (ΔKinase) were examined. The cell lysate was blotted with α-Bub1, α-tubulin (Tub) and α-H3-pS10 antibodies. The immunoprecipitated Cdc20 was blotted with α-Cdc20 and α-Cdc20-pS153 antibodies.

The kinetochore localization of Bub1, BubR1 and Mad1 are normal in Bub1 S459A mutant

Next I tried to determine whether Bub1, BubR1 and Mad1 are still recruited to the kinetochore in Bub1 S459A mutant. Bub1 forms a constitutive complex with Bub3, which facilitates Bub1 to localize to the kinetochore through binding with Knl1 (London et al., 2012; Shepperd et al., 2012; Yamagishi et al., 2012). By immunoprecipitation of over-expressed Bub1 proteins, I was able to show that the Bub1$^{\Delta Kinase}$ and the Bub1$^{\Delta Kinase}$ S459A mutant bound to Knl1 similarly,

suggesting the S459A mutation does not affect the interaction with Knl1 (Figure 4A). Furthermore, mcherry-tagged Bub1$^{\Delta Kinase}$ and Bub1$^{\Delta Kinase}$ S459A mutant both localized to the kinetochore, showing similar intensity in immunofluorescence experiment (Figure 4I).

Depletion of Bub1 leads to loss of Mad1 and BubR1 from the kinetochore (Kim et al., 2012; Overlack et al., 2015)(Figure 4C-F). BubR1 seems to be more dependent on Bub1 to localize to the kinetochore, which is consistent with previous study showing Mad1 in human cells has extensive kinetochore-binding interface (Kim et al., 2012). It was proposed that BubR1 localization to the kinetochore depends on direct binding with Bub1 (Overlack et al., 2015). In an immunoprecipitation experiment, both Bub1$^{\Delta Kinase}$ and the Bub1$^{\Delta Kinase}$ S459A mutant interacted with BubR1 (Figure 4B). Consistently, the BubR1 signal levels on the kinetochore are similar in mcherry-tagged Bub1$^{\Delta Kinase}$ and Bub1$^{\Delta Kinase}$ S459A lines (Figure 4H and 4K).

The interaction between Bub1 and Mad1 cannot be detected using immunoprecipitation from cell lysate. I directly examined the kinetochore localizations of Mad1 in Bub1$^{\Delta Kinase}$ and Bub1$^{\Delta Kinase}$ S459A lines (Figure 4G and 4J), which are also similar.

In conclusion, the Bub1 S459A mutant is not defective in association with kinetochore or the recruitment of downstream checkpoint proteins including BubR1 and Mad1.

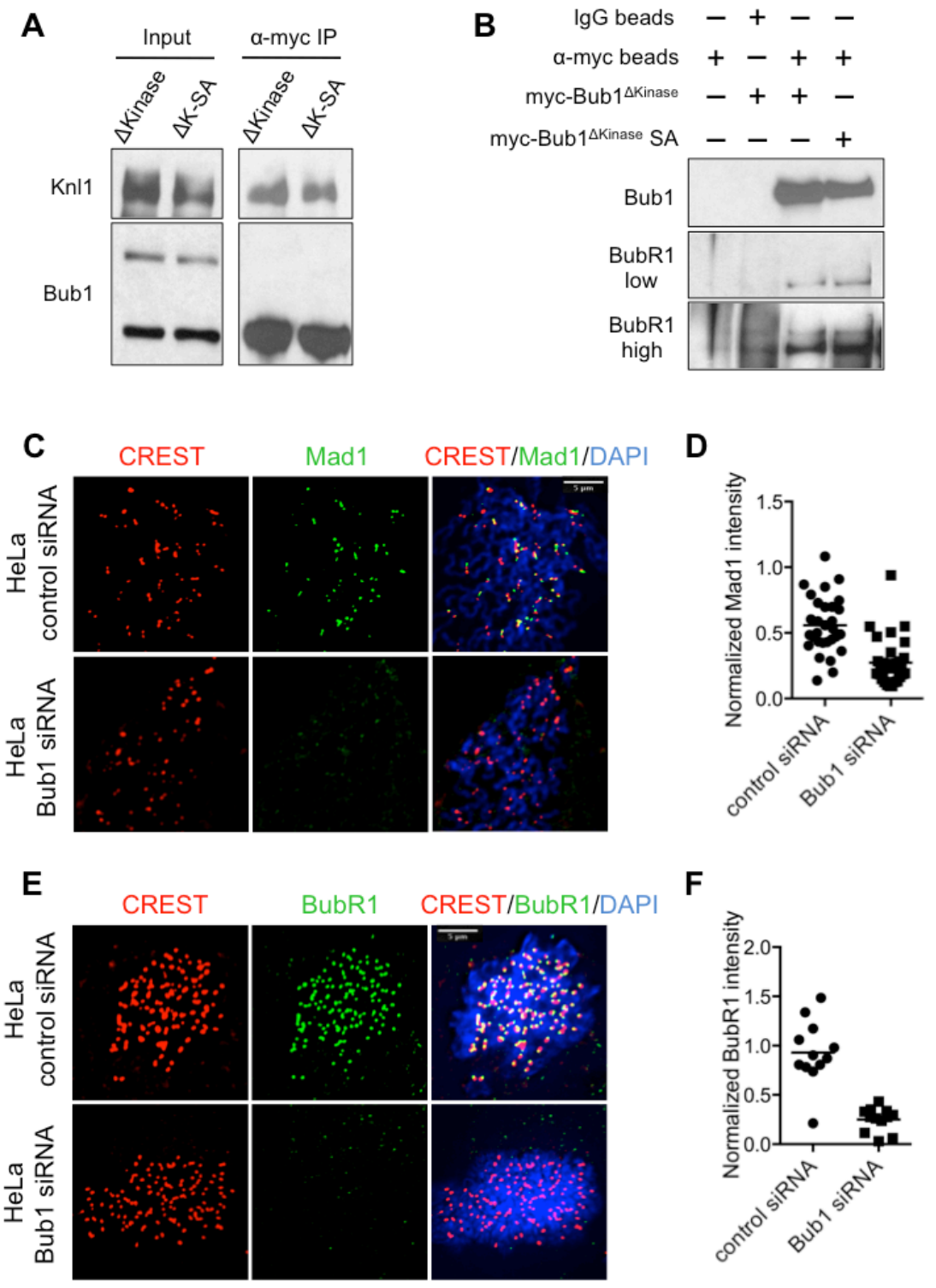
A
Input
α-myc IP
ΔKinase
ΔK-SA
ΔKinase
ΔK-SA
Knl1
Bub1
B
IgG beads
α-myc beads
myc-Bub1ΔKinase
myc-Bub1ΔKinase SA
Bub1
BubR1 low
BubR1 high
C
CREST
Mad1
CREST/Mad1/DAPI
HeLa control siRNA
HeLa Bub1 siRNA
D
Normalized Mad1 intensity
control siRNA
Bub1 siRNA
E
CREST
BubR1
CREST/BubR1/DAPI
HeLa control siRNA
HeLa Bub1 siRNA
F
Normalized BubR1 intensity
control siRNA
Bub1 siRNA

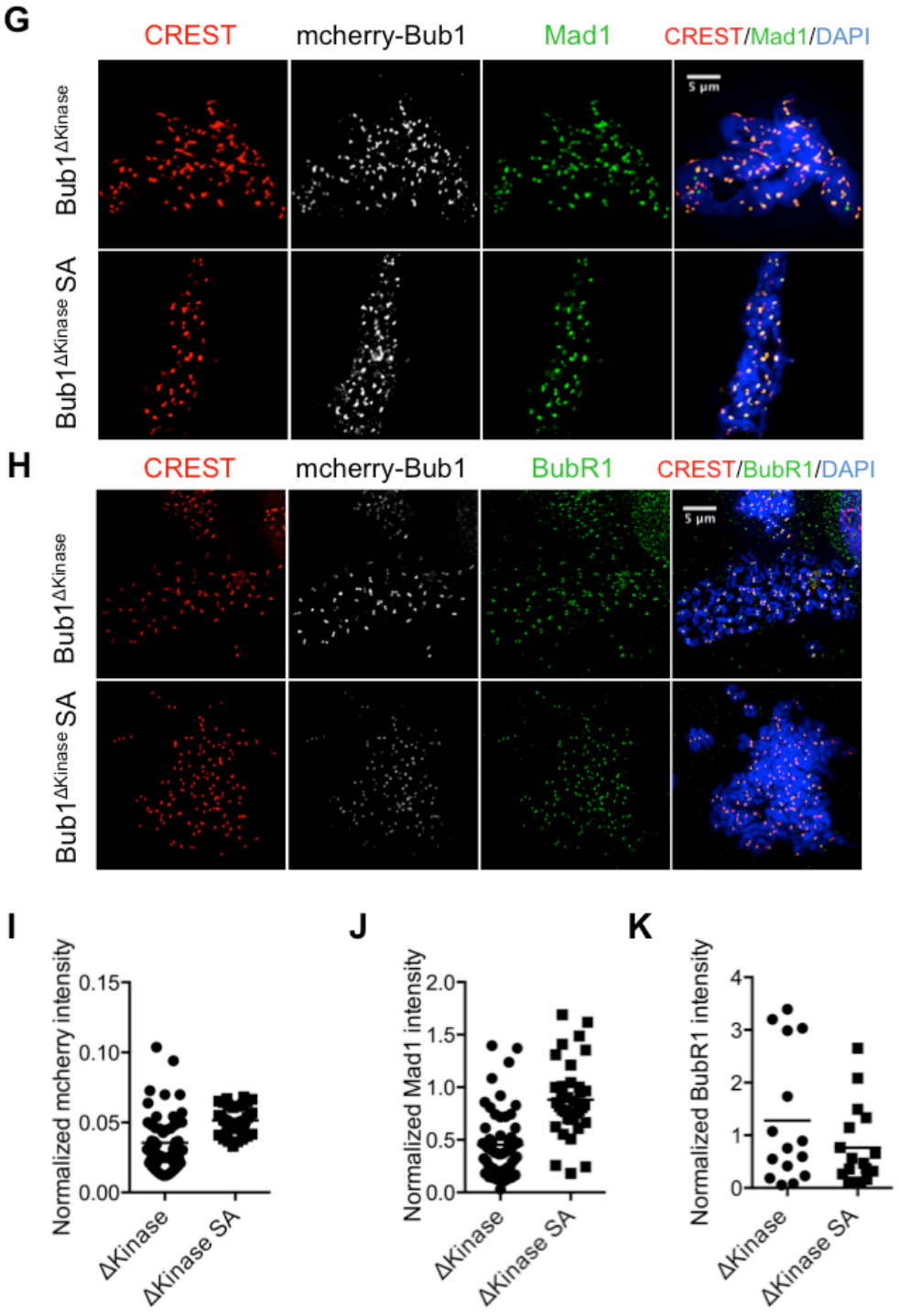

Figure 4. Mad1 and BubR1 are recruited to the kinetochore in Bub1 S459A mutant. (A) HeLa Tet-on cells were transfected with plasmids expressing myc-tagged Bub1$^{\Delta Kinase}$ (ΔKinase) or Bub1$^{\Delta Kinase}$ S459A (ΔK-SA). After arresting cells in mitosis, the over-expressed Bub1 proteins

were pulled down with α-myc beads. The proteins bound to the beads were released using SDS sample buffer. The input samples and the immunoprecipitated samples were analyzed with indicated antibodies. **(B)** HeLa Tet-on cells were transfected with plasmids expressing myc-tagged Bub1$^{\Delta Kinase}$ (ΔKinase) or Bub1$^{\Delta Kinase}$ S459A (ΔK-SA) and were arrested in mitosis. Over-expressed Bub1 proteins were pulled down with α-myc beads. IgG beads was used as control. The immunoprecipitated samples were analyzed with indicated antibodies. **(C)** and **(E)** HeLa cells with or without Bub1 depletion were arrested in mitosis using 1 μM nocodazole. Samples were stained with DAPI (blue in overlay), CREST (Reddy et al.), Mad1 or BubR1 as labeled (green). Scale bar is 5 μm. **(D)** and **(F)** Quantification of the kinetochore Mad1 or BubR1 intensity after normalized to CREST intensity for cells in **(C)** and **(E)**, respectively. **(G-H)** Cell lines stably expressing Bub1$^{\Delta Kinase}$ or Bub1$^{\Delta Kinase}$ S459A were treated with Bub1 siRNA, and were arrested in mitosis using 1 μM nocodazole. Cells were then stained with DAPI and indicated antibodies. Scale bar is 5 μm. **(I-K)** Quantification of the kinetochore signal of mcherry-tagged Bub1 **(I)**, Mad1 **(J)**, and BubR1 **(K)** normalized to CREST for cells in **(G-H)**.

The association between Bub1 and Mad1 is disrupted by the S459A mutation

In order to test the direct interaction between Bub1 and Mad1, which is difficult to show in cells, we used purified proteins in an in vitro binding assay. Mad1E fragment (amino acids 481-718) was immobilized on glutathione-Sepharose beads as the bait to pull down Bub1. It was previously reported that the Bub1-Mad1 interaction in yeast requires Bub1 phosphorylation by Mps1; Mad2 also facilitates this interaction (London and Biggins, 2014). So we tried to incubate Bub1-Mad1 with or without Mps1 or ATP to test whether Mps1 and Mps1 kinase activity are important for Bub1-Mad1 interaction. Mad2 was also added in one group in order to examine the role of Mad2 in this interaction. When Mps1 was added without ATP, both Bub1$^{\Delta Kinase}$ and Bub1$^{\Delta Kinase}$ S459A mutant bound to Mad1E very weakly without any difference. When Mps1 was added with ATP, the interaction between Bub1$^{\Delta Kinase}$ and Mad1E was greatly enhanced.

Strikingly, Bub1$^{\Delta Kinase}$ S459A fail to increase its affinity with Mad1E. When only ATP was added, the two Bub1 proteins again showed weak binding with Mad1E. The results suggest that the enhancement of Bub1-Mad1 interaction requires Bub1 S459 and Mps1 kinase activity. When Mps1, ATP and Mad2 were all added to the mixture, there is no additional enhancement of Bub1$^{\Delta Kinase}$ binding comparing with adding Mps1 and ATP, suggesting the interaction between Bub1 and Mad1 in human cell may be different from that in yeast.

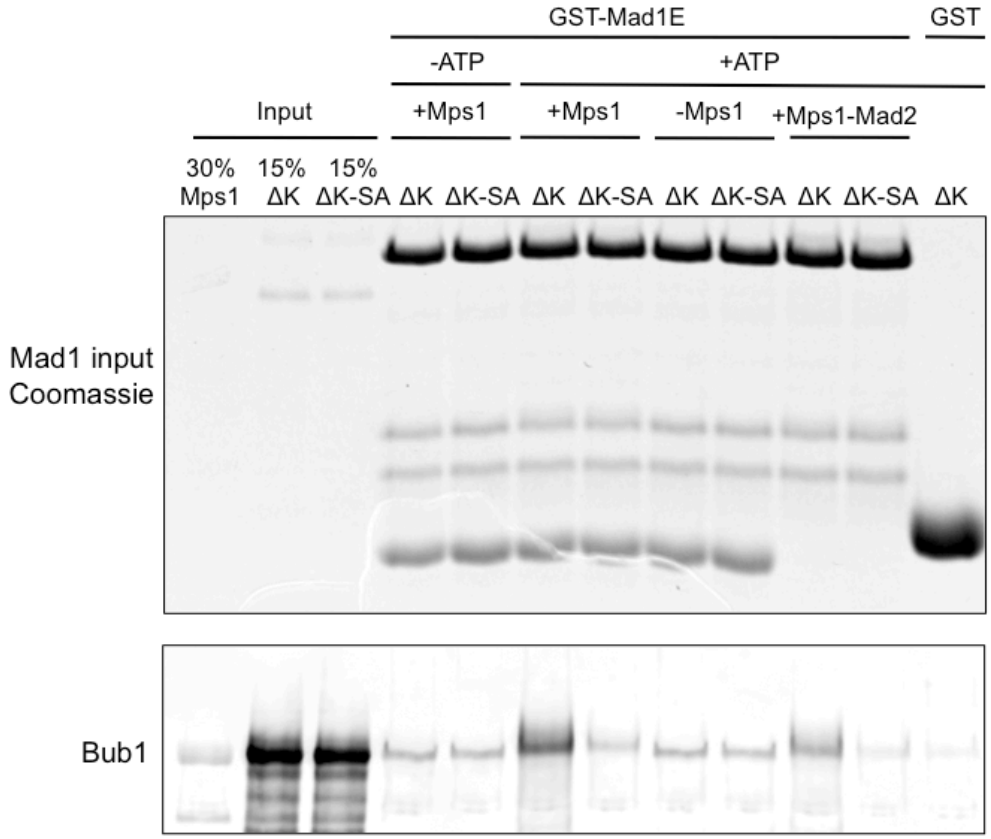

Figure 5. Bub1-Mad1 binding is disrupted in Bub1 S459A. Purified GST-Mad1E fragment (amino acids 481-718) was immobilized on beads and used as bait to pull down Bub1 after incubation with different combinations of ATP, Mps1 kinase and Mad2. GST was used as a control bait. ΔK, Bub1$^{\Delta Kinase}$; ΔK-SA, Bub1$^{\Delta Kinase}$ S459A. (Figure 5 is from Bing Li)

Discussion

The kinetochore targeting of Mad1 is a key event in the spindle checkpoint signaling. In yeast, it was shown that phosphorylation in Bub1 middle region by Mps1 is required for the direct interaction between Bub1 and Mad1-Mad2 complex, and this interaction brings Mad1 to the kinetochore. However, the kinetochore recruitment of Mad1 in human cells seems to be more complicated. Depletion of Bub1 in HeLa cells only reduced Mad1 kinetochore signal to about 50%. It is also very hard to detect the interaction between endogenous Bub1 and Mad1 using immunoprecipitation from cell lysate. Here we show phosphoylation of Bub1 S459 by Cdk1 is essential for the spindle checkpoint. Further analysis using purified protein showed that Bub1-Mad1 binding was enhanced by incubation with Mps1 and ATP. But this enhancement was diminished in the Bub1 S459A mutant.

Interestingly, the Bub1-Mad1 interaction is regulated by Mps1 in yeast; while in human cells, it is regulated by both Cdk1 and Mps1. It will be important to understand why the Cdk1 phosphorylation at Bub1 S459 is required for Bub1-Mad1 interaction; and how Cdk1 and Mps1 coordinate to regulate the Bub1-Mad1 binding, which is key to the spindle checkpoint signaling pathway.

In Bub1 S459A mutant cell line, Mad1 is localized to the kinetochore, while the spindle checkpoint is defective. The conclusion is Bub1-Mad1 interaction is not required for the recruitment of Mad1, but for “activating” Mad1 to be functional in the spindle checkpoint. It is not clear what is the exact function of the Bub1-Mad1 interaction in human cells, which requires further investigation.

Material and methods

Cell culture and transfection

HeLa Tet-on parental cell line and the stable cell lines were cultured in Dulbecco's modified Eagle's medium (DMEM; Life Technologies) supplemented with 10% fetal bovine serum (Life Technologies) and 10 mM L-glutamine (Life Technologies). To arrest cells in mitosis, cells were treated with 2.5 mM thymidine (Sigma) for 16 h, released into fresh medium for 7 h, and then incubated in medium containing 100 nM taxol (Sigma). Aurora B inhibitor ZM447439 was used at 4 μM (Selleck Chemicals).

Lipofectamine RNAiMAX (Life Technologies) and Effectene (QIAGEN), were used for siRNAs and plasmids transfection, respectively. The transfection procedure followed manufacturers' protocols. A final concentration of 5 nM per siRNA was used. Bub1 siRNA, GAGUGAUCACGAUUUCUAA (Klebig et al., 2009)

Antibodies, immunoblotting and immunoprecipitation

The Bub1-pS459 antibody was made in an in-house facility by immunizing rabbits with Bub1-pS459-containing peptides coupled to hemocyanin (Sigma). Antibodies against human Bub1, BubR1, Cdc20, Cdc20-pS153, Knl1 were described before (Lin et al., 2014; Tang et al., 2001; Xia et al., 2004). Mouse anti-tubulin (DM1A) was purchased from Sigma. Rabbit anti-H3-pS10 was purchased from Milipore. Mouse anti-phospho-S/T-P MPM2 antibody used in Flow cytometry was purchased from Milipore. CREST serum used in immunofluorescence experiments was purchased from ImmunoVision.

In immunoprecipitation, cell pellets were lysed with lysis buffer (50 mM Tris-HCl [pH 7.7], 120 mM KCl, 0.1% NP-40, 5 mM NaF, 0.3 mM Na_3VO_4, 10 mM β-glycerophosphate, 0.5 mM okadaic acid, 1 mM DTT) supplemented with protease inhibitor tablets (Roche), 0.5 μM

okadaic acid (LC Labs), and 10 units/ml TurboNuclease (Accelagen). After breaking the cells, the lysate was cleared by centrifugation. The supernatant was incubated with the antibody-coupled protein A beads (Bio-Rad) for 2 hr at 4℃. After washing, the proteins bound on the beads were released by boiling in SDS sample buffer, and the were analyzed by immunoblotting.

Immunofluorescence

Mitotic cells were harvested by shake-off. Harvested cells were washed once with PBS and incubated with 75 mM KCl for 15 min at 37℃. Then the cells were spun onto micro- scope slides with a Shandon Cytospin centrifuge. Cells were first extracted with PBS containing 0.2% Triton X-100 for 2 min and then fixed in 4% paraformaldehyde for 5 min. After washing three times with PBS containing 0.2% Triton X-100, samples were incubated with primary antibodies in PBS containing 0.2% Triton X-100 and 3% BSA at 4℃ for 10 hr. The cells were then washed three times with PBS containing 0.2% Triton X-100 and incubated with fluorescent secondary antibodies (Molecular Probes) in PBS containing 0.2% Triton X-100 and 3% BSA for 1 hr at room temperature. The cells were again washed three times with PBS containing 0.2% Triton X-100 and stained with 1 mg/ml DAPI for 3 min. After the final washes with PBS, the slides were sealed and viewed using a 100× objective on a Deltavision microscope (Applied Precision). A series of z stack images was captured at 0.2 μm intervals, deconvolved, and projected. Image processing and quantification were done with ImageJ.

Protein binding assay

Purified GST-Mad1E fragment or GST was immobilized on glutathione-Sepharose 4B beads (GE Healthcare). After being washed twice, the beads were incubated with different

combinations of Bub1$^{\Delta Kinase}$, Bub1$^{\Delta Kinase}$ S459A, Mps1 and Mad2 proteins. After being washed four times, bound proteins were eluted with SDS sample buffer and analyzed by immunoblotting. The amount of input GST-Mad1 was analyzed by coomassie blue staining.

Reference

Bharadwaj, R., and Yu, H. (2004). The spindle checkpoint, aneuploidy, and cancer. Oncogene *23*, 2016-2027.

Cheeseman, I.M., Chappie, J.S., Wilson-Kubalek, E.M., and Desai, A. (2006). The conserved KMN network constitutes the core microtubule-binding site of the kinetochore. Cell *127*, 983-997.

Heinrich, S., Windecker, H., Hustedt, N., and Hauf, S. (2012). Mph1 kinetochore localization is crucial and upstream in the hierarchy of spindle assembly checkpoint protein recruitment to kinetochores. Journal of cell science *125*, 4720-4727.

Ji, Z., Gao, H., and Yu, H. (2015). CELL DIVISION CYCLE. Kinetochore attachment sensed by competitive Mps1 and microtubule binding to Ndc80C. Science (New York, N.Y.) *348*, 1260-1264.

Jia, L., Kim, S., and Yu, H. (2013). Tracking spindle checkpoint signals from kinetochores to APC/C. Trends in biochemical sciences *38*, 302-311.

Jia, L., Li, B., Warrington, R.T., Hao, X., Wang, S., and Yu, H. (2011). Defining pathways of spindle checkpoint silencing: functional redundancy between Cdc20 ubiquitination and p31(comet). Molecular biology of the cell *22*, 4227-4235.

Kang, J., Yang, M., Li, B., Qi, W., Zhang, C., Shokat, K.M., Tomchick, D.R., Machius, M., and Yu, H. (2008). Structure and substrate recruitment of the human spindle checkpoint kinase Bub1. Molecular cell *32*, 394-405.

Kim, S., Sun, H., Tomchick, D.R., Yu, H., and Luo, X. (2012). Structure of human Mad1 C-terminal domain reveals its involvement in kinetochore targeting. Proceedings of the National Academy of Sciences of the United States of America *109*, 6549-6554.

Klebig, C., Korinth, D., and Meraldi, P. (2009). Bub1 regulates chromosome segregation in a kinetochore-independent manner. The Journal of cell biology *185*, 841-858.

Lin, Z., Jia, L., Tomchick, D.R., Luo, X., and Yu, H. (2014). Substrate-specific activation of the mitotic kinase Bub1 through intramolecular autophosphorylation and kinetochore targeting. Structure (London, England : 1993) *22*, 1616-1627.

London, N., and Biggins, S. (2014). Mad1 kinetochore recruitment by Mps1-mediated phosphorylation of Bub1 signals the spindle checkpoint. Genes & development *28*, 140-152.

London, N., Ceto, S., Ranish, J.A., and Biggins, S. (2012). Phosphoregulation of Spc105 by Mps1 and PP1 regulates Bub1 localization to kinetochores. Current biology : CB *22*, 900-906.

Luo, X., Tang, Z., Rizo, J., and Yu, H. (2002). The Mad2 spindle checkpoint protein undergoes similar major conformational changes upon binding to either Mad1 or Cdc20. Molecular cell *9*, 59-71.

Maldonado, M., and Kapoor, T.M. (2011). Constitutive Mad1 targeting to kinetochores uncouples checkpoint signalling from chromosome biorientation. Nature cell biology *13*, 475-482.

Martin-Lluesma, S., Stucke, V.M., and Nigg, E.A. (2002). Role of Hec1 in spindle checkpoint signaling and kinetochore recruitment of Mad1/Mad2. Science (New York, N.Y.) *297*, 2267-2270.

McCleland, M.L., Gardner, R.D., Kallio, M.J., Daum, J.R., Gorbsky, G.J., Burke, D.J., and Stukenberg, P.T. (2003). The highly conserved Ndc80 complex is required for kinetochore assembly, chromosome congression, and spindle checkpoint activity. Genes & development *17*, 101-114.

Overlack, K., Primorac, I., Vleugel, M., Krenn, V., Maffini, S., Hoffmann, I., Kops, G.J., and Musacchio, A. (2015). A molecular basis for the differential roles of Bub1 and BubR1 in the spindle assembly checkpoint. eLife *4*, e05269.

Pagliuca, C., Draviam, V.M., Marco, E., Sorger, P.K., and De Wulf, P. (2009). Roles for the conserved spc105p/kre28p complex in kinetochore-microtubule binding and the spindle assembly checkpoint. PloS one *4*, e7640.

Peters, J.M. (2006). The anaphase promoting complex/cyclosome: a machine designed to destroy. Nat Rev Mol Cell Biol *7*, 644-656.

Reddy, S.K., Rape, M., Margansky, W.A., and Kirschner, M.W. (2007). Ubiquitination by the anaphase-promoting complex drives spindle checkpoint inactivation. Nature *446*, 921-925.

Rischitor, P.E., May, K.M., and Hardwick, K.G. (2007). Bub1 is a fission yeast kinetochore scaffold protein, and is sufficient to recruit other spindle checkpoint proteins to ectopic sites on chromosomes. PloS one *2*, e1342.

Shepperd, L.A., Meadows, J.C., Sochaj, A.M., Lancaster, T.C., Zou, J., Buttrick, G.J., Rappsilber, J., Hardwick, K.G., and Millar, J.B. (2012). Phosphodependent recruitment of Bub1

and Bub3 to Spc7/KNL1 by Mph1 kinase maintains the spindle checkpoint. Current biology : CB *22*, 891-899.

Sironi, L., Mapelli, M., Knapp, S., De Antoni, A., Jeang, K.T., and Musacchio, A. (2002). Crystal structure of the tetrameric Mad1-Mad2 core complex: implications of a 'safety belt' binding mechanism for the spindle checkpoint. The EMBO journal *21*, 2496-2506.

Tang, Z., Bharadwaj, R., Li, B., and Yu, H. (2001). Mad2-Independent inhibition of APCCdc20 by the mitotic checkpoint protein BubR1. Developmental cell *1*, 227-237.

Tang, Z., Shu, H., Oncel, D., Chen, S., and Yu, H. (2004). Phosphorylation of Cdc20 by Bub1 provides a catalytic mechanism for APC/C inhibition by the spindle checkpoint. Molecular cell *16*, 387-397.

Tighe, A., Staples, O., and Taylor, S. (2008). Mps1 kinase activity restrains anaphase during an unperturbed mitosis and targets Mad2 to kinetochores. The Journal of cell biology *181*, 893-901.

Torres, E.M., Williams, B.R., and Amon, A. (2008). Aneuploidy: cells losing their balance. Genetics *179*, 737-746.

Xia, G., Luo, X., Habu, T., Rizo, J., Matsumoto, T., and Yu, H. (2004). Conformation-specific binding of p31(comet) antagonizes the function of Mad2 in the spindle checkpoint. The EMBO journal *23*, 3133-3143.

Yamagishi, Y., Yang, C.H., Tanno, Y., and Watanabe, Y. (2012). MPS1/Mph1 phosphorylates the kinetochore protein KNL1/Spc7 to recruit SAC components. Nature cell biology *14*, 746-752.

Yu, H. (2007). Cdc20: a WD40 activator for a cell cycle degradation machine. Molecular cell *27*, 3-16.

CHAPTER THREE

SUBSTRATE-SPECIFIC ACTIVATION OF THE MITOTIC KINASE BUB1 THROUGH INTRAMOLECULAR AUTOPHOSPHORYLATION AND KINETOCHORE TARGETING

Summary

During mitosis of human cells, the kinase Bub1 orchestrates chromosome segregation through phosphorylating histone H2A and the anaphase-promoting complex/cyclosome activator Cdc20. Bub1-mediated H2A-T120 phosphorylation (H2A-pT120) at kinetochores promotes centromeric sister-chromatid cohesion, whereas Cdc20 phosphorylation by Bub1 contributes to spindle checkpoint signaling. Here, we show that phosphorylation at the P+1 substrate-binding loop of human Bub1 enhances its activity toward H2A but has no effect on its activity toward Cdc20. We determine the crystal structure of phosphorylated Bub1. A comparison between structures of phosphorylated and unphosphorylated Bub1 reveals phosphorylation-triggered reorganization of the P+1 loop. This activating phosphorylation of Bub1 is constitutive during the cell cycle. Enrichment of H2A-pT120 at mitotic kinetochores requires kinetochore targeting of Bub1. The P+1 loop phosphorylation of Bub1 appears to occur through intramolecular autophosphorylation. Our study provides structural and functional insights into substrate-specific regulation of a key mitotic kinase and expands the repertoire of kinase activation mechanisms.

Introduction

The mitotic serine/threonine kinase Bub1 has multiple functions in chromosome segregation. Mice harboring a catalytically inactive Bub1 mutant exhibit increased chromosome segregation errors and aneuploidy (Ricke et al., 2012). Bub1 has two known substrates in human cells, Cdc20 and histone H2A (Kawashima et al., 2010; Tang et al., 2004a). Cdc20 is an activator of the anaphase promoting complex or cyclosome (APC/C), a ubiquitin ligase essential for anaphase onset (Yu, 2007). In response to kinetochores not properly attached to spindle microtubules, the spindle checkpoint inhibits APC/C^{Cdc20} to delay anaphase onset (Foley and Kapoor, 2013; Jia et al., 2013; Lara-Gonzalez et al., 2012). Phosphorylation of the N-terminal region of Cdc20 by Bub1 contributes to checkpoint-dependent inhibition of APC/C^{Cdc20} (Tang et al., 2004a). Bub1 also phosphorylates histone H2A at threonine 120 (H2A-T120) (Kawashima et al., 2010). H2A-pT120 is enriched at mitotic kinetochores (Liu et al., 2013a) and creates a docking site for the complex of shugoshin (Sgo1) and protein phosphatase 2A (PP2A) (Kawashima et al., 2010; Kitajima et al., 2005, 2006; Riedel et al., 2006; Tang et al., 2004b, 2006), which binds and protects cohesin at centromeres until the metaphase-anaphase transition (Liu et al., 2013b). Thus, the kinase activity of Bub1 is critical for multiple steps of chromosome segregation.

Despite these critical functions, whether and how the kinase activity of Bub1 is regulated during the cell cycle are poorly understood. We have previously determined the crystal structure of the Bub1 kinase domain (Kang et al., 2008). Although much of the activation segment of Bub1 has an ordered conformation characteristic of active kinases in that structure, the P+1 substrate-binding loop partially blocks the active site and is not optimal for substrate binding (Kang et al., 2008). The mechanism by which Bub1 reorganizes its P+1 loop for efficient substrate phosphorylation is unknown.

Here we show that phosphorylation of S969 of the P+1 loop in human Bub1 selectively enhances its activity toward H2A-T120 but does not affect its activity toward Cdc20. We determine the crystal structure of the Bub1 kinase domain containing phospho-S969, revealing a phosphorylation-induced conformational change in the P+1 loop. Surprisingly, the Bub1-pS969 level is not elevated during mitosis. The kinetochore enrichment of H2A-pT120 in mitosis instead relies on the mitosis-specific kinetochore targeting of Bub1. Bub1-pS969 is mediated by intramolecular autophosphorylation, which does not strictly require the catalytic aspartate. Our study thus defines an unusual mode of autoactivation for Bub1 and provides a mechanism by which the activities of a kinase toward different substrates can be differentially regulated.

Results

P+1 loop phosphorylation stimulates the kinase activity of Bub1 toward H2A

Bub1 consists of an N-terminal tetratricopeptide repeat (TPR) domain, a central Cdc20-binding domain (CBD), and a C-terminal serine/threonine kinase domain (Figure 1A). The CBD contains a KEN box that interacts with the C-terminal WD40 repeat domain of Cdc20. Using mass spectrometry, we mapped the phosphorylation sites of recombinant human Bub1 expressed in insect cells, which was active in phosphorylating both Cdc20 and H2A. One of the phosphoresidues, S969, is located in the P+1 loop and is conserved among vertebrate Bub1 proteins (Figure 1B and Figure 2A). To examine the effect of S969 phosphorylation, we mutated this residue to alanine or aspartate. The neighboring residue T968 is also conserved in vertebrates. To avoid potential compensation for the loss of S969 phosphorylation through T968 phosphorylation, we also created the T968A mutant and the T968A/ S969A (AA) double mutant.

We then expressed Myc-Bub1 wild-type (WT) or mutants in HeLa cells, arrested these cells in mitosis with nocodazole, immunoprecipitated Myc-Bub1 proteins, and assayed their activities in vitro toward histone H2A or Cdc20 using phospho-specific antibodies (Figures 1C and 1D). Two different kinase-dead mutants, D917N and D946N, were used as negative controls. The D917N mutant has the catalytic aspartate mutated but is expected to retain ATP binding. The D946N mutation targets a key Mg2+-coordinating residue and disrupts ATP binding. As expected, both mutants were inactive toward H2A or Cdc20. Myc-Bub1 proteins isolated from G1 cells (thymidine-arrested or nocodazole-arrest-release samples) or mitotic cells (nocodazole-arrested samples) had similar activities toward both histone H2A and Cdc20, suggesting that the kinase activity of Bub1 might not be regulated during the cell cycle.

S969A had much weaker activity toward H2A-T120, whereas the activity of S969D was similar to that of WT. Consistent with our previous study (Kang et al., 2008), S969A largely retained its activity toward Cdc20 (Figures 1C and 1D). Similar results were obtained with recombinant purified WT, S969A, and S969D Bub1 kinase domain proteins (containing residues 740–1085) (Figure 1E). These results suggest that S969 phosphorylation of Bub1 is required for its activity toward H2A but appears to be dispensable for Cdc20 phosphorylation.

The T968A mutation greatly reduced the activity of Bub1 toward H2A. As reported previously (Kang et al., 2008), Bub1 T968A had diminished activity toward an N-terminal fragment of Cdc20. Interestingly, the T968A and AA mutants largely retained their activities toward full-length Cdc20. Compared with the N-terminal fragment of Cdc20, the full-length Cdc20 was a better substrate for Bub1 because it could be recruited to Bub1 through a docking interaction between its C-terminal WD40 domain and the CBD of Bub1 (Kang et al., 2008). To clarify the role of T968 in H2A phosphorylation, we immunized rabbits with a mixture of two

phosphopeptides containing either pT968 or pS969 and affinity purified the antibodies using either peptide. The antibody mixture and the pS969 antibody detected the recombinant Bub1 kinase domain protein from insect cells (Figure 1E) and Myc-Bub1 from HeLa cells (Figure 1F), but not the S969A mutant. The Myc-Bub1 signals were abolished by phosphatase treatment (Figure 1F). The pT968 antibody detected no signals (data not shown). Moreover, Myc-Bub1 T968A retained the pS969 signal (Figure 1F). Therefore, Bub1 T968 is itself not phosphorylated and is not required for S969 phosphorylation. T968 likely plays a structural role in phosphorylating substrates and may directly participate in the recognition of the H2A or Cdc20 peptides. The full-length Cdc20 can interact with docking motifs on Bub1 that are outside its kinase domain. This docking mechanism presumably compensates for the weakened local interactions between T968 and residues neighboring the Cdc20 phosphorylation site in Bub1 T968A.

We were intrigued by two previous reports that implicated the N-terminal TPR domain of Bub1 in regulating its kinase activity (Krenn et al., 2012; Ricke et al., 2012), as this result suggested the potential existence of long-range interactions between the TPR and kinase domains. In contrast to these reports, however, we found that the Bub1 mutant with its TPR deleted (ΔTPR) expressed in human or insect cells was fully active in phosphorylating Cdc20 and H2A (Figures 1C, 1D, 2B, and 2C). Consistently, Bub1 ΔTPR had normal levels of S969 phosphorylation (Figures 1F and 2C). Thus, the TPR domain of Bub1 is dispensable for its kinase activity.

Both previous studies relied on kinase assays with tagged Bub1 proteins overexpressed in and immunoprecipitated from mammalian cells. The effects of TPR deletion on the kinase activities of immunoprecipitated Bub1 in these studies were likely indirect and might involve

other Bub1-binding proteins. Because we did not observe activity differences with Myc-Bub1 proteins overexpressed in HeLa cells, the indirect effects of TPR might be variable among cell lines or types or might be sensitive to immunoprecipitation (IP) conditions.

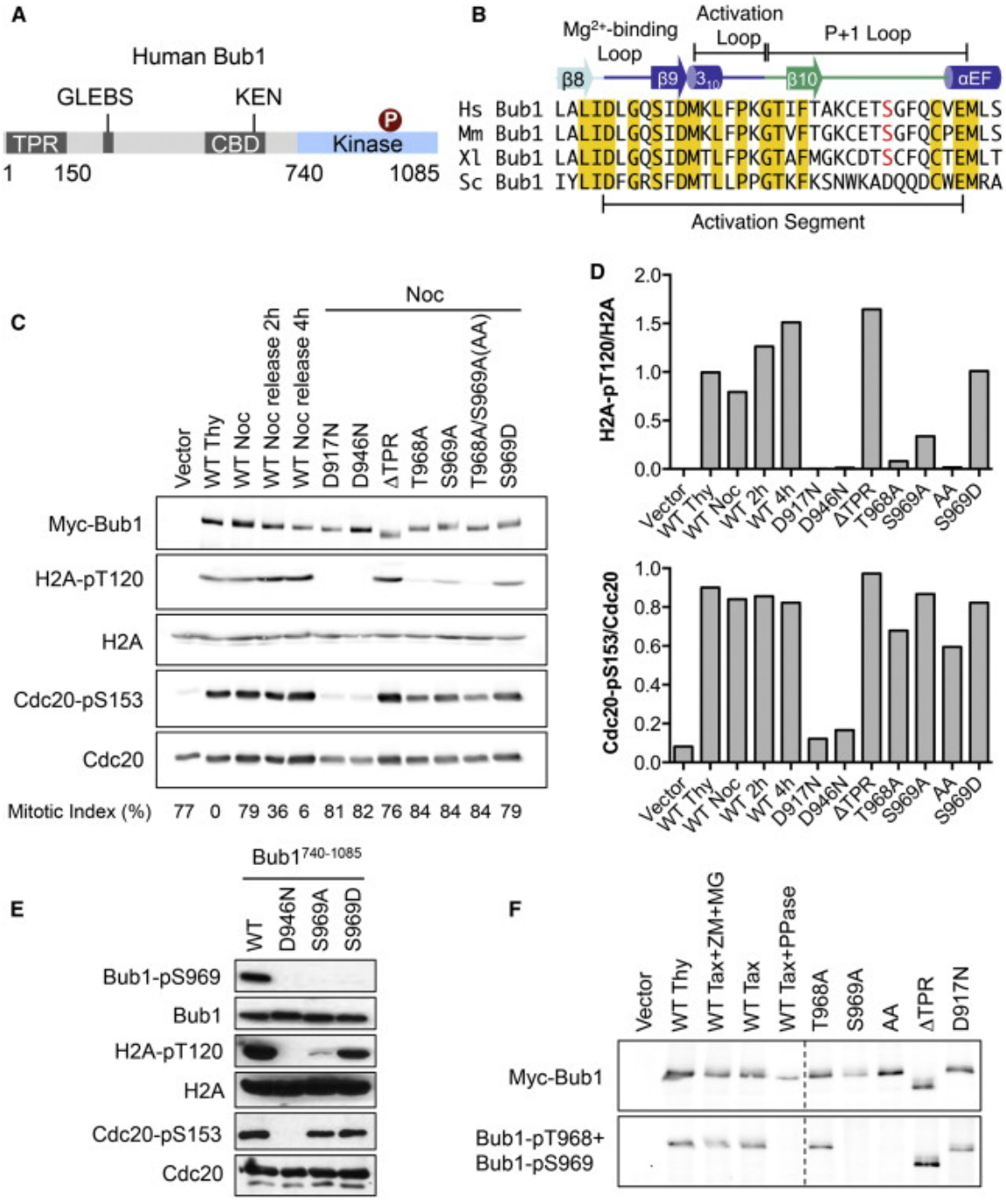

Figure 1. S969 phosphorylation is required specifically for the activity of Bub1 toward H2A. (A) Schematic drawing of the domains and motifs of human Bub1. CBD, Cdc20-binding

domain; GLEBS, Gle2-binding sequence; KEN, Lys-Glu-Asn box; TPR, tetratricopeptide repeat. **(B)** Sequence alignment of the activation segment of Bub1 proteins. Hs, *Homo sapiens*; Mm, *Mus musculus*; Sc, *Saccharomyces cerevisiae*; Xl, *Xenopus laevis*. Identical residues are shaded yellow. S969 in human Bub1 and its corresponding residues are colored red. **(C)** HeLa cells were transfected with the indicated Myc-Bub1 plasmids and synchronized at G1/S with thymidine (Thy), at mitosis with nocodazole (Noc), or at early G1 with nocodazole-arrest release. The mitotic index of each sample was indicated at the bottom. Myc-Bub1 proteins were immunoprecipitated with the anti-Myc antibody beads and subjected to kinase assays with Cdc20 or bulk histones as substrates. The kinase reaction mixtures were blotted with the indicated antibodies. **(D)** The H2A-pT120 and Cdc20-pS153 signals in **(C)** were quantified and normalized against the total H2A and Cdc20 levels, respectively. **(E)** Recombinant purified WT or mutant Bub1$^{740–1085}$ were assayed for their activities toward H2A and Cdc20. The reaction mixtures were blotted with the indicated antibodies. **(F)** HeLa cells were transfected with the indicated Myc-Bub1 vectors and treated with thymidine (Thy), Taxol (Tax), or Taxol followed by MG132 (MG) and the Aurora kinase inhibitor ZM447439 (ZM). Myc-Bub1 proteins were immunoprecipitated from cell lysates, either untreated or treated with λ phosphatase (PPase), and blotted with the indicated antibodies. (Figure 1E is from Zhonghui Lin)

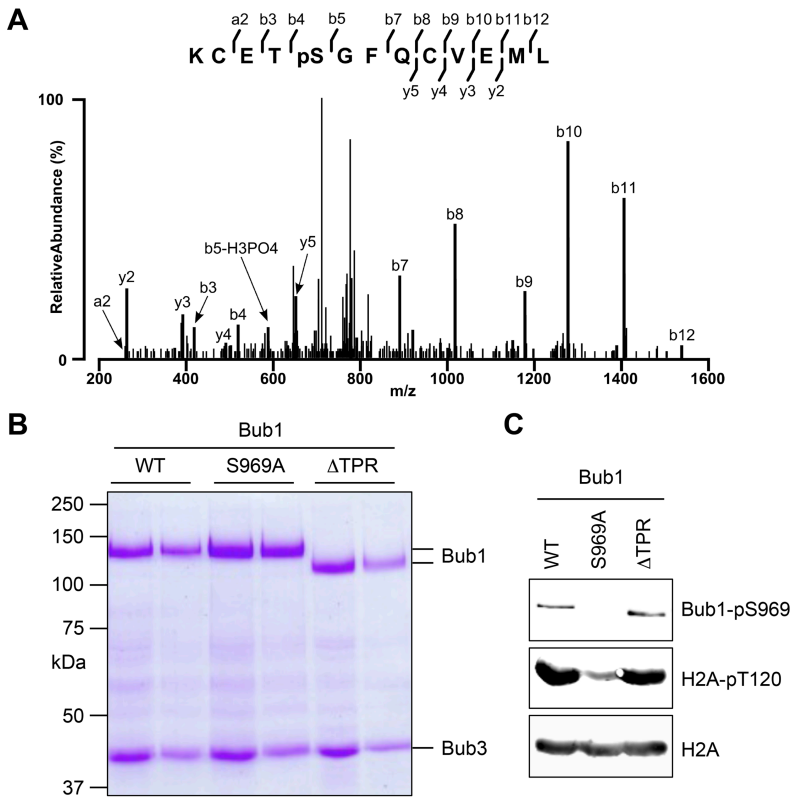

Figure 2. The TPR domain of Bub1 is dispensable for Bub1 S969 and H2A phosphorylation. (A) Mass spectrum of the pS969 peptide derived from recombinant Bub1 purified from Sf9 cells. **(B)** Coomassie blue stained gel of the indicated recombinant full-length Bub1–Bub3 proteins. **(C)** Bub1 proteins in **(B)** were used to phosphorylate bulk histones. The reaction mixtures were blotted with the indicated antibodies. (Figure 2 is from Zhonghui Lin)

Structure of the Bub1 kinase domain with phosphorylated S969

We had previously determined the structure of the extended kinase domain of Bub1 (residues 724–1085), in which S969 was not phosphorylated (Kang et al., 2008). Compared with Bub1$^{724–1085}$, a smaller Bub1 fragment (residues 740–1085) was more efficient in undergoing autophosphorylation at S969 (Figure 3A). Bub1$^{740–1085}$ was also more active in phosphorylating histone H2A. These results provide direct evidence that phospho-Bub1 is more active than the unphosphorylated Bub1 toward H2A, although we cannot rule out the possibility that residues

724–739 (missing in the phospho-Bub1 protein) might have an autoinhibitory role in H2A phosphorylation. Importantly, the phosphorylated and unphosphorylated Bub1 proteins can be separated by cation exchange chromatography (Figure 3B), with pS969 Bub1 eluting at lower salt. About 30% of Bub1$^{740–1085}$ purified from insect cells was already phosphorylated at S969. When the unphosphorylated and phosphorylated Bub1$^{740–1085}$ were incubated with H2A in the kinase buffer for only 15 min, we did not observe substantial differences in pS969 or pH2A levels at the end of the reaction. Thus, the autophosphorylation reaction likely proceeds with kinetics faster than those of the H2A phosphorylation reaction.

We then incubated the unphosphorylated Bub1 fractions with the kinase buffer containing cold ATP. Virtually all of the Bub1 protein was phosphorylated after this incubation, based on its fractionation profile on the cation exchange column. The fractions corresponding to phosphorylated Bub1 was collected and subjected to crystallization. We obtained diffracting crystals of phosphorylated Bub1 and determined its structure using molecular replacement with the structure of unphosphorylated Bub1 (PDB ID 3E7E) as the search model (Figures 3C and 3D).

During the refinement of the phosphorylated Bub1 structure, we discovered that modeling of the bound nucleotide as ATP with one Mg^{2+} ion coordinated to the α and β phosphates resulted in severe distortions of the geometry and regions of large positive and negative density for the atoms of the γ phosphate. Reducing the occupancy of the γ phosphate atoms to less than 1.0 and re-refinement, as had been done in the original refinement for the unphosphorylated Bub1, did not eliminate the geometry distortions and electron density. Inclusion of a fully occupied ADP, with a second Mg^{2+} ion bound to three water molecules (in place of the γ phosphate of ATP that was originally modeled), resolved all refinement issues. A

re-examination of the unphosphorylated Bub1 structure led us to conclude that this structure also contains one fully occupied ADP and two bound Mg^{2+} ions with tightly bound waters. Statistics for data collection and structure refinement for both unphosphorylated and phosphorylated Bub1 are included in Table 1.

The structure of pS969-Bub1 is virtually identical to that of unphosphorylated Bub1, except the conformations of their P+1 loop (Figures 3C–3E). The electron density of the P+1 loop of phospho-Bub1 is generally well defined, with pS969 being clearly visible (Figure 3F). The P+1 loops in both unphosphorylated and phosphorylated Bub1 have B factors higher than those of the rest of the protein, indicative of partial disorder in both cases. S969 phosphorylation substantially reorganized the conformation of the P+1 loop. In the unphosphorylated state, S969 points toward the active site. In the phosphorylated state, a part of P+1 loop containing pS969 forms a 3_{10} helix, with pS969 pointing away from the active site.

Despite repeated attempts, we could not determine the structure of phospho-Bub1 bound to H2A peptides. The underlying reason for why pS969 enhances the Bub1 activity toward H2A remains unclear. Because S969 phosphorylation has little effect on Bub1-catalyzed Cdc20 phosphorylation, the conformation of the phosphorylated P+1 loop of Bub1 may be specifically optimized for H2A binding. For example, pS969 may make direct contact with the H2A peptide (VLLPKK**T**ESHKAK), which has basic residues at −1 and −2 positions. In contrast, the Cdc20 S153 phosphorylation site (RLKVLY**S**QKATPG) has hydrophobic residues at −1, −2, and −3 positions, providing a possible reason for why Cdc20 phosphorylation is insensitive to Bub1 S969 phosphorylation. The two basic residues at −1/−2 positions in H2A may form favorable electrostatic interactions with Bub1 pS969, whereas the hydrophobic residues of Cdc20 at the corresponding positions cannot. Another possible reason for why Cdc20 phosphorylation does

not require Bub1 S969 phosphorylation may be the existence of the distal docking interaction between the WD40 domain of Cdc20 and the CBD of Bub1.

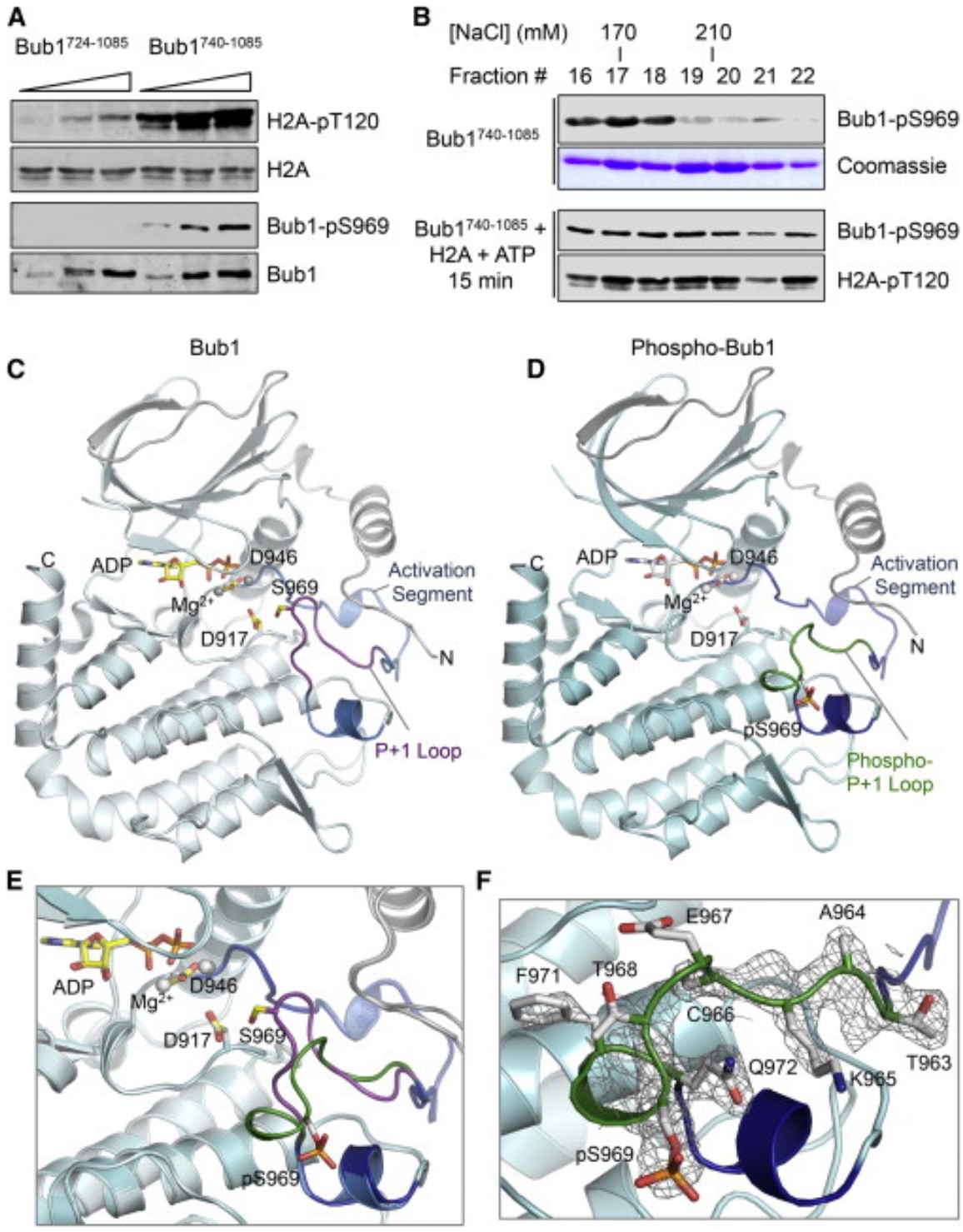

Figure 3. S969 phosphorylation induces localized conformational change of the Bub1 P+1 loop. (A) Recombinant purified Bub1$^{724–1085}$ and Bub1$^{740–1085}$ proteins were assayed for their activities toward H2A. The reaction mixtures were blotted with anti-H2A and anti-H2A-pT120 antibodies. The Bub1 proteins prior to the kinase reactions were also blotted with anti-Bub1 and anti-Bub1-pS969 antibodies. **(B)** Resource S fractions of Bub1$^{740–1085}$ were blotted with the anti-Bub1-pS969 antibody or stained with Coomassie (two top panels). The same fractions were incubated with H2A and cold ATP in the kinase buffer for 15 min. The reaction mixtures were blotted with anti-Bub1-pS969 and anti-H2A-pT120 antibodies (two bottom panels). **(C)** Ribbon diagram of unphosphorylated Bub1, with ADP and key residues shown as sticks. The N-terminal extension is in gray. The activation segment is colored blue. The P+1 loop is colored purple. The rest of the protein is in light cyan. Mg^{2+} ions are shown as gray spheres. The N and C termini are labeled. All structure figures were made with Pymol (http://www.pymol.org). **(D)** Ribbon diagram of phospho-S969 Bub1, with ADP and key residues (including pS969) shown as sticks. The N-terminal extension is in gray. The activation segment is colored blue. The phosphorylated P+1 loop is colored green. The rest of the protein is in cyan. **(E)** Overlay of the active site of unphosphorylated and phosphorylated Bub1. Color schedules are as in **(C)** and **(D). (F)** Electron density (plotted at 1σ) of the phosphorylated P+1 loop. (Figure 3 is from Zhonghui Lin)

Table 1. Data collection and refinement statistics of pS969 Bub1. (From Zhonghui Lin)

Data collection	
Space group	$P12_11$
Cell dimensions	a= 90 Å, b=47 Å, C= 93 Å; α=γ=90, β=107
Energy	12,664.5 eV
Resolution range (Å)	50-2.20 (2.24-2.20)[a]
Unique reflections	37,658 (1,707)
Multiplicity	3.7 (3.0)
Data completeness (%)	98.4 (88.9)
R_{merge} (%)[b]	11.4 (39.4)
I/σ(I)	16.1 (2.4)
Wilson B value (Å^2)	32.3
Refinement statistics	
Resolution range (Å)	36.88 – 2.20 (2.28-2.20)
No. of reflections R_{work}/R_{free}	35,718/1,885 (3,166/176)
Data completeness (%)	98.2 (98.2)
Atoms (non-H protein/ADP/ions/waters)	5,365/54/7/237
R_{work} (%)	22.9
R_{free} (%)	26.8
R.m.s.d. bond length (Å)	0.005
R.m.s.d. bond angle (°)	0.747
Mean B-value (Å^2) (protein/ADP/waters)	50.8/24.9/38.2
Ramachandran plot (%) (favored/additional/disallowed)[c]	95.9/4.1/0
Maximum likelihood coordinate error	0.32
Missing residues	A: 807-814,932-938, 1084-1085. B: 807-815,932-936, 1082-1085.

[a]Data for the outermost shell are given in parentheses.
[b]$R_{merge} = 100\ \Sigma_h\Sigma_i|I_{h,\,i} - \langle I_h\rangle|/\Sigma_h\Sigma_i I_{h,\,i}$, where the outer sum (h) is over the unique reflections and the inner sum (i) is over the set of independent observations of each unique reflection.
[c]As defined by the validation suite MolProbity (Chen, V.B., Arendall, W.B.A., Headd, J.J., Keedy, D.A., Immormino, R.M., Kapral, G.J., Murray, L.W., Richardson, J.S., Richardson, D.C. (2010) *MolProbity*: all-atom structure validation for macromolecular crystallography. *Acta*

Structural basis of the conformational change triggered by S969 phosphorylation

The catalytic loop and activation segment of Bub1 have several unusual features (Figure 4). The N-terminal half of the activation segment is ordered and has virtually identical conformations in both the unphosphorylated and phosphorylated Bub1 (Figures 5A and 5B). The DLG motif (DFG in most other kinases) at the start of the activation segment is critical for Mg^{2+} binding. A highly conserved aspartate (D952) is engaged in electrostatic and hydrogen bonding interactions with R840 and Y832 on the αC helix. Several residues in the N-terminal portion of the activation segment, including I951, M953, L955, F956, P957, T960, and F962, develop extensive hydrophobic interactions with F736, V738, P741, W742, L746, and L750 from the N-terminal extension, I914 from the catalytic loop, and W982 and Y984 N terminal to the αF helix. Most of these interactions are retained in phosphorylated Bub1, except those involving F736 and V738. These residues are deleted in this shorter Bub1 protein. A proline from the cloning sites takes their place. Because the N-terminal extension is critical for the kinase activity of Bub1, this important difference might help to explain why $Bub1^{740–1085}$ is more active than $Bub1^{724–1085}$.

In many kinases in which activation involves activation segment phosphorylation, their catalytic loop contains a characteristic HRD motif, in which the arginine forms favorable electrostatic interactions with the phosphate. Bub1 does not have an HRD motif. It has an HGD motif instead (Figure 4). Indeed, the pS969 residue in Bub1 does not make favorable interactions with the catalytic loop or other structural elements (Figure 3E).

Instead, the unfavorable interactions between pS969 and the negatively charged D917 and E967 residues provide a driving force for the phosphorylation-induced conformation change. In the unphosphorylated conformation, S969 is located in close proximity to D917 and E967

(Figure 5C). If there were no conformational changes, the phosphate group on pS969 would have developed unfavorable electrostatic interactions with these two negatively charged residues. In phosphorylated Bub1, pS969 points away from D917 and E967, alleviating these clashes (Figure 5D).

Finally, most kinases have a characteristic APE motif at the end of the activation segment. The glutamate in this motif forms a salt bridge with a highly conserved arginine in the C-terminal region of the kinase (Figure 4). In Bub1, this APE motif is replaced by a CVE motif. The carboxyl group of the glutamate (E975) does not interact with an arginine, but forms a hydrogen bond with its own backbone amide. In the unphosphorylated conformation, the cysteine in this motif (C973) and M976 participate in hydrophobic interactions with W982 and I986 (Figure 5C). E967 points toward this hydrophobic core. In the phosphorylated conformation, C966 is included in this core, whereas E967 points away (Figure 5D). The inclusion of the hydrophobic C966 (as opposed to the charged E967) in the hydrophobic core provides another driving force for the phosphorylation-dependent conformational change.

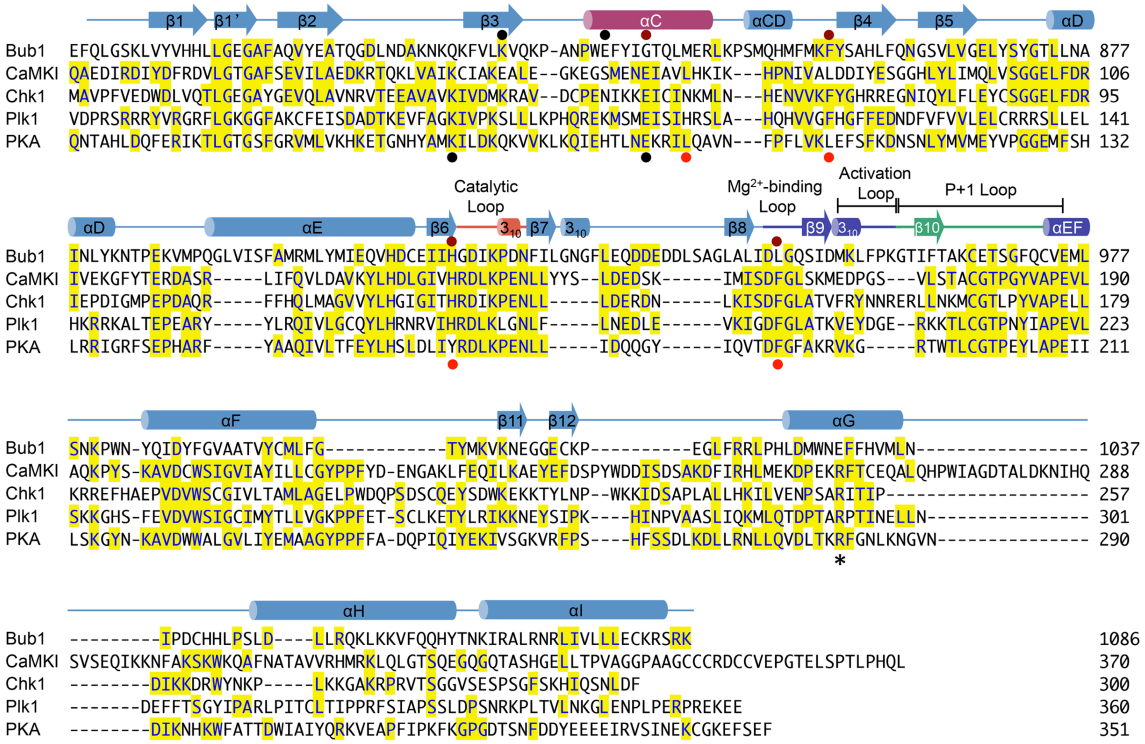

Figure 4. The Bub1 kinase domain has unusual sequence features. Sequence alignment of Bub1 and other human kinases generated with ClustalW. The structural elements of Bub1 are shown on top. The R spine residues of Bub1 and other kinases (including PKA) are indicated by dark and red dots, respectively. The key ATP-binding lysine on β3 and the glutamate on αC that interacts with it in Bub1 and other kinases are indicated by black dots. Note that the positions of these residues and some of the R spine residues in Bub1 are different from those in other kinases. The arginine that forms a salt bridge with the glutamate in the APE motif is indicated by an asterisk. This arginine is missing in Bub1.

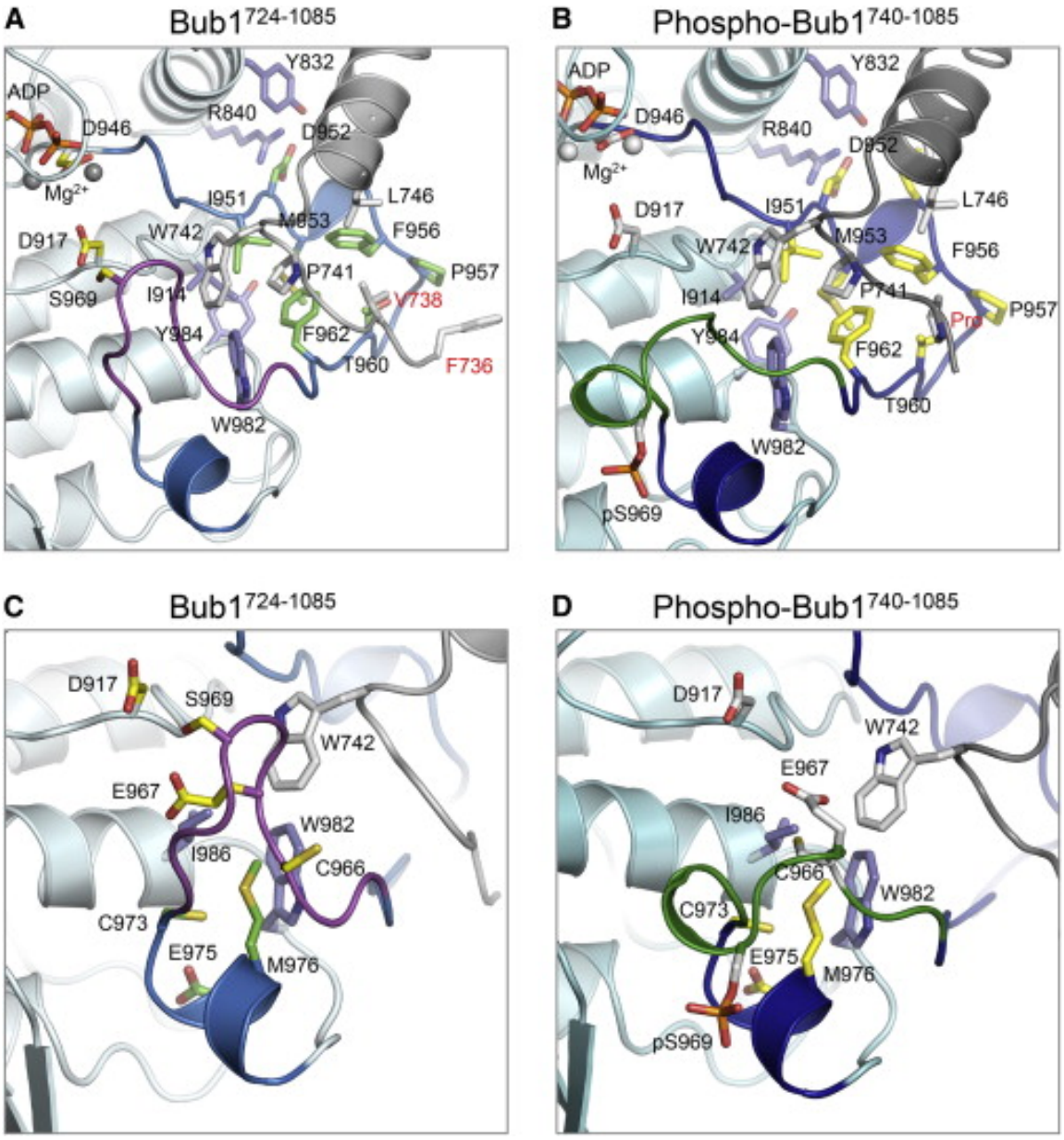

Figure 5. S969 phosphorylation reorganizes the P+1 loop through introducing electrostatic repulsion. (A and B) Zoomed in views of ribbon diagrams of unphosphorylated Bub1$^{724–1085}$ and phosphorylated Bub1$^{740–1085}$ with residues in the N-terminal half of the activation segment and their interacting residues shown in sticks. Color schemes are the same as in Figure 2. F736 and V738 (red labels) in Bub1$^{724–1085}$ are replaced by a proline introduced by the cloning sites in Bub1$^{740–1085}$. **(C and D)** Zoomed in views of ribbon diagrams of unphosphorylated Bub1$^{724–1085}$ and phosphorylated Bub1$^{740–1085}$, with residues in the C-terminal half of the activation segment and their interacting residues shown in sticks. (Figure 5 from Zhonghui Lin)

Bub1 S969 phosphorylation is required for H2A phosphorylation in human cells

To test whether Bub1 S969 phosphorylation was required for Bub1-dependent H2A phosphorylation in human cells, we created HeLa cell lines that stably expressed RNAi-resistant GFP-Bub1 WT or mutants at comparable levels. In HeLa cells depleted of endogenous Bub1 with RNAi, expression of GFP-Bub1 WT, but not the kinase-dead mutant D946N, restored H2A-pT120 levels in mitotic cell lysates (Figure 6A) and on mitotic kinetochores (Figures 6B and 6C). Expression of GFP-Bub1 S969A did not efficiently restore H2A-pT120 in Bub1 RNAi cells, whereas expression of GFP-Bub1 S969D did. Consistent with the role of H2A-pT120 in enriching Sgo1 at centromeres (Kawashima et al., 2010 and Liu et al., 2013a), cells expressing Bub1 S969A had reduced Sgo1 staining at centromeres (Figure 7). These results strongly suggest that S969 phosphorylation of Bub1 is critical for H2A-T120 phosphorylation by Bub1 in human cells. GFP-Bub1 ΔTPR fully supported H2A-T120 phosphorylation and centromeric localization of Sgo1 (Figures 6 and 7), again indicating that the TPR domain of Bub1 is dispensable for its kinase activity.

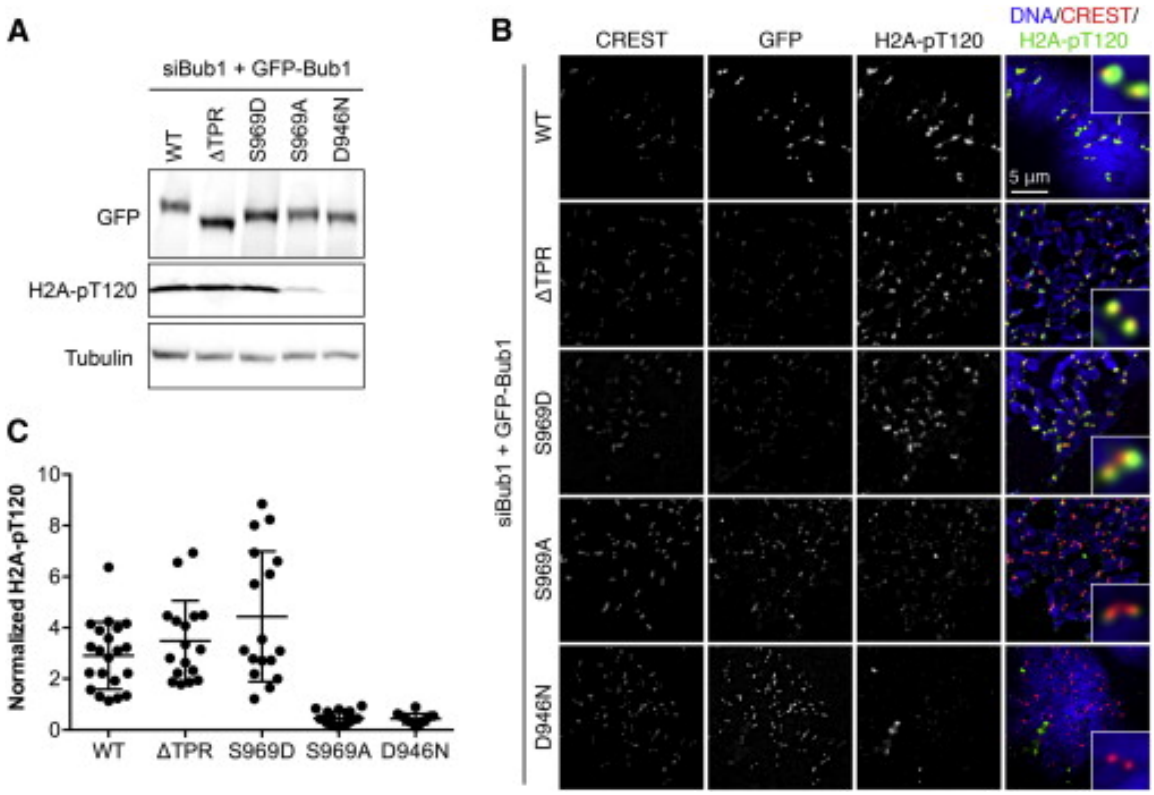

Figure 6. Bub1 S969 phosphorylation is required for H2A-pT120 in human cells. (A) HeLa cells stably expressing the indicated GFP-Bub1 proteins were transfected with siBub1 and arrested in mitosis. Cell lysates were blotted with the indicated antibodies. **(B)** Cells in **(A)** were stained with DAPI (blue in overlay), CREST (red), GFP, or H2A-pT120 (green). Selected regions were magnified in insets. **(C)** Quantification of the normalized kinetochore H2A-pT120 signals of cells in **(B)**.

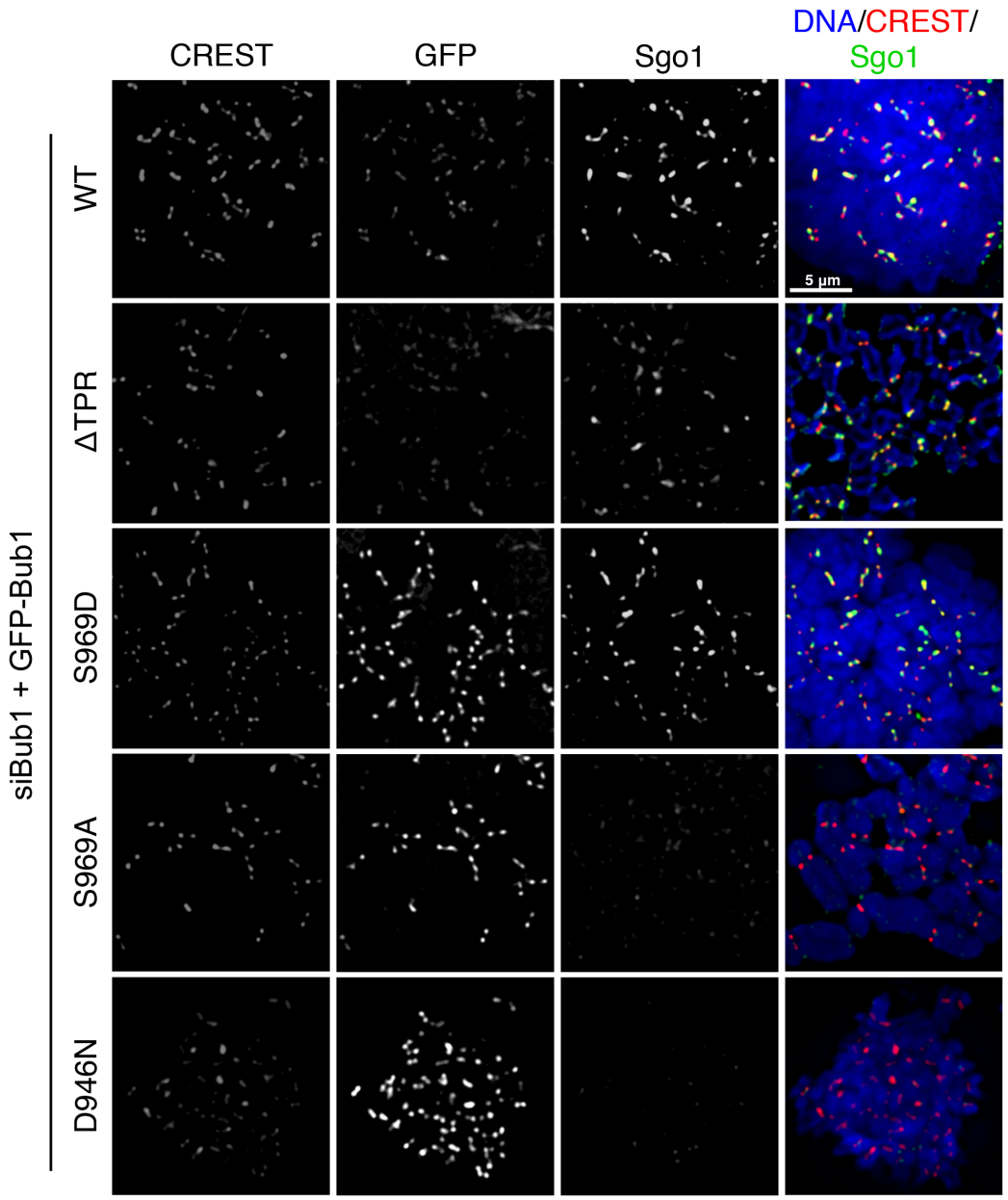

Figure 7. Bub1 S969 phosphorylation is required for centromeric targeting of Sgo1. Mitotic HeLa cells stably expressing the indicated GFP-Bub1 proteins were transfected with siBub1 and stained with DAPI (blue in overlay), CREST (red), GFP, and Sgo1 (green).

Bub1 S969 phosphorylation is constitutive during the cell cycle

H2A-pT120 is enriched at kinetochores only during mitosis, but not in interphase (Kawashima et al., 2010). We tested whether Bub1-pS969 levels were elevated during mitosis. Unexpectedly,

we found that pS969 signals of endogenous Bub1 immunoprecipitated from mitotic (nocodazole-arrested) or G1/S (thymidine-arrested) cells did not change appreciably (Figure 8A). Likewise, inactivation of the spindle checkpoint with the Aurora kinase inhibitor ZM447439 in cells treated with taxol and the proteasome inhibitor MG132 did not reduce pS969 signals of ectopically expressed GFP-Bub1 (Figure 8B). Consistently, pS969 signals of GFP-Bub1 did not change during mitotic exit following nocodazole-arrest release (Figure 8C). These results indicate that Bub1 S969 phosphorylation is not regulated during the cell cycle. This finding is consistent with the fact that Myc-Bub1 proteins isolated from cells in different cell cycle stages have similar kinase activities (Figure 1).

We then tested whether any of known Bub1-interacting proteins regulated S969 phosphorylation (Figure 8D). HeLa cells were depleted of Knl1, BubR1, or Bub3 with siRNAs. We co-depleted Cdc20 from these checkpoint-deficient cells to block them in mitosis. Bub1-pS969 signals remained unchanged in all samples. Thus, binding of Knl1, Bub3, or BubR1 to Bub1 is not required for Bub1 S969 phosphorylation.

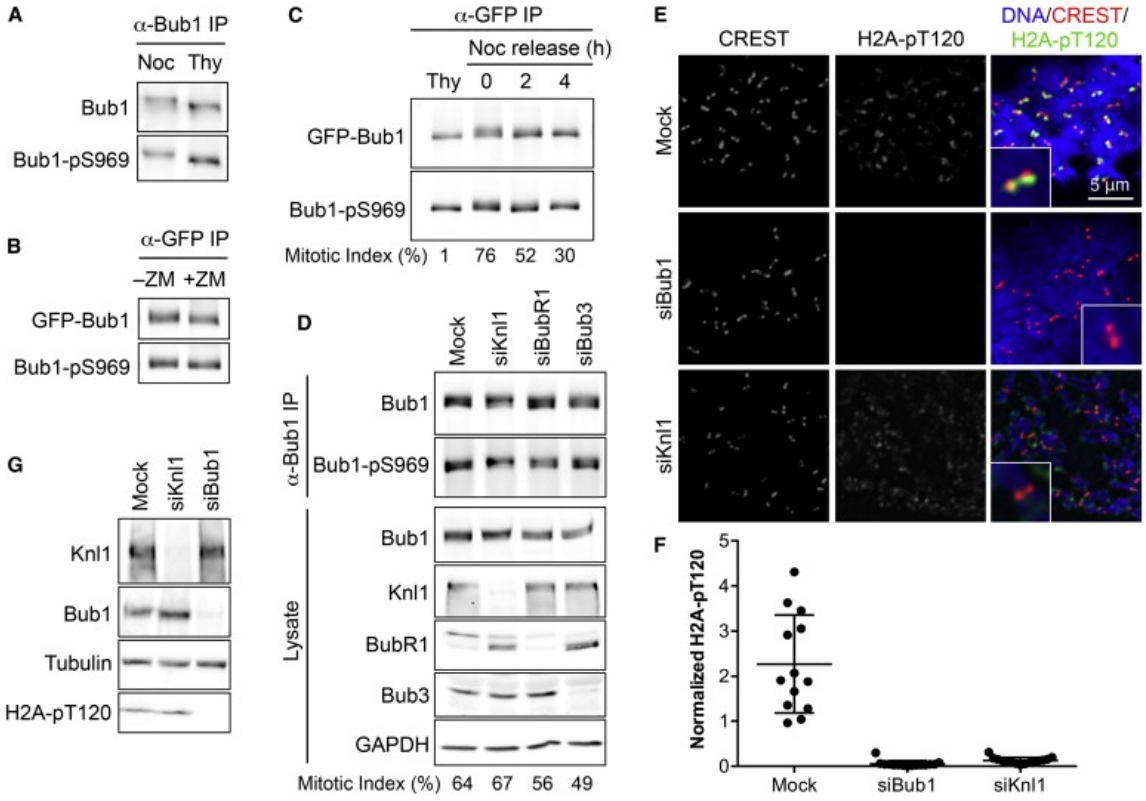

Figure 8. H2A-pT120 accumulation at mitotic kinetochores relies on kinetochore targeting of constitutively active Bub1. (A) Endogenous Bub1 was IPed from nocodazole (Noc) or thymidine (Thy) arrested HeLa cells and blotted with anti-Bub1 or Bub1-pS969 antibodies. **(B)** HeLa cells stably expressing GFP-Bub1 were treated with taxol and MG132 in the absence (−) or presence (+) of ZM447439 (ZM). The anti-GFP IP was blotted with GFP or Bub1-pS969 antibodies. **(C)** HeLa cells stably expressing GFP-Bub1 were treated with thymidine (Thy) or released from nocodazole arrest for the indicated durations. The mitotic index of each sample was shown at the bottom. The anti-GFP IP was blotted with GFP or Bub-pS969 antibodies. **(D)** HeLa cells were transfected with the indicated siRNAs and blocked in mitosis with Cdc20 depletion. The lysates and anti-Bub1 IP were blotted with the indicated antibodies. **(E)** Mitotic HeLa cells mock depleted or depleted of Bub1 or Knl1 were stained with DAPI (blue in overlay), CREST (red), and H2A-pT120 (green). Selected regions were magnified and shown in insets. **(F)** Quantification of the normalized kinetochore H2A-pT120 signals of cells in **(E)**. **(G)** Lysates of cells in **(E)** were blotted with the indicated antibodies.

Kinetochore targeting of Bub1 is required for enriching H2A-pT120 at mitotic kinetochores

Because Bub1 S969 phosphorylation is not elevated during mitosis, increased Bub1 activation during mitosis does not underlie the mitosis-specific enrichment of H2A-pT120 at kinetochores. Bub1 only localizes to kinetochores during mitosis, and this localization relies on the kinetochore scaffolding protein Knl1 (Kiyomitsu et al., 2007, Krenn et al., 2014, Primorac et al., 2013, Vleugel et al., 2013, Yamagishi et al., 2012 and Zhang et al., 2014). We next examined whether the Knl1-dependent kinetochore targeting of Bub1 was required for the kinetochore enrichment of H2A-pT120. As expected, depletion of Bub1 abolished H2A-pT120 signals in mitotic cells, including those at kinetochores (Figures 8E and 8F). Depletion of Knl1 abolished the kinetochore H2A-pT120 signals (Figures 8E and 8F), without reducing the total H2A-pT120 signals in cell lysates (Figure 8G). Consistently, H2A-pT120 staining at other chromosome regions was increased in Knl1 RNAi cells (Figure 8E). Thus, the kinetochore targeting of Bub1 is responsible for enriching H2A-pT120 at kinetochores during mitosis.

Bub1 S969 phosphorylation occurs through intramolecular autophosphorylation

Recombinant human Bub1 WT, but not the kinase-dead mutant D946N, purified from insect cells was phosphorylated at S969, indicating that Bub1 could undergo autophosphorylation at this site (Figure 1E). Consistently, Bub1 D946N expressed in human cells had no detectable S969 phosphorylation with or without the depletion of the endogenous Bub1 (Figure 9A). In contrast, when expressed in human cells, another kinase-dead mutant D917N still had detectable, albeit reduced, S969 phosphorylation (Figures 1F and 9A). S969 phosphorylation of Bub1 D917N was unlikely mediated by the endogenous Bub1 in human cells, as depletion of Bub1 did

not reduce this phosphorylation (Figure 9A). Moreover, recombinant purified Bub1 D917N retained about 30% S969 phosphorylation, whereas D946N had no detectable pS969 signals (Figure 9B).

The different behaviors of the two kinase-dead Bub1 mutants, D946N and D917N, in supporting S969 phosphorylation were unexpected. D946 coordinates Mg^{2+} ions and is required for ATP binding (Figure 9C). D917 acts as the catalytic base to deprotonate the hydroxyl group in substrates, thus promoting γ phosphate transfer. The D946N mutant cannot bind ATP, whereas D917N is expected to retain ATP binding but cannot transfer the γ phosphate to substrates. The fact that Bub1 D946N does not have pS969 signals clearly indicates that S969 phosphorylation occurs through either intermolecular or intramolecular autophosphorylation, as opposed to through another kinase. Because D917N retains ATP binding, it may still support S969 phosphorylation to some degree, provided that the γ phosphate transfer to S969 does not strictly require D917.

Activation of many kinases involves the autophosphorylation of their activation loop (Nolen et al., 2004). These autophosphorylation events have generally been thought to occur through an intermolecular (or trans) mechanism, in which two molecules of the same kinase phosphorylates each other (Figure 9D). Recent studies have shown that certain kinases can undergo intramolecular autophosphorylation (Dodson et al., 2013 and Hu et al., 2013). The structural basis of such a transfer has not been established, however. As discussed above, our unphosphorylated Bub1 structure contains ADP and a second Mg^{2+} ion with three bound water molecules at the site normally occupied by the γ phosphate. The Mg^{2+} and water molecules might serve as a mimic of the γ phosphate, similar to AlF_4^-. S969 in the unphosphorylated Bub1 lies in close proximity to and points toward D917 and the second Mg^{2+} ion bound at the

active site. It is poised to accept the phosphate group from ATP. This conformation of Bub1 is thus compatible for an intramolecular phosphate transfer from ATP to S969.

In the current conformation, the distance between the Mg^{2+} ion (as a putative γ phosphate mimic) and the hydroxyl group of S969 is too far for phosphate transfer. On the other hand, the B factors of the P+1 loop are substantially higher than those of the rest of the protein. The presumed high mobility of this loop might allow S969 to transiently engage the catalytic site and enable phosphate transfer. We note that even though Bub1 was crystalized in the presence of ATP the structures of both phosphorylated and unphosphorylated Bub1 contained ADP at their active site, presumably because Bub1 had measurable ATPase activity in the absence of substrates (Figure 10A). This ATPase activity might compete with and limit the extent of Bub1 autophosphorylation.

Next, we expressed and purified two different human Bub1 fragments containing the kinase domain, $Bub1^{740–1085}$ and $Bub1^{527–1085}$, from insect cells. Both fragments underwent S969 phosphorylation (Figure 9E). Phosphatase treatment greatly reduced pS969 signals of $Bub1^{740–1085}$. Incubation of dephosphorylated $Bub1^{740–1085}$ with ATP restored the pS969 signal. As shown above, $Bub1^{740–1085}$ D946N could not undergo S969 phosphorylation. Importantly, active $Bub1^{527–1085}$ could not phosphorylate the kinase-dead $Bub1^{740–1085}$ D946N at S969, indicating that intermolecular Bub1 autophosphorylation was inefficient. This finding was consistent with the fact that ectopically expressed Bub1 D946N was not phosphorylated by the endogenous Bub1 in human cells (Figure 9A). Moreover, the extent of Bub1 S969 phosphorylation in vitro was relatively insensitive to the concentration of Bub1 (Figure 10B), a phenomenon expected of intramolecular reactions. In contrast, T180 phosphorylation at the activation loop of the kinase Mst2 (which was known to undergo intermolecular autophosphorylation) was greatly reduced at

lower kinase concentrations (Ni et al., 2013). On the other hand, we cannot exclude the possibility that λ phosphatase was not completely inactivated, and Mst2-pT180 was a much better substrate for the phosphatase. Collectively, these results suggest that Bub1 might undergo intramolecular autophosphorylation at S969.

Finally, we tested whether the residual S969 phosphorylation in Bub1 D917N mutant was mediated by E967, which was located near S969 (Figure 9C). Although the E967Q mutation slightly reduced S969 phosphorylation, it did not reduce the residual S969 phosphorylation in the D917N mutant (Figure 9B). Thus, E967 is not responsible for S969 phosphorylation in the kinase-dead D917N mutant. Interestingly, the D917N/E967Q double mutant completely lacked ATPase activity (Figure 10A), indicating that the autophosphorylation and ATPase activities of Bub1 can be uncoupled.

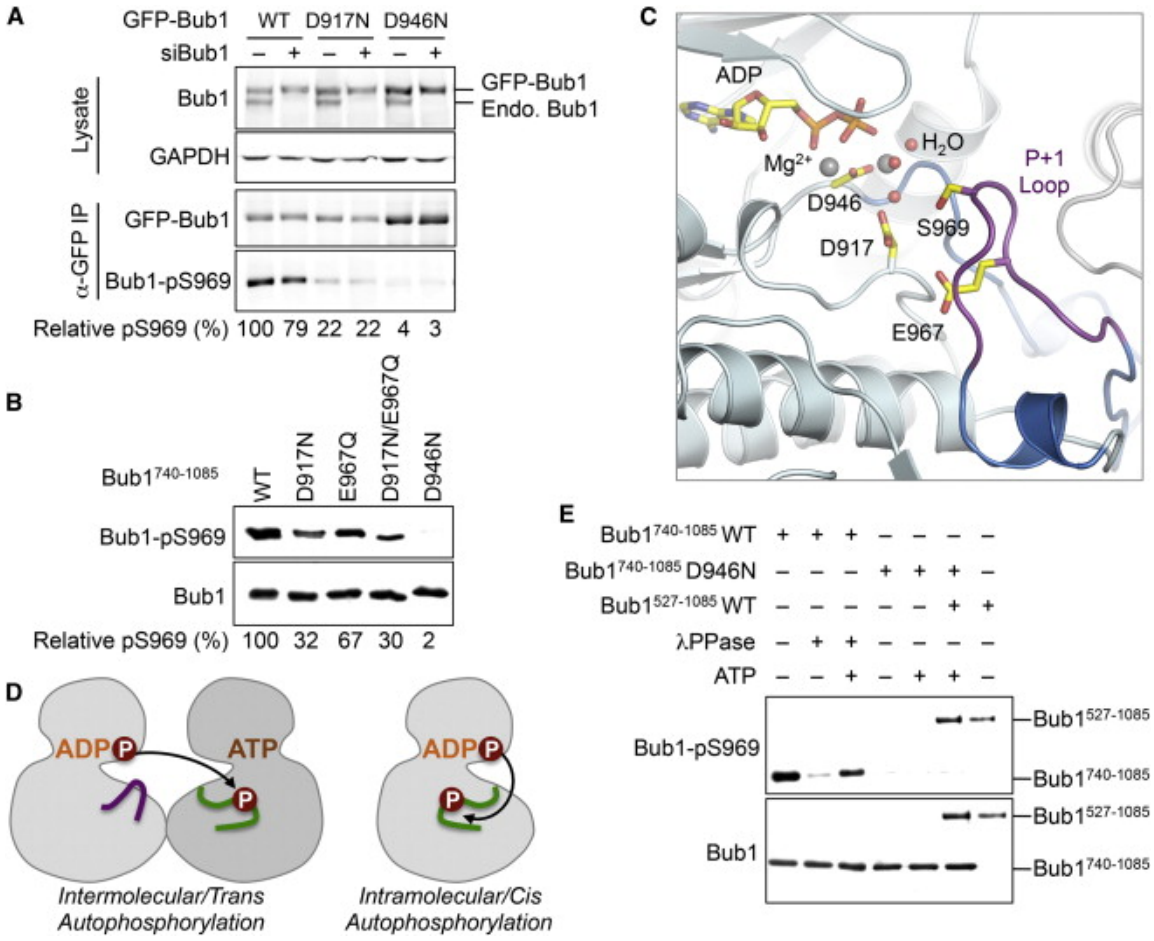

Figure 9. Bub1 S969 phosphorylation occurs through intramolecular auto-phosphorylation. (A) HeLa cells stably expressing the indicated GFP-Bub1 proteins were transfected with (+) or without (−) siBub1 and arrested in mitosis. The total lysates and GFP IP were blotted with the indicated antibodies. The relative intensities of pS969 signals were shown below each sample. **(B)** The indicated recombinant purified Bub1$^{740–1085}$ proteins were blotted with anti-Bub1 and Bub1-pS969 antibodies. The relative intensities of pS969 signals were shown below each sample. **(C)** Ribbon diagram of the active site of unphosphorylated Bub1, with ADP and key residues in sticks. Mg^{2+} ions and water molecules are shown as gray and red spheres, respectively. Color scheme is the same as in Figure 3. **(D)** Schematic drawing of intermolecular and intramolecular autophosphorylation. **(E)** The indicated purified recombinant Bub1 proteins were incubated in the presence (+) or absence (−) of λ phosphatase or ATP. The reaction mixtures were blotted with anti-Bub1 or Bub1-pS969 antibodies. (Figure 9B, 9C, 9E from Zhonghui Lin)

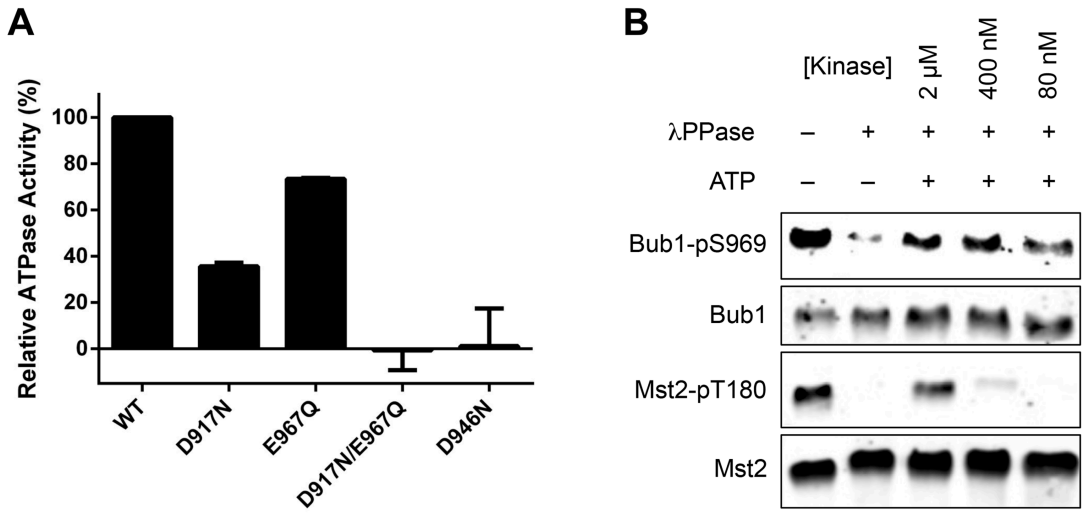

Figure 10. Bub1 S969 phosphorylation can be uncoupled from its ATPase activity and is insensitive to dilution. (A) The relative ATPase activities of the indicated recombinant purified Bub1$^{740\text{-}1085}$ proteins. The mean and standard deviations of two experiments are shown. **(B)** Recombinant human Bub1$^{740\text{-}1085}$ or the Mst2 kinase domain proteins were dephosphorylated by λ phosphatase. After the dephosphorylation reactions, phosphatase inhibitors were added to inactivate λ phosphatase. The reaction mixtures were further incubated with ATP at varying concentrations of the kinase. The same total amount of either kinase was loaded in each lane, and blotted with the indicated antibodies. (Figure 10 from Zhonghui Lin)

Discussion

We have discovered an autophosphorylation event in the activation segment of human Bub1 required for its activation toward histone H2A. This S969 phosphorylation has several unusual features. First, it occurs on the substrate-binding loop, not on the activation loop. Second, activation-loop phosphorylation typically activates the kinase through establishing favorable interactions between the phosphoresidue and a basic residue in the catalytic loop and inducing a disordered-to-ordered conformational transition of the activation loop (Nolen et al., 2004). In contrast, S969 phosphorylation of Bub1 reorganizes the P+1 loop through introducing

unfavorable interactions between the phosphoresidue and neighboring acid residues, including the catalytic aspartate. Third, S969 phosphorylation of Bub1 only stimulates its activity toward H2A but has no effect on its activity toward Cdc20. This substrate-specific activation is unusual. Finally, our structural and biochemical analyses suggest that the activating phosphorylation of Bub1 occurs through an intramolecular reaction and that this reaction does not strictly require the catalytic aspartate. Although intramolecular autophosphorylation has been reported for certain kinases (Dodson et al., 2013 and Hu et al., 2013), our structure of unphosphorylated Bub1 provides the first glimpse of how this intramolecular reaction might proceed.

It is surprising that Bub1 S969 phosphorylation does not strictly require the catalytic aspartate, D917. This suggests that Bub1 uses a non-canonical mechanism for catalysis, at least in the context of autophosphorylation. We initially suspected a neighboring glutamate performing the catalytic functions in the absence of D917, but this was not the case. Because the D946N mutation completely abolishes S969 phosphorylation, it is possible that D946 performs the catalytic function in addition to its known roles in coordinating Mg^{2+} and facilitating ATP binding. Alternatively, the many unique features of Bub1 enable it to undergo cis autophosphorylation to some degree without a catalytic residue. It will be interesting to test whether intramolecular autophosphorylation events in other kinases can also occur in the absence of a catalytic base.

Active kinases contain an internal, spatial motif termed the regulatory (R) spine, which is formed by nonconsecutive hydrophobic residues (Taylor and Kornev, 2011). Both unphosphorylated and pS969 Bub1 have a well-formed R spine (Figures 11A and 4), even though the residues that make up the R spine in Bub1 are different from those in other kinases, such as PKA. Thus, Bub1 is a constitutively active kinase. S969 phosphorylation only enhances

its activity toward H2A, but is not required for all of its activities, including autophosphorylation and phosphorylation of Cdc20.

The kinase RAF undergoes dimerization-dependent autophosphorylation (Hu et al., 2013). In the dimer, one kinase molecule (termed the activator) allosterically activates the other (termed the receiver), which undergoes intramolecular autophosphorylation (Figure 11B). We do not have evidence that dimerization of the Bub1 kinase domain is involved in its autophosphorylation. Unlike RAF, the kinase domain of Bub1 is monomeric in solution. The apparent molecular weight based on gel filtration chromatography is 43 kDa (Figure 11C), whereas the calculated molecular weight of the Bub1 kinase domain is 41 kDa. A crystal contact involving the C-terminal helix of Bub1 exists in both the unphosphorylated and phosphorylated structures, but it is not immediately apparent how this contact could be required for Bub1 activation. More importantly, our previous work on the unphosphorylated Bub1 has established the importance of the N-terminal extension in the activity of Bub1 (Kang et al., 2008). This extension restricts the movement of the αC helix and promotes the formation of the R spine and hence the active conformation of the kinase. Thus, our results favor the possibility that Bub1 undergoes unassisted, intramolecular autophosphorylation (Figure 11B), without the need for allosteric activation from another Bub1 molecule, at least in the context of the isolated Bub1 kinase domain.

Bub1 installs the H2A-pT120 mark at mitotic kinetochores, which recruits Sgo1-PP2A to centromeres to protect centromeric cohesion. The H2A-pT120 mark is not enriched at kinetochores in interphase cells. On the other hand, Bub1 S969 phosphorylation is not regulated during the cell cycle and is not influenced by known Bub1-binding proteins. Consistent with the constitutive nature of S969 phosphorylation, the budding yeast Bub1 has an aspartate, instead of

a serine, at that position (Figure 1B). The mitosis-specific enrichment of H2A-pT120 at kinetochores is thus not caused by enhanced Bub1 autophosphorylation and activation, but is instead controlled by mitosis-specific targeting of already activated Bub1 to kinetochores. Indeed, recent studies have established an elaborate mechanism for targeting Bub1 to kinetochores specifically during mitosis, which involves the binding of Bub1–Bub3 to Mps1-dependent phosphomotifs in Knl1 (Kiyomitsu et al., 2007, Krenn et al., 2014, Primorac et al., 2013, Vleugel et al., 2013, Yamagishi et al., 2012 and Zhang et al., 2014).

In conclusion, this study provides structural and functional insights into the regulation of the key mitotic kinase Bub1 and highlights a mode of substrate-specific kinase activation through intramolecular autophosphorylation of the substrate-binding loop.

Materials and methods

Protein expression and purification

The Bub1 kinase domain (residues 740–1085) was expressed and purified essentially as described (Kang et al., 2008). Briefly, Sf9 cells infected with the human Bub1 baculovirus were harvested at 48 hr after infection and lysed by sonication. His_6-$Bub1^{740–1085}$ was purified with the Ni^{2+}-NTA resin (QIAGEN) and incubated with tobacco etch virus protease and 1 mM ATP overnight at 4°C. Phosphorylated $Bub1^{740–1085}$ was further purified with resource S and Superdex 200 columns (GE Healthcare). $Bub1^{740–1085}$ mutants were expressed and purified similarly. The purified $Bub1^{740–1085}$ was further incubated with 10 mM ATP in the storage buffer (20 mM Tris-HCl [pH 7.7], 150 mM NaCl, 10 mM MgCl2, 10 mM DTT) for 30 min at room temperature and was concentrated to 6 mg/ml for crystallization.

Crystallization, data collection, and structure determination

The Bub1$^{740–1085}$ crystals were grown at 20°C with the hanging drop method by mixing equal volumes of the protein solution with the precipitant solution (20% PEG3350, 1% tryptone, 10 mM dithiothreitol (DTT), 0.1 M 2-[4-(2-hydroxyethyl)piperazin-1-yl]ethanesulfonic acid [HEPES] [pH 7.0]). Crystals grew to full size in 2 days. For X-ray data collection, crystals were transferred to a cryoprotectant solution containing 15% MPD, 22% PEG3350, and 0.1 M HEPES (pH 7.0) and were flash frozen in a liquid nitrogen stream. The crystal diffracted to a minimum Bragg's spacing of 2.20 Å and exhibited the symmetry of space group of P21 with cell dimensions of a = 90 Å, b = 47 Å, c = 93 Å, β = 107°. Diffraction data were collected at 19-ID (SBC-CAT) at the Advanced Photon Source (Argonne National Laboratory) and processed with HKL3000 (Minor et al., 2006).

Phase for Bub1$^{740–1085}$ was obtained by molecular replacement with Phaser using the coordinates of unphosphorylated Bub1 (PDB code: 3E7E) as the initial search model (McCoy, 2007). Iterative model building and refinement were performed with COOT and Phenix (Adams et al., 2010 and Emsley and Cowtan, 2004). The final model of Bub1$^{740–1085}$ (Rwork = 22.9%, Rfree = 26.8%) contained two molecules per asymmetric unit. Each molecule has 331 residues, one ADP, two Mg^{2+} ions, one Cl^{-} ion, and 237 water molecules. The structure has good geometry with 95.8% residues in most favored regions of the Ramachandran plot, 4.2% in the allowed region, and none in the disallowed region, as defined by MolProbity (Chen et al., 2010).

Cell culture and transfection

HeLa Tet-On cells (Invitrogen) were maintained in Dulbecco's modified Eagle's medium (Invitrogen) supplemented with 10% fetal bovine serum (Invitrogen), 10 mM l glutamine

(Invitrogen), and 100 μg/ml penicillin and streptomycin (Invitrogen). To arrest cells at G1/S, cells were treated with 2.5 mM thymidine for 18 hr. To arrest cells in mitosis, cells released from thymidine for 7 hr were treated with 2.5 μM nocodazole or 200 nM Taxol for another 7–8 hr. To inactivate the spindle checkpoint while keeping cells in mitosis, the Aurora kinase inhibitor ZM447439 (4 μM; Selleck Chemicals) and MG132 (10 μM; Boston Biochem) were added to Taxol-treated cells for 1.5 hr.

Plasmid transfection was performed with the Effectene reagent (QIAGEN) following the manufacturer's protocols. GFP-Bub1 WT or mutant stable cell lines were made by transfecting HeLa Tet-On cells with pTRE2-GFP-Bub1 WT or mutant plasmids and selecting resistant colonies with 300 μg/ml hygromycin (Clontech). Single clones were picked and screened for inducible expression of GFP-Bub1 proteins in the presence of 1 μg/ml doxycycline (Clontech).

For RNAi experiments, HeLa Tet-On cells were transfected with 5 nM siRNA using Lipofectamine RNAiMax (Invitrogen) and were harvested at 48–60 hr after transfection. The siRNA oligonucleotides for Bub1, Knl1, BubR1, and Bub3 were purchased from Thermo Scientific. The sequences of these siRNAs are siBub1c, CCCAUUUGCCAGCUCAAGCdTdT; siKnl1, GGAAAUAGAUAACGAAAGU; siBubR1, CAAGAUGGCUGUAUUGUUU; and siBub3, CAAGCAGGGUUAUGUAUUA. The Cdc20 siRNA was purchased from Ambion (Silencer Select Pre-designed siRNA, ID s2748).

Antibodies, immunoblotting, and immunoprecipitation

Antibodies against Bub1, Cdc20, BubR1, and H2A-pT120 were described previously (Liu et al., 2013a and Tang et al., 2001). The α-Cdc20-pS153 antibody was made in an in-house facility by immunizing rabbits with a Cdc20-pS153 containing peptide coupled to hemocyanin (Sigma).

The α-Bub1-pT968/pS969 antibody was produced in the same facility with a mixture of a pT968-containing peptide and a pS969-containing peptide. The α-Bub1-pS969 antibody was subsequently purified with beads immobilized with the pS969 peptide. The following antibodies were purchased from the indicated sources: mouse α-Myc (9E10; Roche), mouse α-H2A (L8846; Cell Signaling), mouse α-tubulin (DM1A; Sigma-Aldrich), mouse α-GAPDH (6C5; Milipore), and CREST (ImmunoVision). For quantitative immunoblotting, α-rabbit immunoglobulin G (IgG) (H+L) (Dylight 800 conjugates) and α-mouse IgG (H+L) (Dylight 680 conjugates) (Cell Signaling) were used as secondary antibodies. The blots were scanned and quantified with the Odyssey Infrared Imaging System (LI-COR).

For IP, antibodies against Myc, Bub1, or GFP were coupled to Affi-Prep Protein A beads (Bio-Rad) at a concentration of 1 mg/ml. Cells were lysed with the lysis buffer (50 mM Tris-HCl [pH 7.7], 120 mM KCl, 0.1% NP-40, 5 mM NaF, 0.3 mM Na_3VO_4, 10 mM β-glycerophosphate, 0.5 μM okadaic acid, 1 mM DTT) supplemented with protease inhibitor tablets (Sigma-Aldrich) and Turbo-nuclease (Accelagen). After 20 min incubation on ice, the lysate was cleared by centrifugation. The supernatant was incubated with the antibody-coupled protein A beads for 2 hr at 4°C. After washing, the beads were boiled in SDS sample buffer and analyzed by SDS-PAGE followed by immunoblotting.

Kinase assays

WT or mutant Bub1 proteins purified from Sf9 cells or immunoprecipitated from human cells were incubated with the kinase buffer (50 mM Tris-HCl [pH 7.7], 100 mM NaCl, 10 mM $MgCl_2$, 5 mM NaF, 0.1 mM Na_3VO_4, 20 mM β-glycerophosphate, 1 mM DTT) for 15 or 30 min at

room temperature or 30° C with 1 μg recombinant Cdc20 protein or 6 μg bulk histones from calf thymus (Sigma-Aldrich) in 20 μl Kinase Buffer supplemented with 100 μM ATP. The reaction mixtures were quenched with SDS sample buffer and analyzed by SDS-PAGE followed by Cdc20-pS153 or H2A-pT120 blotting.

For autophosphorylation experiments, Bub1 proteins purified from Sf9 cells were treated with λ phosphatase (New England Biolabs) for 1 hr at 30° C. The phosphatase reactions were stopped by a buffer containing 5 mM Na_3VO_4, 10 mM NaF, and 20 mM β-glycerophosphate. The reaction mixture was then incubated with 0.1 mM ATP in kinase buffer for another 1 hr at 30°C and blotted with anti-Bub1-pS969.

Immunofluorescence

Mitotic cells were washed once with PBS and incubated with 75 mM KCl for 15 min at 37°C. After the hypotonic treatment, the cells were spun onto microscope slides with a Shandon Cytospin centrifuge. Cells were first extracted with PBS containing 0.2% Triton X-100 for 2 min and then fixed in 4% paraformaldehyde for 5 min. After washing three times with PBS containing 0.2% Triton X-100, the cells were incubated with primary antibodies in PBS containing 0.2% Triton X-100 and 3% BSA at 4°C for 10 hr. The cells were washed three times with PBS containing 0.2% Triton X-100 and incubated with fluorescent secondary antibodies (Molecular Probes) in PBS containing 0.2% Triton X-100 and 3% BSA for 1 hr at room temperature. The cells were again washed three times with PBS containing 0.2% Triton X-100 and stained with 1 μg/ml DAPI for 3 min. After the final washes with PBS, the slides were sealed and viewed using a 100× objective on a Deltavision microscope (Applied Precision). A

series of z stack images was captured at 0.2 μm intervals, deconvolved, and projected. Image processing and quantification were done with ImageJ.

Reference

Adams, P.D., Afonine, P.V., Bunkóczi,, G., Chen, V.B., Davis, I.W., Echols, N., Headd, J.J., Hung, L.W., Kapral, G.J., Grosse-Kunstleve, R.W., et al. (2010). PHENIX: a comprehensive Python-based system for macromolecular struc- ture solution. Acta Crystallogr. D Biol. Crystallogr. 66, 213–221.

Chen, V.B., Arendall, W.B., 3rd, Headd, J.J., Keedy, D.A., Immormino, R.M., Kapral, G.J., Murray, L.W., Richardson, J.S., and Richardson, D.C. (2010). MolProbity: all-atom structure validation for macromolecular crystallography. Acta Crystallogr. D Biol. Crystallogr. 66, 12–21.

Dodson, C.A., Yeoh, S., Haq, T., and Bayliss, R. (2013). A kinetic test charac- terizes kinase intramolecular and intermolecular autophosphorylation mecha- nisms. Sci. Signal. 6, ra54.

Emsley, P., and Cowtan, K. (2004). Coot: model-building tools for molecular graphics. Acta Crystallogr. D Biol. Crystallogr. 60, 2126–2132.

Foley, E.A., and Kapoor, T.M. (2013). Microtubule attachment and spindle as- sembly checkpoint signalling at the kinetochore. Nat. Rev. Mol. Cell Biol. 14, 25–37.

Hu, J., Stites, E.C., Yu, H., Germino, E.A., Meharena, H.S., Stork, P.J., Kornev, A.P., Taylor, S.S., and Shaw, A.S. (2013). Allosteric activation of functionally asymmetric RAF kinase dimers. Cell 154, 1036–1046.

Jia, L., Kim, S., and Yu, H. (2013). Tracking spindle checkpoint signals from ki- netochores to APC/C. Trends Biochem. Sci. 38, 302–311.

Kang, J., Yang, M., Li, B., Qi, W., Zhang, C., Shokat, K.M., Tomchick, D.R., Machius, M., and Yu, H. (2008). Structure and substrate recruitment of the hu- man spindle checkpoint kinase Bub1. Mol. Cell 32, 394–405.

Kawashima, S.A., Yamagishi, Y., Honda, T., Ishiguro, K., and Watanabe, Y. (2010). Phosphorylation of H2A by Bub1 prevents chromosomal instability through localizing shugoshin. Science 327, 172–177.

Kitajima, T.S., Hauf, S., Ohsugi, M., Yamamoto, T., and Watanabe, Y. (2005). Human Bub1 defines the persistent cohesion site along the mitotic chromo- some by affecting Shugoshin localization. Curr. Biol. 15, 353–359.

Kitajima, T.S., Sakuno, T., Ishiguro, K., Iemura, S., Natsume, T., Kawashima, S.A., and Watanabe, Y. (2006). Shugoshin collaborates with protein phospha- tase 2A to protect cohesin. Nature 441, 46–52.

Kiyomitsu, T., Obuse, C., and Yanagida, M. (2007). Human Blinkin/AF15q14 is required for chromosome alignment and the mitotic checkpoint through direct interaction with Bub1 and BubR1. Dev. Cell 13, 663–676.

Krenn, V., Wehenkel, A., Li, X., Santaguida, S., and Musacchio, A. (2012). Structural analysis reveals features of the spindle checkpoint kinase Bub1- kinetochore subunit Knl1 interaction. J. Cell Biol. 196, 451–467.

Krenn, V., Overlack, K., Primorac, I., van Gerwen, S., and Musacchio, A. (2014). KI motifs of human Knl1 enhance assembly of comprehensive spindle checkpoint complexes around MELT repeats. Curr. Biol. 24, 29–39.

Lara-Gonzalez, P., Westhorpe, F.G., and Taylor, S.S. (2012). The spindle as- sembly checkpoint. Curr. Biol. 22, R966–R980.

Liu, H., Jia, L., and Yu, H. (2013a). Phospho-H2A and cohesin specify distinct tension-regulated Sgo1 pools at kinetochores and inner centromeres. Curr. Biol. 23, 1927–1933.

Liu, H., Rankin, S., and Yu, H. (2013b). Phosphorylation-enabled binding of SGO1-PP2A to cohesin protects sororin and centromeric cohesion during mitosis. Nat. Cell Biol. 15, 40–49.

McCoy, A.J. (2007). Solving structures of protein complexes by molecular replacement with Phaser. Acta Crystallogr. D Biol. Crystallogr. 63, 32–41.

Minor, W., Cymborowski, M., Otwinowski, Z., and Chruszcz, M. (2006). HKL- 3000: the integration of data reduction and structure solution—from diffraction images to an initial model in minutes. Acta Crystallogr. D Biol. Crystallogr. 62, 859–866.

Ni, L., Li, S., Yu, J., Min, J., Brautigam, C.A., Tomchick, D.R., Pan, D., and Luo, X. (2013). Structural basis for autoactivation of human Mst2 kinase and its regulation by RASSF5. Structure 21, 1757–1768.

Nolen, B., Taylor, S., and Ghosh, G. (2004). Regulation of protein kinases; con- trolling activity through activation segment conformation. Mol. Cell 15, 661–675.

Primorac, I., Weir, J.R., Chiroli, E., Gross, F., Hoffmann, I., van Gerwen, S., Ciliberto, A., and Musacchio, A. (2013). Bub3 reads phosphorylated MELT re- peats to promote spindle assembly checkpoint signaling. eLife 2, e01030.

Ricke, R.M., Jeganathan, K.B., Malureanu, L., Harrison, A.M., and van Deursen, J.M. (2012). Bub1 kinase activity drives error correction and mitotic checkpoint control but not tumor suppression. J. Cell Biol. 199, 931–949.

Riedel, C.G., Katis, V.L., Katou, Y., Mori, S., Itoh, T., Helmhart, W., Ga´ lova´ , M., Petronczki, M., Gregan, J., Cetin, B., et al. (2006). Protein phosphatase 2A pro- tects centromeric sister chromatid cohesion during meiosis I. Nature 441, 53–61.

Tang, Z., Bharadwaj, R., Li, B., and Yu, H. (2001). Mad2-Independent inhibition of APCCdc20 by the mitotic checkpoint protein BubR1. Dev. Cell 1, 227–237.

Tang, Z., Shu, H., Oncel, D., Chen, S., and Yu, H. (2004a). Phosphorylation of Cdc20 by Bub1 provides a catalytic mechanism for APC/C inhibition by the spindle checkpoint. Mol. Cell 16, 387–397.

Tang, Z., Sun, Y., Harley, S.E., Zou, H., and Yu, H. (2004b). Human Bub1 pro- tects centromeric sister-chromatid cohesion through Shugoshin during mitosis. Proc. Natl. Acad. Sci. USA 101, 18012–18017.

Tang, Z., Shu, H., Qi, W., Mahmood, N.A., Mumby, M.C., and Yu, H. (2006). PP2A is required for centromeric localization of Sgo1 and proper chromosome segregation. Dev. Cell 10, 575–585.

Taylor, S.S., and Kornev, A.P. (2011). Protein kinases: evolution of dynamic regulatory proteins. Trends Biochem. Sci. 36, 65–77.

Vleugel, M., Tromer, E., Omerzu, M., Groenewold, V., Nijenhuis, W., Snel, B., and Kops, G.J. (2013). Arrayed BUB recruitment modules in the kinetochore scaffold KNL1 promote accurate chromosome segregation. J. Cell Biol. 203, 943–955.

Yamagishi, Y., Yang, C.H., Tanno, Y., and Watanabe, Y. (2012). MPS1/Mph1 phosphorylates the kinetochore protein KNL1/Spc7 to recruit SAC compo- nents. Nat. Cell Biol. 14, 746–752.

Yu, H. (2007). Cdc20: a WD40 activator for a cell cycle degradation machine. Mol. Cell 27, 3–16.

Zhang, G., Lischetti, T., and Nilsson, J. (2014). A minimal number of MELT re- peats supports all the functions of KNL1 in chromosome segregation. J. Cell Sci. 127, 871–884.

CHAPTER FOUR

THE BUB1-PLK1 KINASE COMPLEX PROMOTES SPINDLE CHECKPOINT SIGNALING THROUGH CDC20 PHOSPHORYLATION

Summary

The spindle checkpoint senses kinetochores not properly attached to spindle microtubules and inhibits the anaphase-promoting complex or cyclosome (APC/C) bound to its mitotic activator Cdc20 to delay anaphase, thereby preventing aneuploidy. A critical checkpoint inhibitor of APC/C^{Cdc20} is the mitotic checkpoint complex (MCC) consisting of BubR1–Bub3, Cdc20, and Mad2. It is unclear whether MCC suffices to inhibit all cellular APC/C. We show that human checkpoint kinase Bub1 not only directly phosphorylates Cdc20, but also scaffolds Plk1-mediated phosphorylation of Cdc20. Phosphorylation of Cdc20 by Bub1–Plk1 inhibits APC/C^{Cdc20} in vitro, and is required for checkpoint signaling in human cells. Bub1–Plk1-dependent Cdc20 phosphorylation requires upstream checkpoint signals, and is dispensable for MCC assembly. A phospho-mimicking Cdc20 mutant restores nocodazole-induced mitotic arrest in Mad2/BubR1-depleted cells. Thus, Bub1–Plk1-mediated phosphorylation of Cdc20 constitutes an APC/C-inhibitory pathway parallel to MCC formation. Both pathways cooperate to sustain mitotic arrest in response to spindle defects.

Introduction

The spindle checkpoint ensures the fidelity of chromosome segregation during mitosis and meiosis (Gorbsky, 2014; Jia et al., 2013; London and Biggins, 2014b; Sacristan and Kops, 2015).

Chromosome missegregation during mitosis can result in aneuploidy, which is a hallmark of cancer cells and can promote tumorigenesis depending on context (Holland and Cleveland, 2012). For sister chromatids to be evenly partitioned into two daughter cells during mitosis, cells must not initiate the molecular program of sister-chromatid separation until all pairs of sister kinetochores attach to microtubules emanating from opposite spindle poles (bi-orientation). Unattached or improperly attached kinetochores recruit and activate checkpoint proteins to produce diffusible anaphase inhibitors, which inhibit the ubiquitin ligase activity of the anaphase-promoting complex/cyclosome (APC/C) bound to its mitotic activator Cdc20 (Chang and Barford, 2014; Sivakumar and Gorbsky, 2015; Yu, 2007). Inhibition of APC/C^{Cdc20} stabilizes its key substrates, securin and cyclin B1, and delays sister-chromatid separation and exit from mitosis. Among other mechanisms, proper microtubule attachment to kinetochores releases the checkpoint proteins and turns off the checkpoint (Gorbsky, 2014; Jia et al., 2013; London and Biggins, 2014b; Sacristan and Kops, 2015). APC/C^{Cdc20} then ubiquitinates securin and cyclin B1 to trigger their degradation, promoting the onset of anaphase and exit from mitosis.

Cdc20 activates APC/C in part through directly contributing to binding of APC/C degrons found in substrates, including the destruction (D) box, the KEN box, and the recently discovered Phe box (also called ABBA motif) (Buschhorn et al., 2011; Chang et al., 2014; da Fonseca et al., 2011; Di Fiore et al., 2015; Diaz-Martinez et al., 2015; Lu et al., 2014; Tian et al., 2012). The checkpoint proteins BubR1 and Mad2 can each independently inhibit APC/C^{Cdc20} using different mechanisms in vitro (Diaz-Martinez et al., 2015; Fang et al., 1998; Tang et al., 2001), and can collaborate to inhibit APC/C^{Cdc20} in vivo by forming the mitotic checkpoint complex (MCC) that consists of the constitutive BubR1–Bub3 complex, Cdc20, and Mad2 (Chao

et al., 2012; Sudakin et al., 2001). Unattached kinetochores promote the conformational activation of Mad2, which enables Mad2 binding to Cdc20 (Luo and Yu, 2008; Mapelli and Musacchio, 2007). The Mad2–Cdc20 complex then associates with BubR1–Bub3 at kinetochores to form MCC (Kulukian et al., 2009). MCC blocks substrate recruitment by APC/C^{Cdc20} in two ways: anchoring Cdc20 to a binding site on APC/C incompatible for substrate ubiquitination, and acting as a competitive inhibitor of substrate recruitment through D and KEN boxes of BubR1 (Chao et al., 2012; Diaz-Martinez et al., 2015; Herzog et al., 2009; Izawa and Pines, 2011, 2015; Lara-Gonzalez et al., 2011; Tian et al., 2012).

Kinetochore-enhanced MCC production is clearly required for APC/C^{Cdc20} inhibition during checkpoint signaling (Jia et al., 2013; London and Biggins, 2014b; Sacristan and Kops, 2015). It is less clear whether MCC as a stoichiometric inhibitor is sufficient to inhibit all cellular APC/C. We have previously shown that the checkpoint kinase Bub1 directly phosphorylates Cdc20 and inhibits APC/C^{Cdc20} (Tang et al., 2004), implicating the existence of other APC/C inhibitory mechanisms. On the other hand, the kinase activity of Bub1 is not strictly required for the spindle checkpoint in human cells (Kang et al., 2008; Klebig et al., 2009). Furthermore, in the mouse, the checkpoint functions of the Bub1 kinase activity have been attributed to mechanisms aside from Cdc20 phosphorylation (Ricke et al., 2012). The functional relevance of Bub1-dependent Cdc20 phosphorylation needs to be further clarified.

Plk1 is a cell cycle kinase with myriad functions, including spindle assembly and chromosome alignment (Archambault et al., 2015). Both Bub1 and BubR1 contain a STP motif that, when phosphorylated by Cdk1 in mitosis, binds to the polo-box domain of Plk1 (Elowe et al., 2007; Qi et al., 2006). Plk1 phosphorylates the KARD motif of BubR1 to enable PP2A binding (Suijkerbuijk et al., 2012). BubR1–Plk1-dependent recruitment of PP2A to kinetochores

promotes chromosome alignment at metaphase (Suijkerbuijk et al., 2012). The Bub1–Plk1 interaction recruits a population of Plk1 to kinetochores (Qi et al., 2006), but the functional substrate of Bub1–Plk1 at kinetochores remains to be identified.

In this study, we show that, in addition to directly phosphorylating Cdc20, the non-kinase domains of Bub1 bind to both Plk1 and Cdc20, thus providing a scaffold for Cdc20 phosphorylation by Plk1. Phosphorylation of Cdc20 by the Bub1–Plk1 kinase complex inhibits APC/C^{Cdc20} in vitro, and is required for and regulated by checkpoint signaling in human cells, but is dispensable for MCC formation. A Cdc20 mutant mimicking a major Plk1 phosphorylation event rescues the checkpoint defects of cells partially depleted of Mad2 or BubR1. Our study extends the scaffolding roles of the checkpoint kinase Bub1, and establishes Cdc20 phosphorylation by Bub1–Plk1 as a critical mechanism that acts in parallel to MCC formation to inhibit APC/C^{Cdc20} in the spindle checkpoint.

Results

Plk1 is required for the spindle checkpoint in human cells with partial depletion of Bub1

Bub1 is a well-established, critical component of the spindle checkpoint. However, it was exceedingly difficult to produce checkpoint defects in human cells depleted of Bub1 with RNA interference (RNAi) (Figure 2A). Only Bub1 siRNA-d (initially reported by Meraldi and coworkers) produced checkpoint defects (Klebig et al., 2009). Multiple other Bub1 siRNAs failed to produce checkpoint defects, despite their ability to deplete Bub1 as efficiently as did Bub1 siRNA-d (Figure 2B). The checkpoint defects caused by Bub1 siRNA-d were rescued by an RNAi-resistant Bub1 transgene, indicating that the effects of this siRNA were Bub1-dependent (Klebig et al., 2009) (Figure 2C). Based on quantitative RT-PCR, Bub1 siRNA-d

depleted Bub1 mRNA slightly more efficiently than siRNA-b and siRNA-c (Figure 2D). Thus, it is possible that only siRNA-d depleted Bub1 to a level below the threshold required for checkpoint signaling. Alternatively, in addition to depleting Bub1, siBub1d might have depleted other proteins that cooperated with Bub1 in the checkpoint. Regardless, these results indicate that a small amount of Bub1 is sufficient to support the spindle checkpoint. The fact that partial depletion of Bub1 does not produce checkpoint defects afforded us an opportunity to identify other regulators that collaborate with Bub1 to sustain the checkpoint.

Inactivation or partial depletion of several important mitotic regulators, including Aurora B, Ndc80, and Plk1, does not cause cells to escape from nocodazole-triggered mitotic arrest (Kim and Yu, 2015; Santaguida et al., 2011; Saurin et al., 2011; Sumara et al., 2004), despite their known roles in regulating checkpoint proteins. We thus tested whether their inactivation synergized with Bub1 siRNA-b or siRNA-c to override the mitotic arrest exerted by nocodazole. Consistent with previous studies (Kim and Yu, 2015; Santaguida et al., 2011; Saurin et al., 2011), inhibition of Aurora B with ZM44739 synergized with depletion of Ndc80 to produce strong checkpoint defects in HeLa cells (Figure 1B), validating the approach. Inhibition of Aurora B or depletion of Ndc80 did not synergize with Bub1 depletion by siRNA-c to produce checkpoint defects. Addition of the Plk1 inhibitor BI2536 to cells transfected with Bub1 siRNA-c and arrested in nocodazole caused them to undergo mitotic exit (Figure 1B). Because BI2536 had other molecular targets aside from Plk1 in human cells (Ciceri et al., 2014), we tested another Plk1 inhibitor GSK461364 in this assay. GSK461364 also produced strong checkpoint defects in cells transfected with Bub1 siRNA-c (Figure 1C). Without Bub1 depletion, BI2536 or GSK461364 alone caused mitotic arrest in the absence of nocodazole (Figure 2E), and did not cause escape from nocodazole-mediated mitotic arrest (Figure 1B and 1C). Bub1 depletion and

BI2536 treatment also caused HeLa cells to escape from taxol-induced mitotic arrest (Figure 2F). BI2536 also synergized with Bub1 siRNA-b to produce checkpoint defects in HeLa cells (Figure 2G). Similar synergy between Plk1 inhibition by BI2536 and Bub1 depletion by siRNA-b or siRNA-c was also observed in U2OS cells (Figure 2G). Therefore, our results reveal a critical role of Plk1 in the spindle checkpoint. Bub1 and Plk1 cooperate to maintain checkpoint-dependent mitotic arrest exerted by spindle poisons. The checkpoint becomes dependent on the kinase activity of Plk1 in cells with a compromised Bub1 function.

To understand the mechanism by which Bub1 and Plk1 collaborated to promote checkpoint signaling, we tested whether the kinase activity of Bub1 was involved in this cooperation. Unlike Bub1 depletion, inhibition of the kinase activity of Bub1 with 2OH-BNPP1 did not synergize with Plk1 inhibition to produce strong checkpoint defects in HeLa cells (Kang et al., 2008) (Figure 1D). 2OH-BNPP1 effectively inhibited the kinase activity of Bub1 in these cells, as evidenced by the greatly reduced phosphorylation of H2A, a known Bub1 substrate (Kawashima et al., 2010) (Figure 2H). Furthermore, expression of the RNAi-resistant kinase-dead (KD) mutant of Bub1 rescued the checkpoint defects caused by Bub1 depletion and Plk1 inhibition (Figure 1E and 1F). Thus, the cooperation between Bub1 and Plk1 appears to be mediated by the non-kinase domains of Bub1.

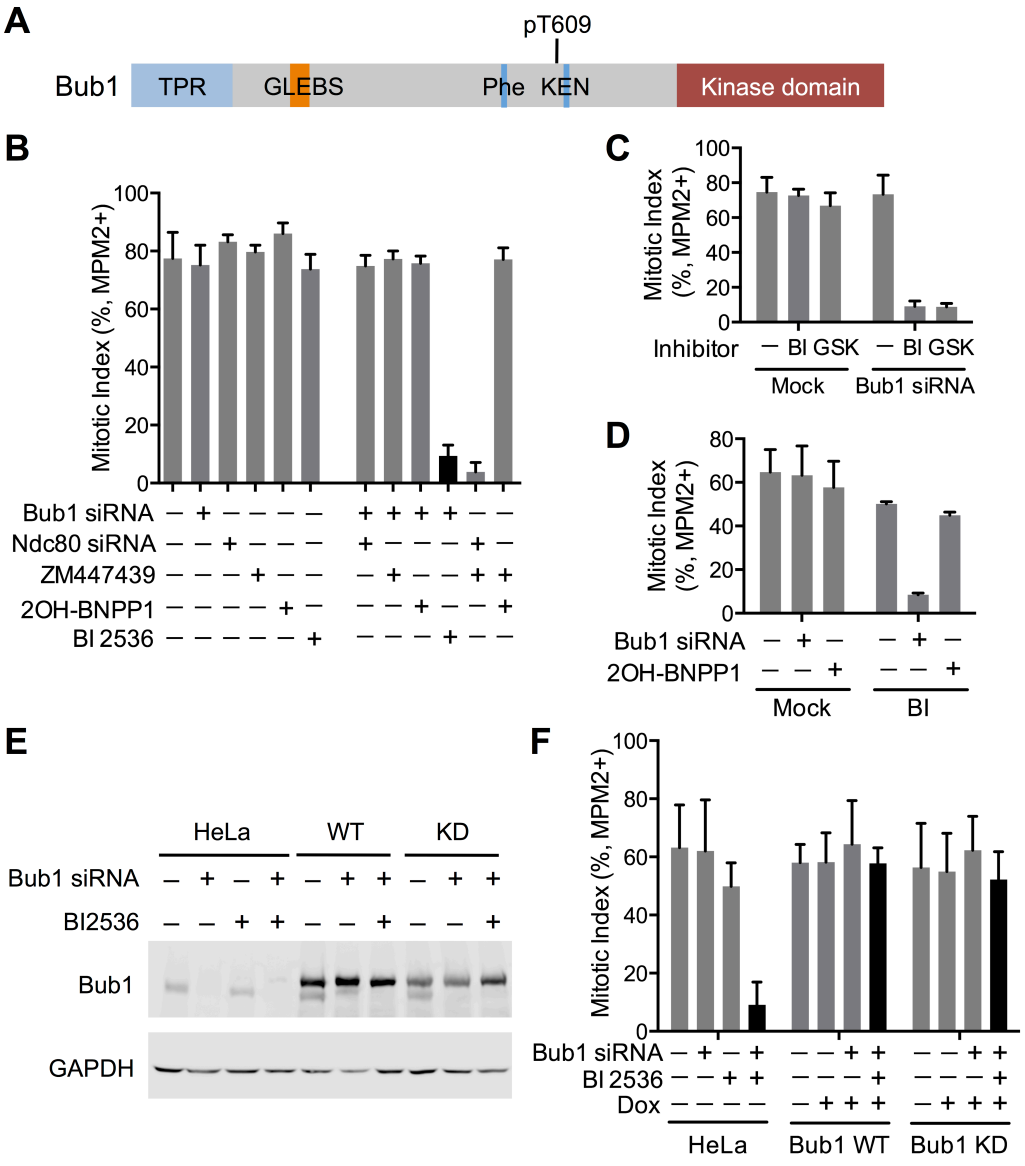

Figure 1. Bub1 depletion and Plk1 inhibition synergizes to inactivate the spindle checkpoint. (**A**) Domains and motifs of Bub1. TPR, tetratricopeptide repeat; GLEBS, Gle2-binding sequence. **(B)** Quantification of the mitotic index (defined as the percentage of MPM2+, 4N cells) of HeLa Tet-On cells treated with 5 μM nocodazole and the indicated siRNAs and kinase inhibitors. Mean ± SD for columns 1, 2, 5, 6, and 10 (three or more independent experiments); mean ± range for other columns (two independent experiments). (**C**) Quantification of the mitotic index of HeLa Tet-On cells treated with 500 nM nocodazole and the indicated siRNA and Plk1 inhibitors (BI, BI2536; GSK, GSK461364). Mean ± SD (n = 3 independent

experiments). (**D**) Quantification of the mitotic index of HeLa Tet-On cells treated with 200 nM taxol in the presence or absence of Bub1 siRNA or inhibitor (2OH-BNPP1) kinase inhibitor treatment in 200 nM taxol. Mean ± range (n = 2 independent experiments). (**E**) Immunoblots of lysates of parental HeLa Tet-On cells and cells stably expressing GFP-Bub1 wild type (WT) or kinase-dead mutant (KD) treated with doxycycline in the presence or absence of Bub1 siRNA and BI2536. (**F**) Quantification of the mitotic index of HeLa Tet-On parental cells and cells expressing GFP-Bub1 WT and KD treated with 200 nM taxol in the presence or absence of doxycycline (Dox), Bub1 siRNA, and BI2536. Mean ± SD (n = 3 independent experiments).

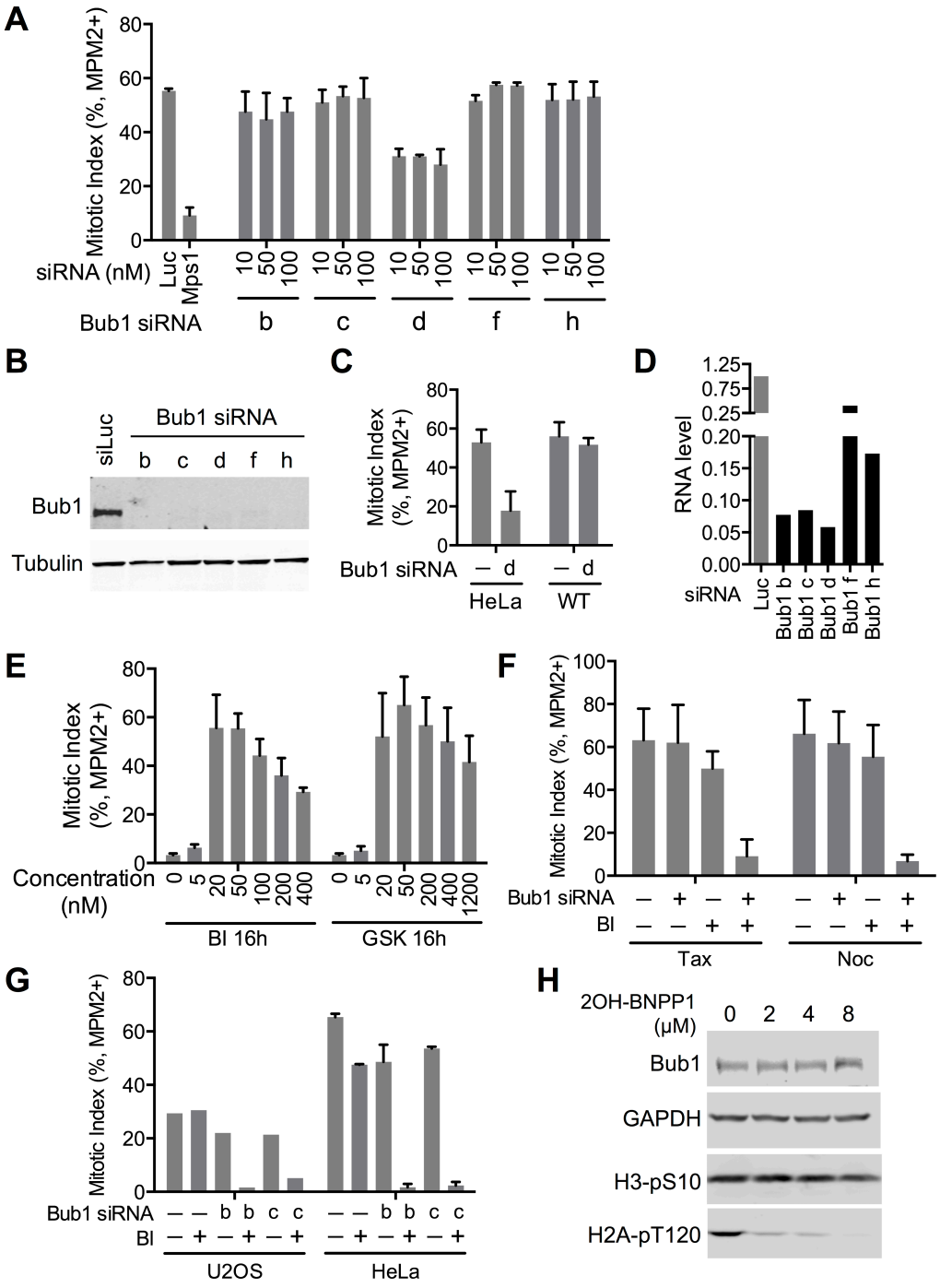

Figure 2. Bub1 depletion and Plk1 inhibition cause strong spindle checkpoint defects. (**A**) Quantification of the mitotic index of HeLa Tet-On cells treated with the indicated siRNAs and 500 nM nocodazole (mean ± SD; n = 3 independent experiments). Luc, Luciferase. **(B)** Blots of lysates of HeLa Tet-On cells treated with the indicated siRNAs. (**C**) Quantification of the mitotic index of HeLa Tet-On cells treated with 200 nM taxol and the indicated siRNAs (mean ± SD; n

= 3 independent experiments). (**D**) Quantification of the relative RNA levels in log-phase HeLa Tet-On cells treated with the indicated siRNAs using quantitative RT-PCR. (**E**) Quantification of the mitotic index of HeLa Tet-On cells treated with BI2536 (BI) or GSK461364 (GSK) at the indicated concentrations (mean ± SD; n = 3 independent experiments). (**F**) Quantification of the mitotic index of HeLa Tet-On cells treated with or without Bub1 siRNA and BI2536 (BI) and incubated with 200 nM taxol (Tax) or 500 nM nocodazole (Noc) (mean ± SD; n = 3 independent experiments). (Lara-Gonzalez et al.) Quantification of the mitotic index of HeLa Tet-On or U2OS cells treated with or without the indicated Bub1 siRNAs and BI2536 (BI), and incubated with 200 nM taxol (mean ± range; n = 2 independent experiments). (**H**) HeLa Tet-On cells were arrested in mitosis with 500 nM nocodazole, and then treated with different doses of the Bub1 inhibitor 2OH-BNPP1. Cell lysates were blotted with the indicated antibodies.

The Bub1–Plk1 complex phosphorylates Cdc20 and inhibits APC/C^{Cdc20}

Bub1 and Plk1 form a complex specifically in mitosis, in a mechanism that requires the binding of the polo-box of Plk1 to a Cdk1-dependent phosphorylation site (T609) in Bub1 (Qi et al., 2006). Furthermore, Bub1 binds to Cdc20 through the Phe and KEN boxes (Di Fiore et al., 2015; Diaz-Martinez et al., 2015; Kang et al., 2008), and is required for the kinetochore localization of Cdc20 (Di Fiore et al., 2015) (Figure 4A and 4B). We next tested whether, through binding to both Plk1 and Cdc20 with distinct motifs, Bub1 might scaffold Plk1- dependent Cdc20 phosphorylation. Because Bub1 could directly phosphorylate Cdc20 and because the kinase activity of Bub1 was not required for its functional cooperation with Plk1, we used the Bub1 truncation mutant lacking the kinase domain (Bub1$^{\Delta Kinase}$) bound to Bub3 (to stabilize the Bub1 protein) in our assays. Bub1$^{\Delta Kinase}$–Bub3 was co-expressed with cyclin B1– Cdk1 to introduce the Cdk1-dependent phosphorylation at T609, which was required for Plk1 binding. Plk1 alone did not phosphorylate Cdc20 efficiently, as only a small fraction of Cdc20 underwent gel mobility shift (Figure 3A). Addition of Bub1$^{\Delta Kinase}$–Bub3 to this reaction caused about 50% of

Cdc20 to undergo gel mobility shift, and this shift was abolished by BI2536, suggesting that Bub1$^{\Delta Kinase}$ stimulated Cdc20 phosphorylation by Plk1. Consistent with previous studies (Kang et al., 2008; Lin et al., 2014; Tang et al., 2004), full-length Bub1 phosphorylated Cdc20 at S153. This phosphorylation was inhibited by 2OH-BNPP1, and did not retard the gel mobility of Cdc20. Even in the presence of Bub1$^{\Delta Kinase}$, Plk1 did not phosphorylate Cdc20 S153, indicating that Plk1 and Bub1 phosphorylated different Cdc20 residues.

Several residues in the N-terminal region of Cdc20 undergo phosphorylation in mitotic HeLa cells, including S72, S92, S153, T157, and S161 (Tang et al., 2004) (Figure 3B). We constructed a Cdc20 5A mutant that replaced all five phospho-residues with alanines. The Cdc20 5A mutation greatly reduced the extent of the gel mobility shift caused by Bub1$^{\Delta Kinase}$– Plk1 (Figure 3A), suggesting that one or more of these mitotic phosphorylation events of Cdc20 might be mediated by Plk1.

Bub1-dependent phosphorylation of Cdc20 inhibits its ability to activate the ubiquitin ligase activity of APC/C (Tang et al., 2004). We tested whether phosphorylation of Cdc20 by Plk1 (as a component of the Bub1–Plk1 complex) also inhibited APC/C^{Cdc20} . APC/C^{Cdc20} converted nearly all of cyclin B1 to ubiquitin-conjugated forms (Figure 3C). Whereas Bub1$^{\Delta Kinase}$ or Plk1 alone did not appreciably inhibit APC/C^{Cdc20} , addition of both reduced the activity of APC/C^{Cdc20} . The Plk1 inhibitor BI2536 reversed this inhibition. Taken together, our results indicate that Bub1 stimulates Cdc20 phosphorylation by Plk1, which can inhibit APC/C^{Cdc20} in vitro.

We next analyzed Cdc20 phosphorylated by Bub1$^{\Delta Kinase}$–Plk1 with mass spectrometry (Figure 4C and 4D). This analysis identified several phosphorylation sites in Cdc20, including T70, S92, S96, and T106, with T70 and S92 being the most prominent ones. We thus made

phospho-specific antibodies against Cdc20-pT70 and Cdc20-pS92, and expressed and purified Cdc20 T70A and S92A proteins from Sf9 insect cells. Bub1$^{\Delta Kinase}$ stimulated Plk1- dependent phosphorylation of Cdc20 at S92 (Figure 3D). As specificity controls, two other mitotic kinases, Cdk1 and Mps1, did not phosphorylate S92. The pS92 band co-migrated with the slow-migrating Cdc20 species (Figure 3D), and the S92A mutation diminished the gel mobility shift of Cdc20, suggesting that phosphorylation of this residue retarded the gel mobility of Cdc20. Phosphorylation of T70 was already detected in Cdc20 purified from Sf9 cells (Figure 4E). This residue is located in a Cdk1 consensus motif, suggesting that it might be phosphorylated by Cdk1 in insect cells. T70 is thus not a Plk1 site. The T70A mutation did not affect the S92 phosphorylation by Bub1$^{\Delta Kinase}$–Plk1 (Figure 3D), indicating that phosphorylation of T70 is not a prerequisite for S92 phosphorylation. Our results establish Cdc20 S92 as a major Plk1 phosphorylate site in vitro.

We then tested whether the phospho-deficient Cdc20 mutants were refractory to Bub1$^{\Delta Kinase}$–Plk1 inhibition. We expressed and purified additional Cdc20 mutants from Sf9 cells, including S72A, T70A/S72A/S92A (3A), and 5A. Compared to Cdc20 WT, T70A, and S72A, Cdc20 S92A was much less efficiently inhibited by Bub1$^{\Delta Kinase}$–Plk1 (Figure 3E), indicating that S92 phosphorylation contributed to Plk1-dependent inhibition of APC/C^{Cdc20}. On the other hand, Cdc20 S92A was still slightly inhibited by Bub1$^{\Delta Kinase}$–Plk1, while Cdc20 5A was completely resistant to Bub1$^{\Delta Kinase}$–Plk1 inhibition (Figure 3E). We had previously shown that Cdc20 5A was also not phosphorylated by Bub1, and was resistant to Bub1 inhibition (Tang et al., 2004). Therefore, we have identified the major phosphorylation sites of Bub1–Plk1 on Cdc20 that are functionally important for APC/C^{Cdc20} inhibition in vitro.

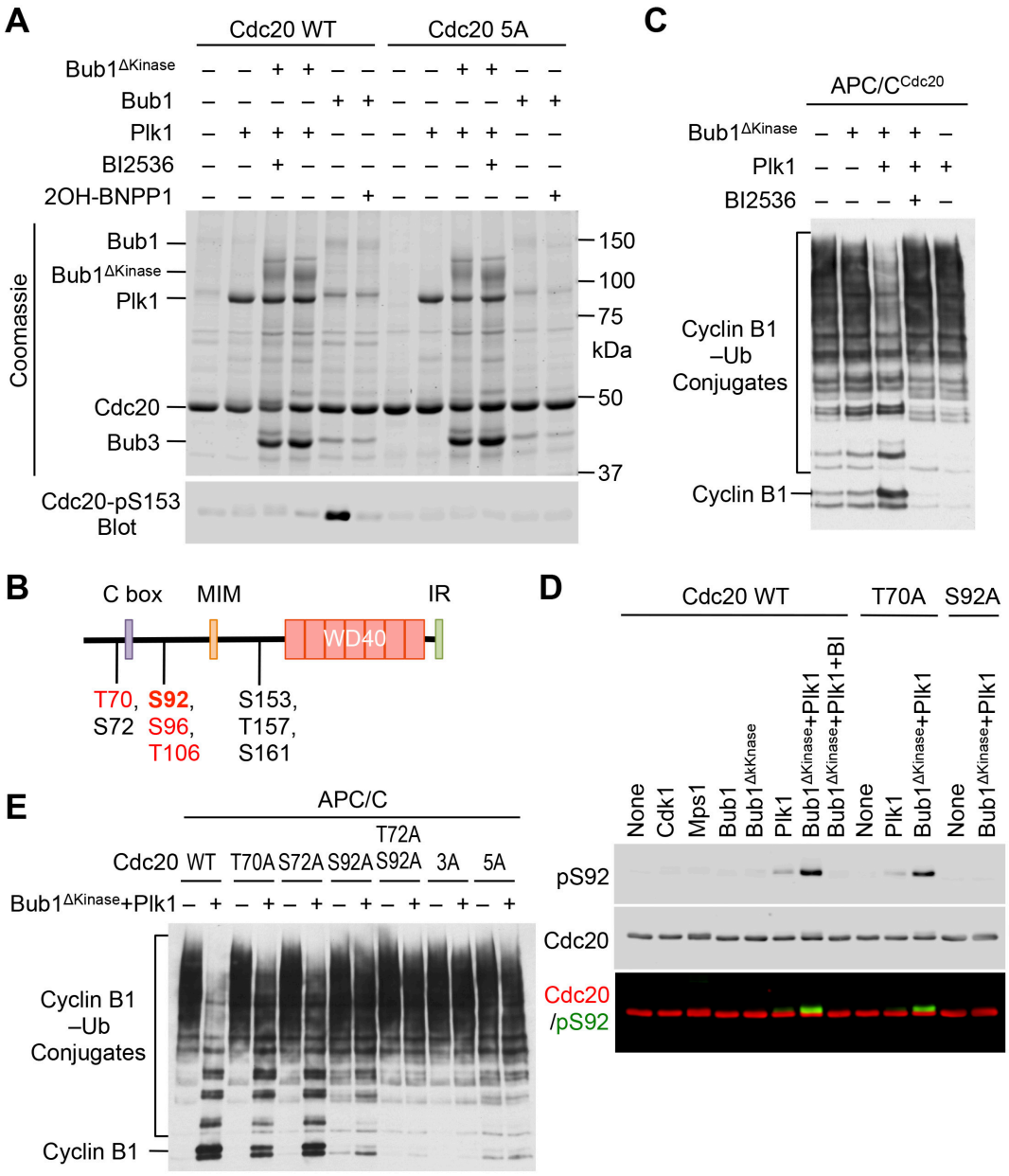

Figure 3. Bub1 promotes Plk1-mediated Cdc20 phosphorylation and APC/C inhibition. (**A**) Coomassie stained gel (top) and Cdc20-pS153 blot (bottom) of kinase reactions containing the indicated recombinant proteins and inhibitors. WT, wild type; Cdc20 5A, S72A/S92A/S153A/T157A/S161A. **(B)** Domains and motifs of human Cdc20 with the important phosphorylation sites indicated. Sites in Bub1–Plk1-treated Cdc20 identified by mass spectrometry in this study are labeled in red. MIM, Mad2-interacting motif; IR, isoleucine-

arginine tail. (**C**) Anti-Myc blot of the in vitro ubiquitination reactions of APC/C^{Cdc20} using cyclin $B1_{1-97}$-Myc as the substrate. Cdc20 was first incubated with the kinase buffer in the presence or absence of indicated proteins and BI2536 before being added to APC/C isolated from *Xenopus* egg extract. (**D**) Quantitative immunoblots of the kinase reactions containing the indicated recombinant kinases and Cdc20 proteins as substrates. BI2536 (BI) was added to one of these reactions. The Cdc20-pS92 and total Cdc20 signals on the same membrane were detected in the 800-nm and 700-nm channels, respectively. The two channels were pseudo-colored (Cdc20-pS92, green; Cdc20, red) and overlaid in the bottom panel. (**E**) Anti-Myc blot of the in vitro ubiquitination reactions of APC/C^{Cdc20} using cyclin $B1_{1-97}$-Myc as the substrate. The indicated Cdc20 proteins were first incubated with the kinase buffer in the presence and absence of $Bub1^{\Delta Kinase}$ and Plk1, and then added APC/C isolated from *Xenopus* egg extracts. Cdc20 3A, T70A/S72A/S92A.

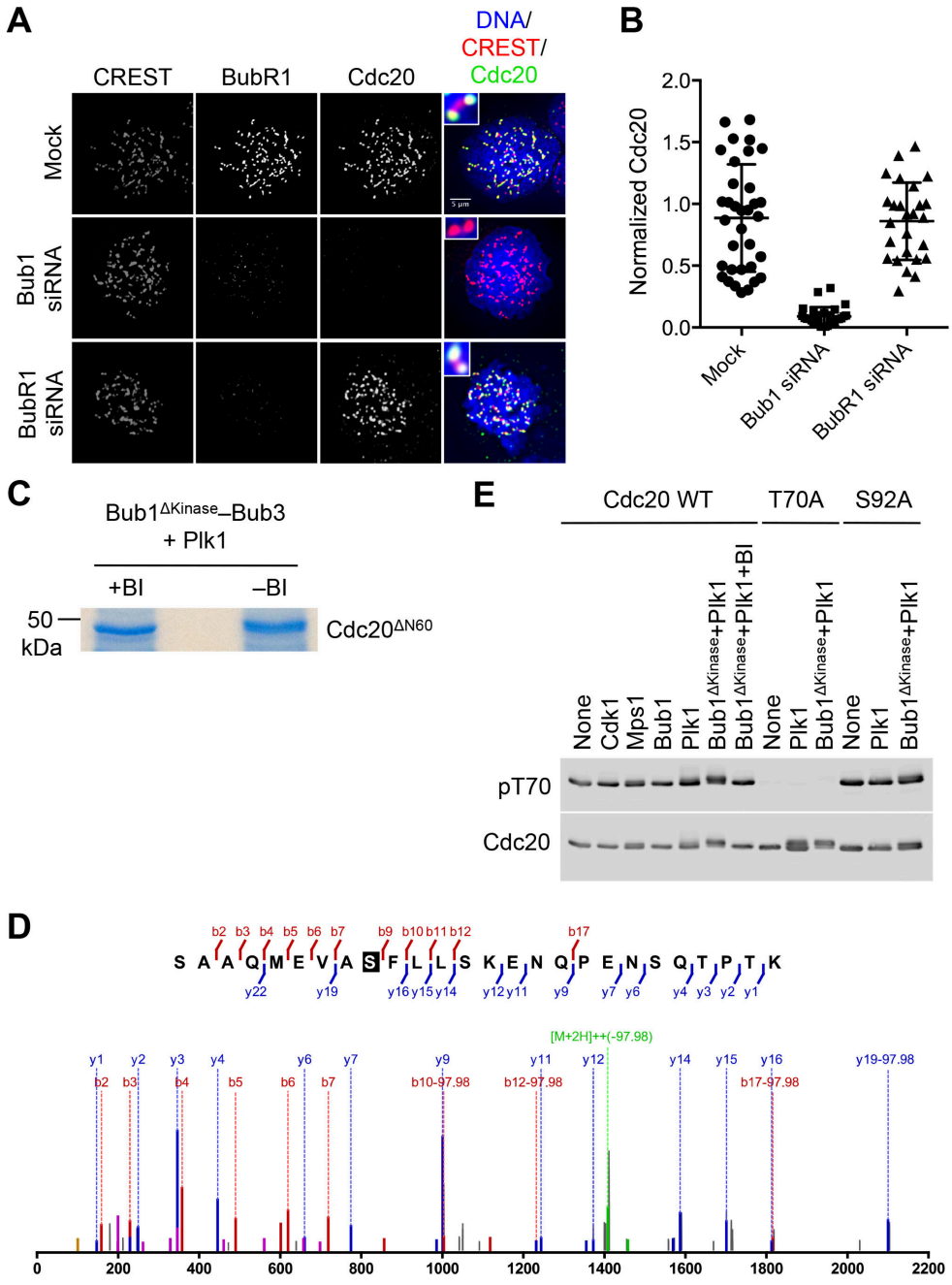

Figure 4. Identification of Cdc20 phosphorylation sites. (**A**) HeLa Tet-On cells were treated with Bub1 or BubR1 siRNAs, and arrested in mitosis with 250 nM nocodazole. Cells were stained with DAPI and the indicated antibodies. Colors of the overlaid channels match those of the label. Selected regions were magnified and shown in insets. Scale bar, 5 μm. **(B)** Quantification of the Cdc20 kinetochore staining intensity in (**A**) normalized to that of CREST

(mean ± SD; each dot represents one cell). (**C**) Coomassie blue stained gel of Cdc20$^{\Delta N60}$ treated with Bub1$^{\Delta Kinase}$–Bub3 and Plk1 in the presence or absence of BI2536. The Cdc20 bands were excised and analyzed by mass spectrometry. (**D**) Mass spectrum showing the fragmentation pattern of a phospho-S92-containing Cdc20 peptide. **(E)** Immunoblots of the kinase reactions containing the indicated recombinant kinases and Cdc20 proteins as substrates. BI2536 (BI) was added to one of these reactions. The Cdc20-pT70 and total Cdc20 signals were detected.

Cdc20 phosphorylation by Bub1–Plk1 is required for spindle checkpoint signaling

We next tested whether Bub1–Plk1 phosphorylated Cdc20 in human cells. HeLa cells were released from a thymidine block at G1/S, arrested in mitosis by nocodazole or taxol, and treated with MG132 and various kinase inhibitors. MG132 was added to prevent mitotic exit of cells with an inactive spindle checkpoint. The endogenous Cdc20 protein was indeed phosphorylated at S92 and S153 in mitotic HeLa cell lysates (Figure 5A). Bub1 depletion greatly reduced S153 phosphorylation, indicating that this phosphorylation was mediated by Bub1. Either Plk1 inhibition by BI2536 or Bub1 depletion reduced Cdc20 S92 phosphorylation, and a combination of both treatments completely abolished this phosphorylation (Figure 5A). Inhibition of Plk1 by GSK461364 together with Bub1 depletion also abolished S92 phosphorylation (Figure 5B). These results indicate that Bub1–Plk1 phosphorylate Cdc20 in human cells during mitosis.

The Bub1 paralog BubR1 can also bind to Plk1 through a phosphorylated STP motif and Cdc20 through Phe and D boxes in the middle region (Diaz-Martinez et al., 2015; Qi and Yu, 2007). We wondered if BubR1 could also scaffold Plk1-mediated phosphorylation of Cdc20. Indeed, recombinant purified BubR1 stimulated Plk1-dependent phosphorylation of Cdc20, as evidenced by the gel mobility shift of Cdc20 (Figure 5C).

Because BubR1 was critical for the spindle checkpoint, we could not effectively synchronize cells depleted of BubR1 in mitosis with the thymidine-arrest-release protocol. To

test whether BubR1–Plk1 contributed to Cdc20 phosphorylation in human cells, we thus constructed a HeLa cell line stably expressing a Cdc20 mutant with its C-terminal IR motif depleted (Cdc20 ΔIR). Cdc20 ΔIR could not bind to or activate APC/C, but retained all other functional motifs. Depletion of the endogenous Cdc20 with siRNA arrested Cdc20 ΔIR-expressing cells in mitosis in a checkpoint-independent manner, allowing us to synchronize cells depleted of BubR1 or Mad2 in mitosis. Similar to Bub1 depletion, depletion of BubR1 reduced S92 phosphorylation on Myc-Cdc20 ΔIR (Figure 5D). As a control, depletion of Mad2 did not affect this phosphorylation. Thus, BubR1–Plk1 can mediate Plk1-dependent phosphorylation of Cdc20 in human cells. Furthermore, Myc-Cdc20 ΔIR still bound to Mad2 and BubR1 in cells depleted of Bub1 and treated with BI2536 (Figure 5D). Because these cells had much reduced levels of Cdc20 S92 phosphorylation, Cdc20 phosphorylation at this and possibly other Plk1 sites might not be required for MCC formation.

BubR1 interacts with both Cdc20 and PP2A through neighboring motifs (Diaz-Martinez et al., 2015; Suijkerbuijk et al., 2012). We tested whether the BubR1–PP2A interaction affected Cdc20 S92 phosphorylation. The Cdc20-pS92 level of cells overexpressing the BubR1 mutant with its KARD motif mutated (mKARD) was about three fold that of cells expressing BubR1 wild type (WT) (Figure 5E). This result is consistent with a role of BubR1-bound PP2A in dephosphorylating Cdc20 S92. Thus, BubR1–Plk1 may also contribute to Cdc20 phosphorylation in human cells, but this mechanism may be limited by BubR1-bound PP2A.

The kinase activities of Mps1 and Aurora B are both required for spindle checkpoint signaling in taxol-treated human cells. The Mps1 inhibitor reversine and the Aurora B inhibitor ZM447439 reduced S92 phosphorylation in mitotic cells (Figure 5B), indicating that this phosphorylation requires active, upstream checkpoint signaling. As a control, Cdc20 T70

phosphorylation was not affected by reversine or ZM447439, suggesting that this phosphorylation is not sensitive to checkpoint status. More importantly, ectopic expression of the phospho-deficient Cdc20 5A, but not Cdc20 WT, in cells depleted of endogenous Cdc20 caused these cells to escape from nocodazole-mediated mitotic arrest (Figure 5F). Taken together, these results indicate that Bub1–Plk1-dependent phosphorylation of Cdc20 is regulated by upstream checkpoint signaling, and is required for checkpoint-dependent mitotic arrest in human cells.

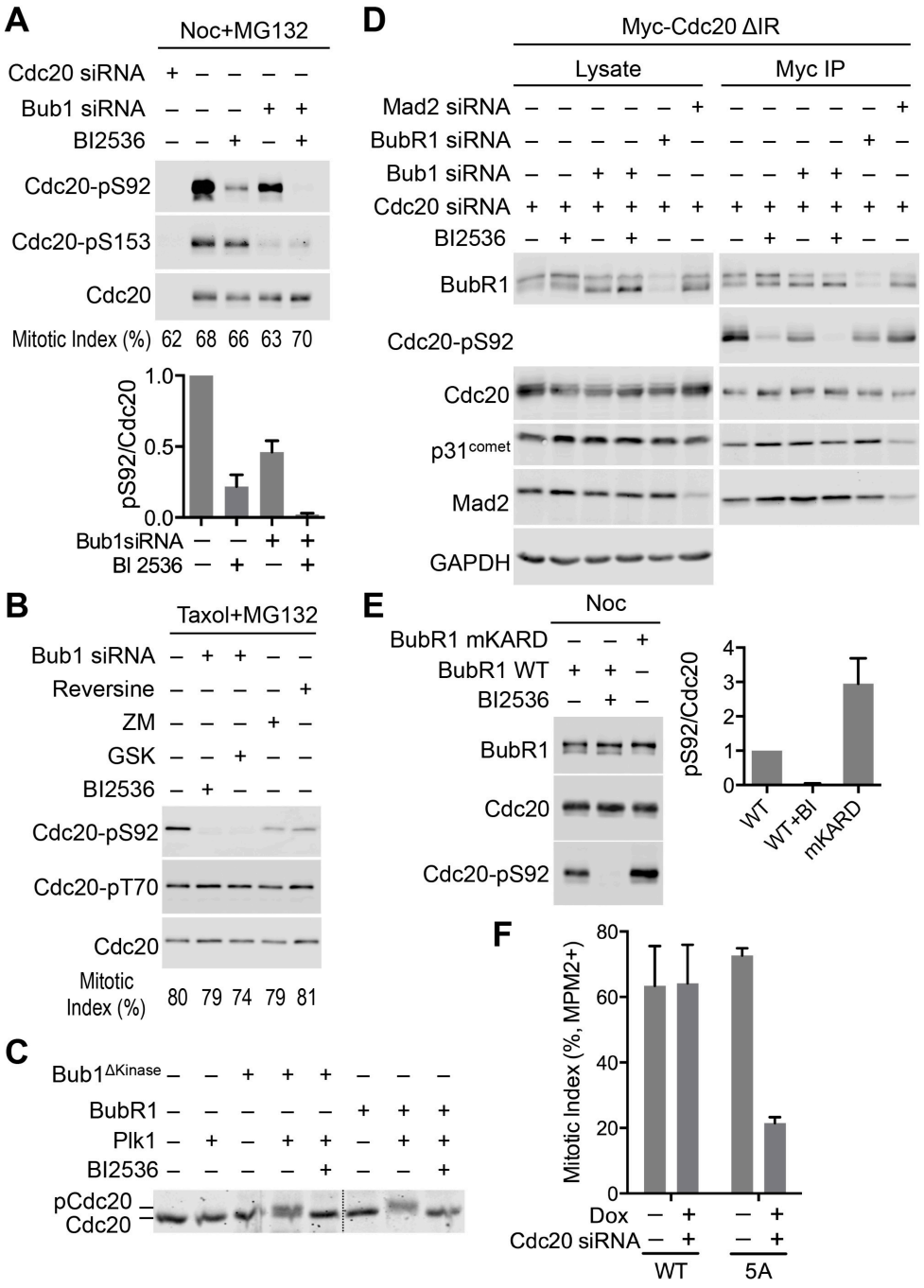

Figure 5. Cdc20 phosphorylation by Bub1–Plk1 is required for the spindle checkpoint. (**A**) HeLa Tet-On cells were treated with the indicated siRNAs, arrested in mitosis using 500 nM nocodazole (Noc) and 10 μM MG132, and then treated with or without BI2536. The endogenous Cdc20 was immunoprecipitated from these cells and blotted with the indicated antibodies. The mitotic index of each sample is indicated below each lane. The bottom graph shows the

quantification of the Cdc20-pS92 signal normalized to the total Cdc20 signal (mean ± range; n = 2 independent experiments). **(B)** HeLa Tet-On cells were treated with or without Bub1 siRNA and arrested in mitosis by 200 nM taxol and 10 μM MG132, and then incubated with the indicated kinase inhibitors (ZM, ZM447439; GSK, GSK461364). The endogenous Cdc20 was immunoprecipitated from these cells and blotted with the indicated antibodies. The mitotic index of each sample is indicated below each lane. (**C**) Coomassie stained gel of the kinase reactions of recombinant Cdc20 and other indicated proteins. The positions of unphosphorylated Cdc20 and the slower migrating, phosphorylated Cdc20 (pCdc20) were indicated. The lanes were from the same gel and were spliced together for clarity. (**D**) HeLa Tet-On cells stably expressing Myc-Cdc20 ΔIR were treated with the indicated siRNAs and 500 nM nocodazole, and then treated with or without BI2536. Cell lysates and anti-Myc immunoprecipitates (IP) were blotted with the indicated antibodies. Note that the Cdc20-pS92 antibody could not detect S92 phosphorylation in cell lysates. GAPDH served as a loading control for the lysates. (**E**) HeLa Tet-On cells were transfected with BubR1 siRNA and plasmids encoding siRNA-resistant Myc- BubR1 wild type (WT) or the KARD motif mutant (mKARD), arrested in mitosis with 500 nM nocodazole (Noc), and treated with or without BI2536. The endogenous Cdc20 was immunoprecipitated from these cells, and the IP was blotted with the indicated antibodies. Right graph shows the quantification of the Cdc20-pS92 signal normalized to that of total Cdc20 (mean ± range; n = 2 independent experiments). (**F**) Quantification of the mitotic index of HeLa Tet- On cells stably expressing Flag-Cdc20 WT or 5A treated with or without doxycycline (Dox) or Cdc20 siRNA, and then incubated with 500 nM nocodazole. Mean ± SD; n = 3 independent experiments.

Bub1 acts as a scaffold to promote Cdc20 phosphorylation and checkpoint signaling

To further probe the mechanism by which Bub1 promoted Plk1-dependent Cdc20 phosphorylation and APC/C^{Cdc20} inhibition, we tested which motifs of Bub1 were critical for $Bub1^{\Delta Kinase}$–Plk1-dependent inhibition of APC/C^{Cdc20}. Bub1 contains two Cdc20-binding motifs, the Phe box and the KEN box, which bind cooperatively to Cdc20 (Di Fiore et al., 2015; Diaz-

Martinez et al., 2015; Kang et al., 2008). A Bub1 mutant with both motifs mutated (mPheK) is deficient in Cdc20 binding (Kang et al., 2008). Because Plk1 binding to Bub1 requires phosphorylation of T609 of the STP motif in Bub1, the Bub1 T609A mutant is deficient in Plk1 binding (Qi et al., 2006). Both Bub1 mPheK and T609A mutants failed to support Plk1-dependent inhibition of APC/C^{Cdc20} in an in vitro ubiquitination assay with cyclin B1 as the substrate (Figure 6A). Therefore, binding of both Cdc20 and Plk1 by Bub1 is required for APC/C^{Cdc20} inhibition.

Depletion of Bub1 by RNAi in HeLa cells abolished the kinetochore localization of Cdc20 during mitosis (Figure 4A). Ectopic expression of Bub1 WT, but not mPheK, in Bub1 RNAi cells restored Cdc20 to kinetochores (Figure 6B), indicating that the Bub1–Cdc20 interaction is required for the kinetochore targeting of Cdc20. Consistent with previous studies (Kang et al., 2008), Bub1 mPheK failed to support Bub1-dependent phosphorylation of Cdc20 S153 (Figure 6C), validating the requirement for the docking interaction between Cdc20 and the non-kinase domains of Bub1 in this phosphorylation event. Bub1 T609A was functional in supporting Cdc20 S153 phosphorylation, confirming that Plk1 does not phosphorylate this site. Both Bub1 mPheK and T609A were deficient in supporting Cdc20 phosphorylation at S92, with mPheK being more defective (Figure 6C). The Bub1 kinase-dead (KD) mutant was fully functional in supporting Cdc20 S92 phosphorylation. Finally, we created stable HeLa cell lines that inducibly expressed Myc-Bub1 WT, mPheK, or T609A (Figure 6D). Consistent with their inability to support Cdc20 phosphorylation, both Bub1 mPheK and T609A were defective in restoring nocodazole-induced mitotic arrest in these cells depleted of endogenous Bub1 and treated with BI2536 (Figure 6E). Bub1 T609A was less defective than mPheK, presumably because Bub1 T609A still supported Bub1-dependent phosphorylation of Cdc20, including S153.

Taken together, our results are consistent with the following mechanism for Bub1–Plk1-dependent Cdc20 phosphorylation (Figure 6F). Bub1 binds to Cdc20 and Plk1 through distinct functional motifs, forming a transient Cdc20–Bub1–Plk1 complex. The kinase domains of both Plk1 and Bub1 then phosphorylate different sets of residues in the N-terminal region of Cdc20, including S92 and S153. Because Bub1 is required for the kinetochore localization of both Cdc20 and Plk1, these phosphorylation events may occur at kinetochores. Cdc20 phosphorylation by Bub1–Plk1 inhibits APC/C^{Cdc20} and contributes spindle checkpoint signaling.

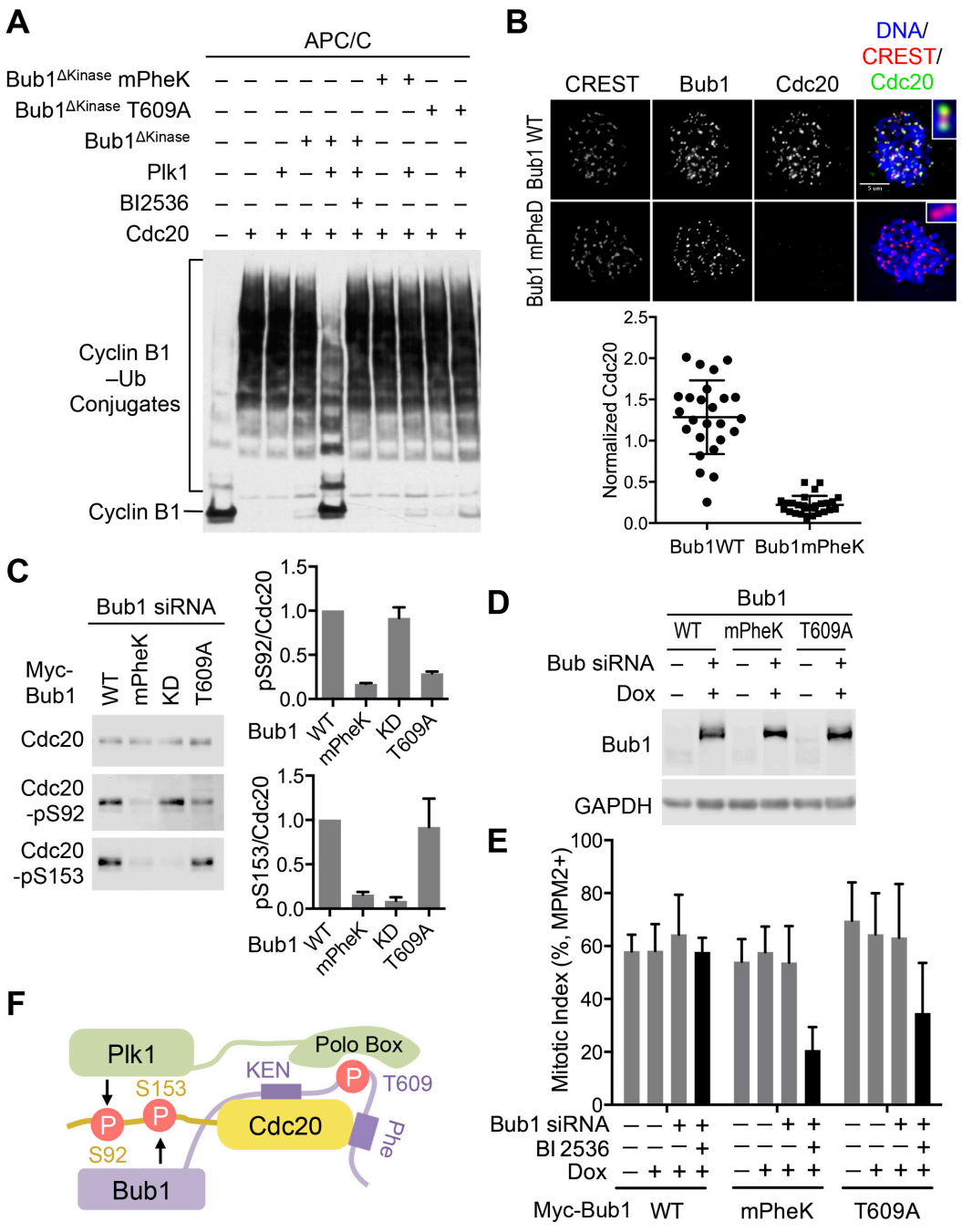

Figure 6. Bub1 acts as a scaffold to promote Plk1-mediated Cdc20 phosphorylation and APC/C^{Cdc20} inhibition. (**A**) Anti-Myc blot of the in vitro ubiquitination reactions of APC/C^{Cdc20} using cyclin B1$_{1-97}$-Myc as the substrate. Cdc20 was first incubated in the kinase buffer in the presence or absence of indicated proteins and BI2536 before being added to APC/C isolated from *Xenopus* egg extract. Bub1$^{\Delta Kinase}$ mPheK, the Bub1$^{\Delta Kinase}$ mutant with the Phe and KEN

boxes mutated, which contains the K535A, E536A, N537A, K625A, E626A, and N627A mutations. **(B)** HeLa Tet-On cells stably expressing GFP-Bub1 WT or mPheK were treated with Bub1 siRNA and arrested in mitosis with 250 nM nocodazole. Cells were stained with DAPI and the indicated antibodies. Colors of the overlaid channels match those of the label. Selected regions were magnified and shown in insets. Scale bar, 5 μm. The bottom graph shows the quantification of the Cdc20 kinetochore staining intensity normalized to that of CREST (mean ± SD; each dot represents one cell). (**C**) HeLa Tet-On cells stably expressing GFP-Bub1 WT or mutants were treated with Bub1 siRNA and 500 nM nocodazole. The endogenous Cdc20 was immunoprecipitated from these cells and blotted with the indicated antibodies. Graphs on the right show the quantification of Cdc20-pS92 (top) or Cdc20-pS153 (bottom) signals normalized to that of total Cdc20 (mean ± range; n = 2 independent experiments). (**D**) HeLa Tet-On cells stably expressing GFP-Bub1 WT or mutants were treated with or without Bub1 siRNA and doxycycline (Dox) and arrested in mitosis with 500 nM nocodazole. Cell lysates were blotted with the indicated antibodies. (**E**) Quantification of the mitotic index of HeLa Tet-On cells stably expressing GFP-Bub1 WT, mPheK, or T609A treated with 200 nM taxol and the indicated siRNA and compounds (mean ± SD; n = 3 independent experiments). Data of GFP-Bub1 WT in this figure were the same as those in Figure 1F. (**F**) Model explaining how the non-kinase domains of Bub1 act as a scaffold to promote Cdc20 phosphorylation by both the kinase domains of Bub1 and Plk1.

A phospho-mimicking Cdc20 mutant lessens the requirement for Mad2 and BubR1 in the spindle checkpoint

Plk1-dependent phosphorylation of Cdc20 inhibits APC/C^{Cdc20} in vitro (Figure 3C, 3E, and 6A). Because Cdc20 S92 is a major Plk1 phosphorylation site, we made the phospho-mimicking Cdc20 S92E mutant and tested its ability to activate APC/C in vitro. UbcH10 is the ubiquitin-conjugating enzyme that initiates ubiquitin chain assembly on APC/C substrates, and Ube2S then elongates these ubiquitin chains (Williamson et al., 2009). Cdc20 S92E was less effective than WT to activate APC/C-dependent ubiquitination of cyclin B1 in the presence of UbcH10 alone

(Figure 7A). The activity difference between Cdc20 WT and S92E appeared to be greater when both UbcH10 and Ube2S were used as ubiquitin-conjugating enzymes (Figure 7B). Thus, Cdc20 S92E is deficient in activating APC/C, and has a strong effect on Ube2S-dependent elongation of ubiquitin chains. This result indicates that Cdc20 S92E can functionally mimic the effects of Plk1-dependent phosphorylation, at least to some degree.

To understand the function of Cdc20 phosphorylation by Plk1 in human cells, we made stable HeLa cell lines that inducibly expressed RNAi-resistant Flag-Cdc20 WT or S92E. Depletion of Cdc20 from parental HeLa cells by RNAi produced strong mitotic arrest in the absence of spindle poisons, confirming the requirement for APC/C^{Cdc20} in mitotic progression (Huang et al., 2009) (Figure 7C). Expression of Cdc20 WT completely rescued the mitotic arrest phenotype caused by Cdc20 depletion. Consistent with its weaker APC/C-stimulatory activity in vitro, Cdc20 S92E only partially rescued the mitotic arrest phenotype (Figure 7C). Moreover, about 25% of HeLa cells treated with nocodazole underwent mitotic adaption or slippage after a prolonged mitotic arrest (Diaz-Martinez et al., 2014), as indicated by the population of cells that had 4N DNA content but were negative for MPM2 staining (Figure 8A). Expression of Cdc20 S92E, but not Cdc20 WT, in cells depleted of endogenous Cdc20 greatly reduced mitotic adaptation in the presence of nocodazole (Figure 8A and 8B). Thus, Cdc20 S92E is partially defective in activating APC/C^{Cdc20} in human cells. Finally, expression of S92E completely restored nocodazole-induced mitotic arrest in cells depleted of Bub1 and Cdc20 and treated with BI2536 (Figure 7D). This result strongly suggests that phosphorylation of Cdc20 S92 is a major function of Plk1 in the spindle checkpoint.

To explore the relationship between MCC and Plk1-dependent Cdc20 phosphorylation in APC/C^{Cdc20} inhibition, we examined the phenotypes of Cdc20 S92E-expressing cells depleted of

Mad2 or BubR1. Strikingly, the phospho-mimicking Cdc20 S92E restored nocodazole-induced mitotic arrest of cells partially depleted of Mad2 or BubR1 (Figure 7E, 7F, and 8C). This result suggests that phosphorylation of Cdc20 might inhibit APC/C^{Cdc20} in a pathway parallel to MCC-dependent inhibition of APC/C^{Cdc20} . Alternatively, Cdc20 S92 phosphorylation might enhance the activity of the residual MCC in Mad2- or BubR1-depleted cells.

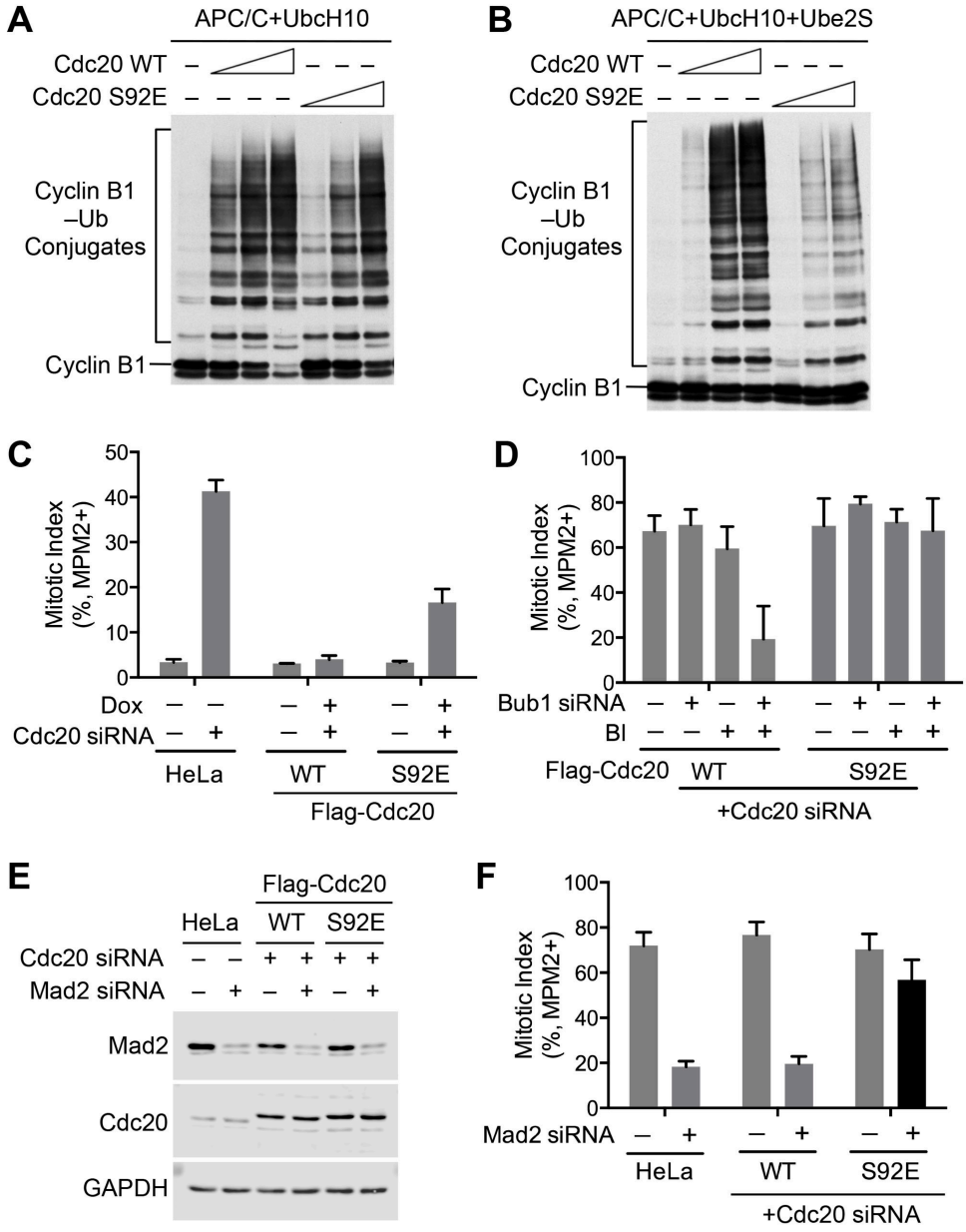

Figure 7. The Cdc20 phospho-mimicking mutant S92E is defective in APC/C activation. (**A–B**) Anti-Myc blot of the in vitro ubiquitination reactions of APC/C^{Cdc20} using cyclin $B1_{1-97}$-Myc as the substrate and UbcH10 (**A**) or both UbcH10 and Ube2S **(B)** as ubiquitin-conjugating enzymes. Recombinant Cdc20 WT or S92E at different concentrations (16.6 nM, 66.4 nM, and 332 nM) were incubated with APC/C isolated from *Xenopus* egg extract. (**C**) Quantification of the mitotic index of HeLa Tet-On parental cells and cells stably expressing Flag-Cdc20 WT or S92E that were treated with or without Cdc20 siRNA or Dox (mean ± SD; n = 3 independent experiments). (**D**) Quantification of the mitotic index of HeLa Tet-On cells stably expressing Flag-Cdc20 WT or S92E that were treated with Cdc20 siRNA, Dox, and 200 nM taxol in the presence or absence of Bub1 siRNA or BI2536 (BI) (mean ± SD; n = 3 independent experiments). (**E**) HeLa Tet-On parental cells and cells stably expressing Flag-Cdc20 WT or S92E were treated with the indicated siRNAs and 500 nM nocodazole. Cell lysates were blotted with the indicated antibodies. (**F**) Quantification of the mitotic index of cells in (**E**) (mean ± SD; n = 3 independent experiments).

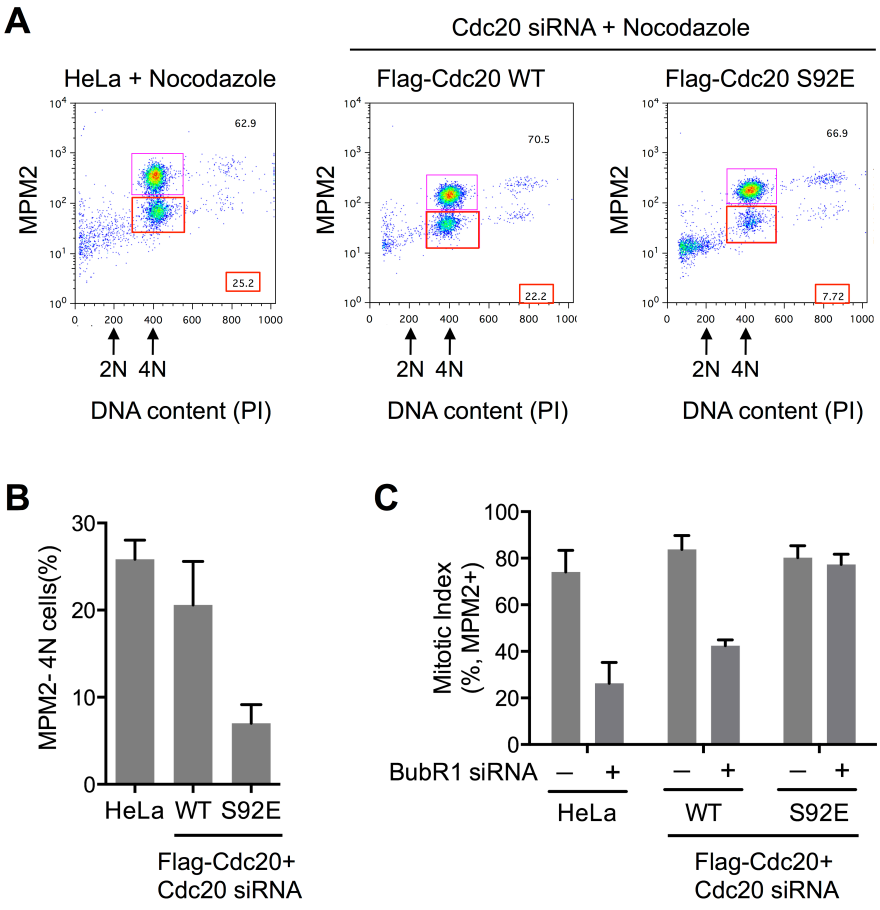

Figure 8. Expression of the phospho-mimicking Cdc20 S92E in HeLa cells suppresses mitotic adaption and alleviates the requirement for BubR1 in the spindle checkpoint. (**A**) Flow cytometry analysis of nocodazole-treated HeLa Tet-On parental cells and cells stably expressing Flag-Cdc20 WT or S92E (with the endogenous Cdc20 depleted). Mitotic cells (defined as MPM2+/4N cells) are indicated by pink boxes. Cells that underwent adaptation and escaped from mitosis (defined as MPM2-/4N cells) are labeled by red boxes, with their percentages indicated. **(B)** Quantification of the percentage of cells in (**A**) that underwent adaptation (mean ± SD; n = 3 independent experiments). (**C**) Quantification of the mitotic index of HeLa Tet-On parental cells and cells stably expressing Flag-Cdc20 WT or S92E treated with the indicated siRNAs and 500 nM nocodazole (mean ± SD; n = 3 independent experiments).

Cdc20 phosphorylation is dispensable for the formation or activity of MCC

To test whether Bub1–Plk1-dependent Cdc20 phosphorylation was required for MCC formation in human cells, we immunoprecipitated Cdc20 WT and the phospho-deficient 5A mutant from HeLa cells stably expressing them, and examined their association with BubR1 and Mad2. Cdc20 5A bound to BubR1 and Mad2 as efficiently as Cdc20 WT did (Figure 9A). This result suggests that Cdc20 phosphorylation is not required for MCC assembly in human cells. We next reconstituted a mini-MCC with recombinant human Mad2, Cdc20, and the N-terminal fragment of BubR1 (BubR1N; residues 1–370) proteins. In the absence of Mad2, BubR1N bound weakly to Cdc20 (Figure 7B). Addition of Mad2 greatly stimulated BubR1N binding to Cdc20, indicative of the formation of the BubR1N–Cdc20–Mad2 complex (mini-MCC). The phospho-mimicking Cdc20 S92E did not exhibit increased binding to Mad2 or BubR1N. Thus, Cdc20 phosphorylation at S92 does not stimulate MCC formation in vitro.

The Mad2 inhibitor $p31^{comet}$ promotes MCC disassembly though multiple mechanisms, including stimulation of Cdc20 autoubiquitination (Eytan et al., 2014; Jia et al., 2011; Reddy et al., 2007; Varetti et al., 2011; Wang et al., 2014; Westhorpe et al., 2011; Xia et al., 2004; Yang et al., 2007; Ye et al., 2015). The phospho-deficient Cdc20 5A mutation did not appreciably alter $p31^{comet}$ binding to Cdc20 (Figure 9A). Moreover, the phospho-mimicking Cdc20 S92E mutant still underwent autoubiquitination in vitro (Figure 10A). Therefore, we have no evidence to indicate that Cdc20 phosphorylation can regulate MCC disassembly.

Although Cdc20 phosphorylation does not appear to be required for MCC assembly, it remains possible that it might enhance the APC/C-inhibitory activity of MCC. MCC not only sequesters one Cdc20 molecule, but also inhibits another Cdc20 molecule that is already bound to APC/C (Izawa and Pines, 2015). We directly examined the effect of the phospho-mimicking Cdc20 S92E mutation on MCC-mediated inhibition of APC/C^{Cdc20}. First, we activated APC/C

with Cdc20 WT and then tested its inhibition by mini-MCC containing either Cdc20 WT or S92E (Figure 9C), with either securin (Figure 9D) or cyclin B1 (Figure 10B) as the substrate. Mad2 and BubR1N did not inhibit the already activated APC/C^{Cdc20}. Addition of Cdc20 along with Mad2 and BubR1N led to the formation of mini-MCC, which inhibited the already activated APC/C^{Cdc20} (Figure 9D and 10B). Importantly, mini-MCC containing Cdc20 S92E did not inhibit APC/C bound to Cdc20 WT more efficiently than mini-MCC containing Cdc20 WT did.

Second, we activated APC/C with Cdc20 S92E and then tested its inhibition by mini- MCC containing Cdc20 WT or S92E (Figure 9C, 9D, and 10B). Because Cdc20 S92E was less active in stimulating APC/C, we used higher doses of this mutant to normalize the activities of APC/C bound to Cdc20 WT and S92E. Again, Cdc20 S92E did not enhance MCC-mediated inhibition of APC/C^{Cdc20}, even when both copies of Cdc20 contained the phospho-mimicking mutation (Figure 9D and 10B). Thus, Cdc20 phosphorylation does not appear to stimulate the APC/C-inhibitory activity of MCC. Taken together, our results suggest that Cdc20 phosphorylation by Bub1–Plk1 directly inhibits APC/C^{Cdc20}, and acts in a pathway that is parallel to MCC formation.

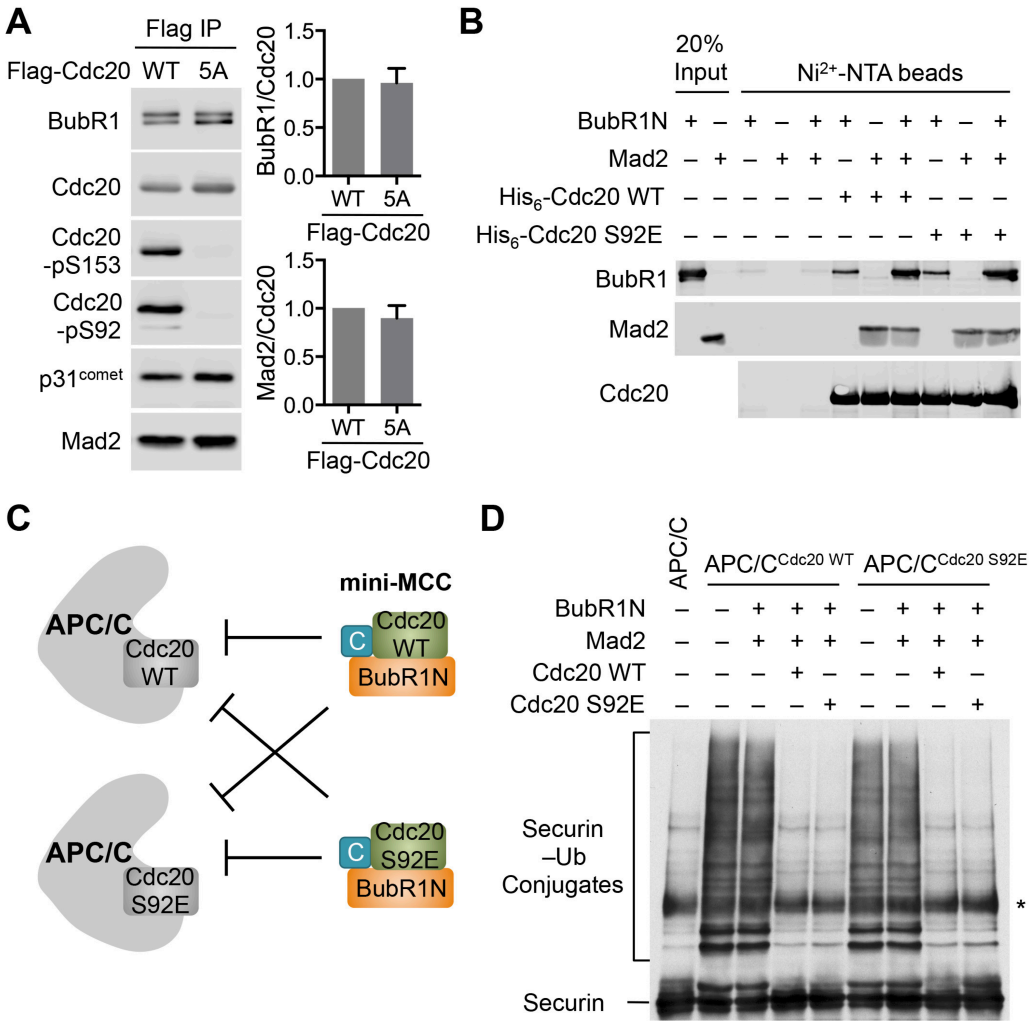

Figure 9. Cdc20 phosphorylation by Bub1–Plk1 is dispensable for MCC formation. (**A**) HeLa Tet-On cells stably expressing Flag-Cdc20 WT or 5A were arrested in mitosis by 5 μM nocodazole. The anti-Flag immunoprecipitates (IP) of these cells were blotted with the indicated antibodies. The graphs on the right show the quantification of the relative BubR1 and Mad2 signals normalized to that of total Cdc20 (mean ± range; n = 2 independent experiments). **(B)** Blots of the input and beads-bound proteins of the binding reactions among the indicated proteins. (**C**) Schematic drawing of the experimental design in (**D**) and Figure 10B. APC/C is pre-activated with Cdc20 WT or S92E and then incubated with mini-MCC comprising BubR1N, Mad2 in the closed conformation, and Cdc20 (WT or S92E). (**D**) Anti-Myc blot of the in vitro

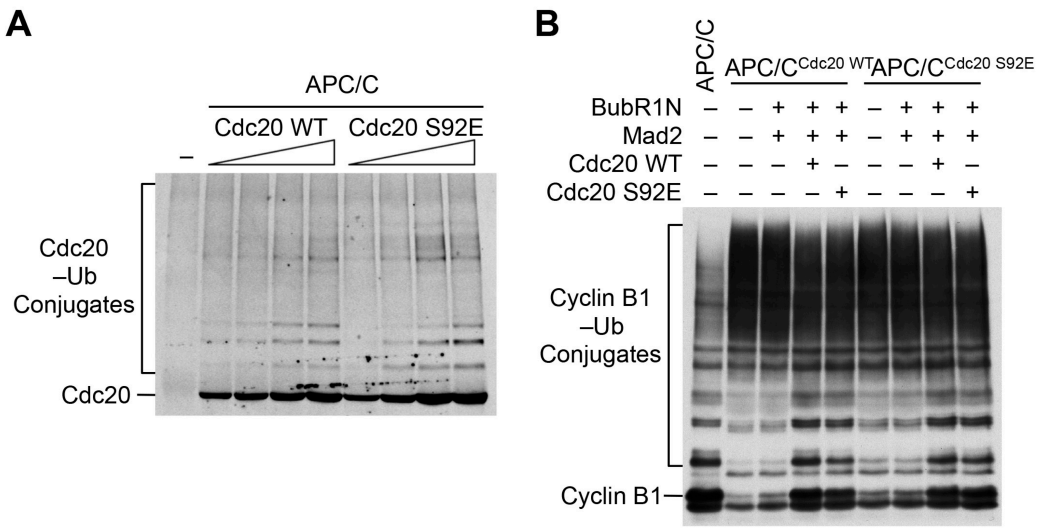

Figure 10. The phospho-mimicking Cdc20 S92E mutation does not affect Cdc20 autoubiquitination or MCC activity. (**A**) Anti-Cdc20 blot of the in vitro autoubiquitination reactions of APC/C^{Cdc20} with increasing amounts of recombinant Cdc20 WT or S92E. APC/C was isolated from mitotic HeLa Tet-On cells depleted of endogenous Cdc20. **(B)** Anti-Myc blot of the in vitro ubiquitination reactions of the indicated APC/C^{Cdc20} incubated with the indicated proteins and using cyclin $B1_{1\text{-}97}$-Myc as the substrate. See Figure 9C for experimental design.

Discussion

A few kinetochores unattached or improperly attached to spindle microtubules within a human cell are capable of activating the spindle checkpoint and delaying the onset of anaphase (Collin et al., 2013; Dick and Gerlich, 2013; Heinrich et al., 2013). The current model of spindle checkpoint signaling posits that these unattached kinetochores produce diffusible wait-anaphase entities to inhibit the checkpoint target APC/C^{Cdc20} throughout the cell. MCC is a critical inhibitor of APC/C^{Cdc20} in the spindle checkpoint and is quite possibly a diffusible wait-anaphase entity. On the other hand, MCC involves the physical binding of BubR1 and Mad2 to Cdc20, and is thus a stoichiometric inhibitor of APC/C^{Cdc20} . It is unclear whether a few unattached kinetochores are sufficient to produce enough MCC to inhibit all cellular APC/C.

In this study, we establish Cdc20 phosphorylation by the heterodimeric Bub1–Plk1 kinase complex as another critical APC/C-inhibitory mechanism in the spindle checkpoint. The kinase domains of both Bub1 and Plk1 in this complex can directly phosphorylate distinct residues in the N-terminal flexible region of Cdc20. Bub1 interacts with Cdc20 through the Phe and KEN motifs and with Plk1 through a phosphorylated STP motif. The Bub1–Cdc20 interaction promotes phosphorylation of Cdc20 by both Bub1 and Plk1, whereas Plk1-mediated phosphorylation of Cdc20 additionally requires the Bub1–Plk1 interaction. We previously showed that Cdc20 phosphorylation by Bub1 inhibits APC/C^{Cdc20} (Tang et al., 2004). We have shown herein that Plk1-dependent phosphorylation of Cdc20 (stimulated by the non-kinase domains of Bub1) also inhibits APC/C^{Cdc20}. Human cells expressing a Cdc20 mutant deficient for Bub1–Plk1 phosphorylation fail to maintain mitotic arrest induced by spindle poisons. We further identify Cdc20 S92 as a key functional site phosphorylated by Plk1. Cdc20 S92 phosphorylation is regulated by upstream checkpoint signals. The Cdc20 S92E mutant that mimics this phosphorylation bypasses the need for the kinase activity of Plk1 in the spindle checkpoint. Collectively, these results establish Cdc20 phosphorylation by Bub1–Plk1 as a functionally relevant, catalytic mechanism for checkpoint-dependent inhibition of APC/C.

The biochemical mechanism by which Cdc20 phosphorylation inhibits APC/C^{Cdc20} is unknown at present. Several phosphorylation sites are located in close proximity to the C box and the Mad2-interacting motif (MIM), which mediate the productive binding of Cdc20 to APC/C (Izawa and Pines, 2012; Labit et al., 2012). It is possible that phosphorylation of Cdc20 might alter the mode of Cdc20 binding to APC/C, or anchor Cdc20 at an APC/C site that is not conducive to catalysis.

We had previously shown that Cdc20 phosphorylation by Bub1 inhibited APC/C^{Cdc20} in vitro, and expression of a Cdc20 mutant deficient for Bub1 phosphorylation causes checkpoint defects in human cells (Tang et al., 2004). These results suggested that Cdc20 phosphorylation by Bub1 provided a catalytic mechanism for checkpoint-dependent inhibition of APC/C. Subsequent studies showed that the kinase activity of Bub1 was not strictly required for the spindle checkpoint in human cells (Kang et al., 2008; Klebig et al., 2009). Mouse cells with the kinase activity of Bub1 genetically inactivated had mild spindle checkpoint defects that were attributed to the function of Bub1 in phosphorylating histone H2A and installing Aurora B at centromeres (Ricke et al., 2012). These results casted doubts on the relevance of Cdc20 phosphorylation by Bub1 in checkpoint signaling, and suggested that the non-kinase domains of Bub1 might play important roles in the spindle checkpoint.

Indeed, the non-kinase region of Bub1 interacts with BubR1–Bub3, Mad1–Mad2, and Cdc20 through distinct conserved motifs in human and yeast cells (Di Fiore et al., 2015; Kang et al., 2008; Kim et al., 2012; London and Biggins, 2014a; Overlack et al., 2015). An emerging picture is that Bub1 acts as a scaffold to promote the kinetochore targeting of other checkpoint proteins. On the other hand, in human cells, it is exceedingly difficult to deplete Bub1 with RNAi to below the threshold needed for checkpoint signaling (Figure 2). Thus, a very small amount of Bub1 in human cells suffices to promote checkpoint signaling, a notion seemingly at odds with a simple scaffolding role of Bub1.

Our study now clarifies the roles of the kinase and non-kinase domains of Bub1, and resolves these long-standing conundrums in the field. Our results show that the non-kinase domains of Bub1 recruit Plk1 and enable Plk1-dependent phosphorylation of Cdc20 and inhibition of APC/C^{Cdc20} . Thus, the non-kinase domains of Bub1 have an unconventional

"catalytic" role indirectly through the associated kinase Plk1, reconciling why the kinase activity of Bub1 is not strictly required for the checkpoint and yet a small amount Bub1 is sufficient to maintain checkpoint signaling. Because this heterodimeric Bub1–Plk1 kinase complex has two catalytic activities with partially redundant functions in APC/C^{Cdc20} inhibition, it is difficult to inactivate this catalytic engine of the checkpoint in human cells. Only the combination of chemical inhibition of Plk1 and depletion of Bub1 can substantially weaken both activities and produce strong checkpoint defects.

BubR1 also stimulates Cdc20 phosphorylation by Plk1 in vitro and may contribute to Cdc20 phosphorylation in human cells. On the other hand, Plk1-dependent phosphorylation of the KARD motif in BubR1 enables the binding of PP2A (Suijkerbuijk et al., 2012). BubR1-bound PP2A might suppress Cdc20 phosphorylation by Plk1, because a BubR1 mutant with its KARD motif mutated supported more Cdc20 phosphorylation as compared to the wild-type BubR1 in human cells. This notion needs to be further tested, but is in general agreement with unpublished findings of Rape and coworkers, which implicate PP2A as an important regulator of APC/C activity and checkpoint silencing in human cells (M. Rape, personal communication).

Several lines of evidence suggest that Cdc20 phosphorylation by Bub1–Plk1 acts in a pathway parallel to MCC formation in APC/C inhibition. First, Cdc20 phosphorylation by Bub1–Plk1 directly inhibits APC/C^{Cdc20} in vitro, in the absence of Mad2 and BubR1. Second, the Cdc20 mutant deficient for Bub1–Plk1 phosphorylation is capable of forming MCC in human cells. Third, the phospho-mimicking Cdc20 S92E mutation lessens the requirement for Mad2 or BubR1 in the spindle checkpoint in human cells, without affecting MCC formation or activity in vitro. On the other hand, our results do not rule out the possibility that Cdc20 phosphorylation

contributes to MCC formation or activity in vivo, where additional regulators of this process are present.

Our results presented herein, along with published results from others (London and Biggins, 2014a; Overlack et al., 2015), suggest the following Bub1 scaffolding model for spindle checkpoint signaling (Figure 11). During early mitosis, the constitutive Bub1–Bub3 complex is phosphorylated by Cdk1 at T609, binds to Plk1, and is recruited to kinetochores. Bub1–Bub3 further recruits BubR1–Bub3, Mad1–Mad2, and Cdc20 to kinetochores. In one pathway, through its physical interactions with all components of MCC, Bub1 promotes the formation of MCC comprising BubR1–Bub3, Mad2, and Cdc20, which can inhibit free APC/C or APC/C already bound to Cdc20. In a second, parallel pathway, the kinase domains of Bub1 and Bub1- bound Plk1 can both phosphorylate Cdc20 and inhibits APC/C^{Cdc20} catalytically. Both MCC formation and Cdc20 phosphorylation are required for proper spindle checkpoint signaling.

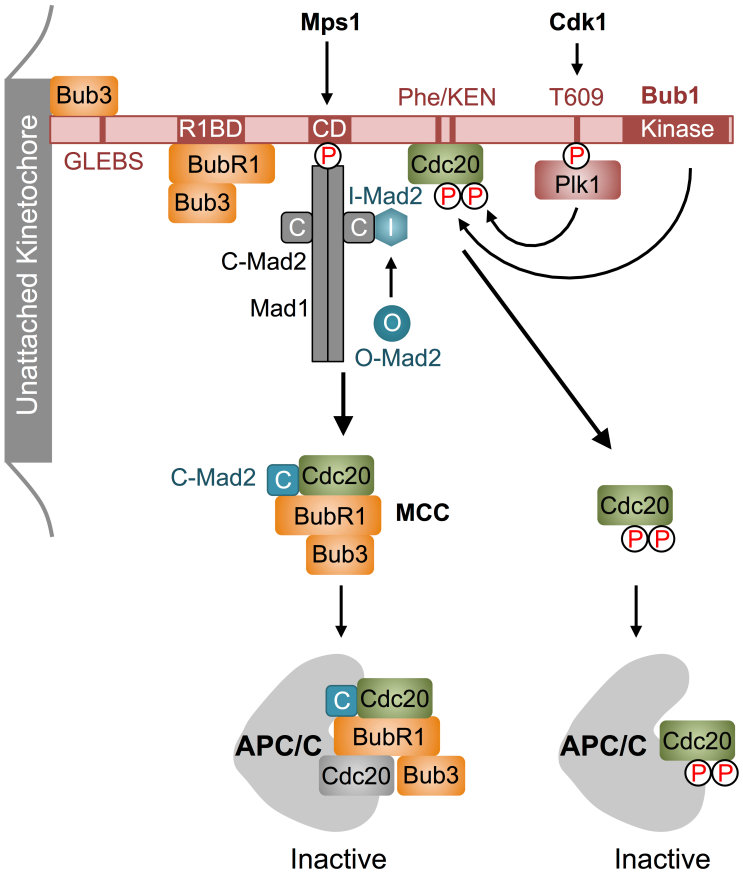

Figure 11. Model explaining the relationship between MCC and Cdc20 phosphorylation by Bub1–Plk1 in checkpoint-dependent inhibition of APC/C. In this model, Bub1 acts as a scaffold at kinetochores to recruit Plk1 and all components of MCC. It promotes MCC formation and Cdc20 phosphorylation by both Bub1 and Plk1, which form two parallel pathways to inhibit APC/C. GLEBS, Gle2-binding sequence; R1BD, BubR1-binding domain; CD, conserved domain.

Materials and methods

Cell culture and transfection

HeLa Tet-On and U2OS cells were cultured in Dulbecco's modified Eagle's medium (DMEM; Life Technologies) with 10% fetal bovine serum (Life Technologies) and 10 mM L-glutamine (Life Technologies). For cell cycle arrest in mitosis, cells were incubated in medium containing

2.5 mM thymidine (Sigma) for 16 h, released into fresh medium for 7 h, and incubated in medium containing nocodazole (500 nM or 5 μM; Sigma) or taxol (200 nM; Sigma) for another 3-5 h. Inhibitors were added at 1-3 h before sample collection. Inhibitors used in this study were: the Aurora kinase inhibitor ZM447439 (used at 2 μM; Selleck Chemicals), the Bub1 kinase inhibitor 2OH-BNPP1 (used at 4 μM), the Plk1 kinase inhibitors BI2536 (used at 100 nM; Selleck Chemicals) and GSK461364 (used at 200 nM; Selleck Chemicals), the Mps1 kinase inhibitor reversine (used at 100 nM; Cayman Chemical), and the proteasome inhibitor MG132 (used at 10 μM; Boston Biochem). For the BI2536 and GSK461364 titration experiment, various concentrations of the two inhibitors were added to log-phase cells. Cells were harvested after a 16-h incubation.

Transfection of siRNAs and plasmids was performed using Lipofectamine RNAiMAX (Life Technologies) and Effectene (QIAGEN), respectively, following manufacturers' protocols. A final concentration of 5 nM per siRNA was used, unless otherwise stated. The Cdc20 siRNA was the Silencer Select Pre-designed siRNA from Ambion (ID s2758) with following sequence: CGAAAUGACUAUUACCUGA. All other siRNAs were synthesized at Thermo Scientific. The sequences of these siRNAs were: Luciferase (Luc) siRNA, UCAUUCCGGAUACUGCGAU; Mps1 siRNA, UGAACAAAGUGAGAGACAU; Bub1 siRNA-b, CCAUGGGAUUGGAACCCUG; Bub1 siRNA-c, CCCAUUUGCCAGCUCAAGC; Bub1 siRNA-d, GAGUGAUCACGAUUUCUAA (Klebig et al., 2009); Bub1 siRNA-f, GGCAAAAGCUGAAGAAAGU; Bub1 siRNA-h, GAAACGGAUUUUUGGAACA; Hec1 siRNA, GAGUAGAACUAGAAUGUGA; BubR1 siRNA, CAAGAUGGCUGUAUUGUUU; and Mad2 siRNA, UACGGACUCACCUUGCUUG.

For the generation of stable cell lines, HeLa Tet-On cells were transfected with pTRE2hygro vectors encoding GFP-Bub1 WT or mutants (resistant to Bub1 siRNA-b, -c, and -d), Flag-Cdc20 WT or mutants, or Myc-Cdc20 ΔIR (resistant to Cdc20 siRNA from Ambion), and selected with 400 μg/ml hygromycin (Clontech). Single colonies were picked, expanded, and screened for desired protein expression in the presence of 1 μg/ml doxycycline (Clontech).

Antibodies, immunoblotting and immunoprecipitation

The Cdc20-pT70 and Cdc20-pS92 antibodies were made in an in-house facility by immunizing rabbits with Cdc20-pT70 or Cdc20-pS92-containing peptides coupled to hemocyanin (Sigma). Antibodies against human Bub1, BubR1, Mad2, Cdc20, Cdc20-pS153, $p31^{comet}$, H2A-pT120 and Hec1 were described previously (Kim et al., 2012; Lin et al., 2014; Liu et al., 2013; Tang et al., 2001; Xia et al., 2004). The following antibodies were purchased from the indicated commercial sources: mouse anti-Cdc20 and goat anti-Cdc20 (Santa Cruz), mouse anti-GAPDH (6C5; Milipore), mouse anti-Myc (9E10; Roche), mouse anti-tubulin (DM1A; Sigma), rabbit anti-H3-pS10 (Milipore), mouse anti-phospho-S/T-P MPM2 (Milipore), and CREST serum (ImmunoVision).

For quantitative immunoblotting, anti-rabbit IgG (H+L) (Dylight 800 conjugates), anti-mouse IgG (H+L) (Dylight 680 conjugates) (Cell Signaling), and anti-goat IgG (H+L) IRDye 680RD (LI-COR) were used as secondary antibodies. The membranes were scanned with the Odyssey Infared Imaging system (LI-COR).

For immunoprecipitation, cell pellets were lysed with the lysis buffer (50 mM Tris-HCl, pH 7.7, 120 mM KCl, 0.1% NP-40, 1 mM dithiothreitol) supplemented with protease inhibitor tablets (Roche), 0.5 μM okadaic acid (LC Labs), and 10 units/ml TurboNuclease (Accelagen).

After centrifugation, the supernatants were incubated with antibody-coupled protein A beads (Bio-Rad) for 1-2 h at 4℃. After being washed, the beads were boiled in SDS sample buffer and analyzed by SDS-PAGE and immunoblotting.

Flow cytometry

Cells were harvested by trypsinization or by shake-off in cases that involved the collection of only mitotic cells. After being washed once with PBS, samples were fixed with cold 70% ethanol. Fixed cells were washed with PBS, permeabilized with 0.25% Triton X-100 (Sigma) in PBS, and incubated with the MPM2 antibody (Millipore) diluted in PBS containing 2% BSA. After being washed with PBS containing 2% BSA, cells were incubated with Alexa Fluor 488 donkey anti-mouse secondary antibody (Life Technologies) diluted in PBS containing 2% BSA. After the antibody incubation, cells were washed again with PBS and resuspended in PBS containing 200 μg/ml DNase-free RNase A (QIAGEN) and 2 μg/ml propidium iodide (Sigma). Samples were analyzed with a FACSCalibur flow cytometer (BD Biosciences), and the data were processed with the FlowJo software (Tree Star).

Immunofluorescence

Cells were cultured in 4-well chamber slides, and were transfected with the desired siRNAs. At 20 h after transfection, 2.5 mM thymidine (Sigma) was added for 16 h. Cells were released into fresh medium for another 9 h. Nocodazole (250 nM; Sigma) was added at 2 h before fixation to depolymerize microtubules and enrich mitotic cells. Cells were washed once with PBS, pre-fixed with ice-cold 0.5% formaldehyde (Sigma) in PBS, and pre-extracted with ice-cold 0.2% Triton X-100 (Sigma) in PBS. Cells were then fixed with ice-cold 4% formaldehyde in PBS for

15 min. After being washed with PBS twice, cells were permeabilized with 0.2% Triton X-100 in PBS for another 20 min at room temperature. Cells were stained with mouse anti-Cdc20, human CREST serum, and rabbit anti-Bub1 or BubR1 antibodies diluted in PBS containing 3% BSA and 0.2% Triton X-100. After being washed three times with PBS containing 0.2% Triton X-100, cells were incubated with Alexa Fluor 647 goat anti-mouse, Alexa Fluor 568 goat anti- human, and Alexa Fluor 488 goat anti-rabbit secondary antibodies (Life Technologies) diluted in PBS containing 3% BSA and 0.2% Triton X-100. After another three washes with PBS containing 0.2% Triton X-100, samples were stained with 1 μg/ml DAPI diluted in PBS for 3 min. After a final wash, slides were mounted and analyzed with a DeltaVision deconvolution fluorescence microscope (DeltaVision, GE Healthcare).

Images were acquired with a 100X 1.40 NA UPLS Apochromat N objective (Olympus). A series of z-stack images were captured at 0.5-μm intervals. The z-stack images were deconvolved using the provided algorithm with the "conservative" setting, and projected with the "sum" method. All images in one experiment were taken with the same light intensity and exposure times. Quantification of the kinetochore signal intensity was performed in ImageJ. A rectangle mask enclosing the CREST signal from a pair of kinetochores was drawn and defined as the region of interest (ROI). The integrated density for the selected ROI was measured in each channel. The normalized intensity was defined as the ratio between the Cdc20 (or Bub1) intensities and the CREST intensities. 10 ROIs per cell were chosen at random, and the normalized intensity was calculated for each ROI. The mean value of the 10 normalized intensities is used as the normalized intensity of one cell. 25-34 cells were quantified for each sample. The graphs and statistics were generated with Prism (GraphPad Software).

Protein expression and purification

Recombinant human Bub1–Bub3, BubR1–Bub3, Mps1, and Mad2 proteins were purified as previously described (Luo et al., 2004; Tang and Yu, 2004). Wild-type and mutant His_6-tagged human $Cdc20^{\Delta N60}$ proteins containing residues 61-499 were purified as previously described (Tang and Yu, 2004) with the following modifications. Sf9 cells expressing various His_6-Cdc20 proteins were lysed in buffer A (50 mM HEPES, pH 6.8, 250 mM KCl, 5% glycerol, 0.1% Triton X-100, 5 mM β-mercaptoethanol) supplemented with 10 mM imidazole, protease inhibitor tablets (Roche), 0.5 μM okadaic acid (LC Labs), and 10 units/ml TurboNuclease (Accelagen). After incubation, the Cdc20-bound Ni^{2+}-NTA beads (QIAGEN) were washed with buffer A containing 20 mM imidazole and then with buffer A containing 50 mM imidazole. Purified proteins were eluted with buffer A containing 250 mM imidazole. After elution, samples were exchanged into storage buffer I (40 mM HEPES, pH 6.8, 200 mM KCl, 5% glycerol, 2 mM dithiothreitol) with PD-10 columns (GE Healthcare).

Wild-type and mutant human Strep-His_6-Bub1 fragments containing residues 1–723 ($Bub1^{\Delta Kinase}$) were co-expressed with His_6-Bub3 in Sf9 cells. Cells were lysed in buffer B (50 mM Tris-HCl, pH 7.7, 200 mM NaCl, 1 mM $MgCl_2$, 0.3 mM Na_3VO_4, 5 mM NaF, 10 mM β-glycerophosphate, 1 mM dithiothreitol, 5% glycerol) supplemented with protease inhibitor tablets (Roche) and 0.5 μM okadaic acid (LC Labs). Strep-His_6-$Bub1^{\Delta Kinase}$–Bub3 complexes were affinity-purified using Strep-Tactin Superflow Plus resin (QIAGEN), and eluted with buffer B supplemented with 15 mM D-desthiobiotin (Sigma). Purified proteins were exchanged into storage buffer II (25 mM Tris-HCl, pH 7.4, 200 mM NaCl, 1 mM $MgCl_2$, 1.5 mM dithiothreitol, 5% glycerol).

Human GST-Plk1 T210D (a constitutively active mutant) and GST-Cdk1–cyclin B1 kinases were expressed in Sf9 cells. Cells were lysed with buffer B supplemented with protease inhibitor tablets (Sigma). Cleared lysates were incubated with glutathione-Sepharose 4B beads (GE Healthcare). Proteins bound to beads were eluted with buffer B supplemented with 25 mM reduced glutathione (Sigma). Purified Plk1 and Cdk1 were exchanged into storage buffer II and stored at -80℃.

His_6-tagged human BubR1 N-terminal fragment (BubR1N) containing residues 1-370 was expressed in bacteria and purified with Ni^{2+}-NTA beads (QIAGEN). After the removal of the His_6-tag by TEV digestion, the BubR1N protein was further purified with Resource Q and Superdex 200 gel filtration columns (GE Healthcare).

Ubiquitination assays

APC/C ubiquitination assays were performed as previously described (Tang and Yu, 2004). Ube2S (a gift from Michael Rape, University of California at Berkeley, Berkeley, CA) was included in certain assays.

Kinase and protein-binding assays

For kinase assays, 1 μM $Cdc20^{\Delta N60}$ WT or mutants were incubated with different kinases at room temperature for 30 min in 20-μl reactions in the kinase buffer (50 mM Tris-HCl, pH 7.7, 100 mM NaCl, 10 mM $MgCl_2$, 5 mM NaF, 0.1 mM Na_3VO_4, 20 mM β-glycerophosphate, 1 mM dithiothreitol) supplemented with 100 μM ATP. Kinases used in this study were: 50 nM Plk1 (with or without 500 nM $Bub1^{\Delta Kinase}$–Bub3), 40 nM Bub1, 50 nM Cdk1, and 100 nM Mps1. The

reaction mixtures were quenched with SDS sample buffer, and analyzed by SDS-PAGE followed by Coomassie blue staining or immunoblotting.

For protein-binding assays, purified His_6-$Cdc20^{\Delta N60}$ WT or the S92E mutant were immobilized on Ni^{2+}-NTA beads (QIAGEN). After being washed twice, the beads were incubated with different combinations of BubR1N and Mad2 proteins for 1 h at room temperature. After being washed five times, bound proteins were eluted with SDS sample buffer and analyzed by SDS-PAGE followed by immunoblotting.

Reference

Archambault, V., Lepine, G., and Kachaner, D. (2015). Understanding the Polo Kinase machine. Oncogene.

Buschhorn, B.A., Petzold, G., Galova, M., Dube, P., Kraft, C., Herzog, F., Stark, H., and Peters, J.M. (2011). Substrate binding on the APC/C occurs between the coactivator Cdh1 and the processivity factor Doc1. Nat Struct Mol Biol *18*, 6-13.

Chang, L., and Barford, D. (2014). Insights into the anaphase-promoting complex: a molecular machine that regulates mitosis. Curr Opin Struct Biol *29C*, 1-9.

Chang, L., Zhang, Z., Yang, J., McLaughlin, S.H., and Barford, D. (2014). Molecular architecture and mechanism of the anaphase-promoting complex. Nature *513*, 388-393.

Chao, W.C., Kulkarni, K., Zhang, Z., Kong, E.H., and Barford, D. (2012). Structure of the mitotic checkpoint complex. Nature *484*, 208-213.

Ciceri, P., Muller, S., O'Mahony, A., Fedorov, O., Filippakopoulos, P., Hunt, J.P., Lasater, E.A., Pallares, G., Picaud, S., Wells, C., Martin, S., Wodicka, L.M., Shah, N.P., Treiber, D.K., and

Knapp, S. (2014). Dual kinase-bromodomain inhibitors for rationally designed polypharmacology. Nat Chem Biol *10*, 305-312.

Collin, P., Nashchekina, O., Walker, R., and Pines, J. (2013). The spindle assembly checkpoint works like a rheostat rather than a toggle switch. Nat Cell Biol *15*, 1378-1385.

da Fonseca, P.C., Kong, E.H., Zhang, Z., Schreiber, A., Williams, M.A., Morris, E.P., and Barford, D. (2011). Structures of APC/C^{Cdh1} with substrates identify Cdh1 and Apc10 as the D-box co-receptor. Nature *470*, 274-278.

Di Fiore, B., Davey, N.E., Hagting, A., Izawa, D., Mansfeld, J., Gibson, T.J., and Pines, J. (2015). The ABBA Motif Binds APC/C Activators and Is Shared by APC/C Substrates and Regulators. Dev Cell *32*, 358-372.

Diaz-Martinez, L.A., Karamysheva, Z.N., Warrington, R., Li, B., Wei, S., Xie, X.J., Roth, M.G., and Yu, H. (2014). Genome-wide siRNA screen reveals coupling between mitotic apoptosis and adaptation. EMBO J.

Diaz-Martinez, L.A., Tian, W., Li, B., Warrington, R., Jia, L., Brautigam, C.A., Luo, X., and Yu, H. (2015). The Cdc20-binding Phe box of the spindle checkpoint protein BubR1 maintains the mitotic checkpoint complex during mitosis. J Biol Chem *290*, 2431-2443.

Dick, A.E., and Gerlich, D.W. (2013). Kinetic framework of spindle assembly checkpoint signalling. Nat Cell Biol *15*, 1370-1377.

Elowe, S., Hummer, S., Uldschmid, A., Li, X., and Nigg, E.A. (2007). Tension-sensitive Plk1 phosphorylation on BubR1 regulates the stability of kinetochore microtubule interactions. Genes Dev *21*, 2205-2219.

Eytan, E., Wang, K., Miniowitz-Shemtov, S., Sitry-Shevah, D., Kaisari, S., Yen, T.J., Liu, S.T.,

and Hershko, A. (2014). Disassembly of mitotic checkpoint complexes by the joint action of the AAA-ATPase TRIP13 and p31comet. Proc Natl Acad Sci U S A *111*, 12019-12024.

Fang, G., Yu, H., and Kirschner, M.W. (1998). The checkpoint protein MAD2 and the mitotic regulator CDC20 form a ternary complex with the anaphase-promoting complex to control anaphase initiation. Genes Dev *12*, 1871-1883.

Gorbsky, G.J. (2014). The spindle checkpoint and chromosome segregation in meiosis. FEBS J, in press.

Heinrich, S., Geissen, E.M., Kamenz, J., Trautmann, S., Widmer, C., Drewe, P., Knop, M., Radde, N., Hasenauer, J., and Hauf, S. (2013). Determinants of robustness in spindle assembly checkpoint signalling. Nat Cell Biol *15*, 1328-1339.

Herzog, F., Primorac, I., Dube, P., Lenart, P., Sander, B., Mechtler, K., Stark, H., and Peters, J.M. (2009). Structure of the anaphase-promoting complex/cyclosome interacting with a mitotic checkpoint complex. Science *323*, 1477-1481.

Holland, A.J., and Cleveland, D.W. (2012). Losing balance: the origin and impact of aneuploidy in cancer. EMBO Rep *13*, 501-514.

Huang, H.C., Shi, J., Orth, J.D., and Mitchison, T.J. (2009). Evidence that mitotic exit is a better cancer therapeutic target than spindle assembly. Cancer Cell *16*, 347-358.

Izawa, D., and Pines, J. (2011). How APC/C-Cdc20 changes its substrate specificity in mitosis. Nat Cell Biol *13*, 223-233.

Izawa, D., and Pines, J. (2012). Mad2 and the APC/C compete for the same site on Cdc20 to ensure proper chromosome segregation. J Cell Biol *199*, 27-37.

Izawa, D., and Pines, J. (2015). The mitotic checkpoint complex binds a second CDC20 to inhibit active APC/C. Nature *517*, 631-634.

Jia, L., Kim, S., and Yu, H. (2013). Tracking spindle checkpoint signals from kinetochores to APC/C. Trends Biochem Sci *38*, 302-311.

Jia, L., Li, B., Warrington, R.T., Hao, X., Wang, S., and Yu, H. (2011). Defining pathways of spindle checkpoint silencing: functional redundancy between Cdc20 ubiquitination and $p31^{comet}$. Mol Biol Cell *22*, 4227-4235.

Kang, J., Yang, M., Li, B., Qi, W., Zhang, C., Shokat, K.M., Tomchick, D.R., Machius, M., and Yu, H. (2008). Structure and substrate recruitment of the human spindle checkpoint kinase Bub1. Mol Cell *32*, 394-405.

Kawashima, S.A., Yamagishi, Y., Honda, T., Ishiguro, K., and Watanabe, Y. (2010). Phosphorylation of H2A by Bub1 prevents chromosomal instability through localizing shugoshin. Science *327*, 172-177.

Kim, S., Sun, H., Tomchick, D.R., Yu, H., and Luo, X. (2012). Structure of human Mad1 C-terminal domain reveals its involvement in kinetochore targeting. Proc Natl Acad Sci U S A *109*, 6549-6554.

Kim, S., and Yu, H. (2015). Multiple assembly mechanisms anchor the KMN spindle checkpoint platform at human mitotic kinetochores. J Cell Biol *208*, 181-196.

Klebig, C., Korinth, D., and Meraldi, P. (2009). Bub1 regulates chromosome segregation in a kinetochore-independent manner. J Cell Biol *185*, 841-858.

Kulukian, A., Han, J.S., and Cleveland, D.W. (2009). Unattached kinetochores catalyze production of an anaphase inhibitor that requires a Mad2 template to prime Cdc20 for BubR1 binding. Dev Cell *16*, 105-117.

Labit, H., Fujimitsu, K., Bayin, N.S., Takaki, T., Gannon, J., and Yamano, H. (2012). Dephosphorylation of Cdc20 is required for its C-box-dependent activation of the APC/C.

EMBO J *31*, 3351-3362.

Lara-Gonzalez, P., Scott, M.I., Diez, M., Sen, O., and Taylor, S.S. (2011). BubR1 blocks substrate recruitment to the APC/C in a KEN-box-dependent manner. J Cell Sci *124*, 4332-4345.

Lin, Z., Jia, L., Tomchick, D.R., Luo, X., and Yu, H. (2014). Substrate-Specific Activation of the Mitotic Kinase Bub1 through Intramolecular Autophosphorylation and Kinetochore Targeting. Structure *22*, 1616-1627.

Liu, H., Jia, L., and Yu, H. (2013). Phospho-H2A and cohesin specify distinct tension-regulated Sgo1 pools at kinetochores and inner centromeres. Curr Biol *23*, 1927-1933.

London, N., and Biggins, S. (2014a). Mad1 kinetochore recruitment by Mps1-mediated phosphorylation of Bub1 signals the spindle checkpoint. Genes Dev *28*, 140-152.

London, N., and Biggins, S. (2014b). Signalling dynamics in the spindle checkpoint response. Nat Rev Mol Cell Biol *15*, 736-747.

Lu, D., Hsiao, J.Y., Davey, N.E., Van Voorhis, V.A., Foster, S.A., Tang, C., and Morgan, D.O. (2014). Multiple mechanisms determine the order of APC/C substrate degradation in mitosis. J Cell Biol *207*, 23-39.

Luo, X., Tang, Z., Xia, G., Wassmann, K., Matsumoto, T., Rizo, J., and Yu, H. (2004). The Mad2 spindle checkpoint protein has two distinct natively folded states. Nat Struct Mol Biol *11*, 338-345.

Luo, X., and Yu, H. (2008). Protein metamorphosis: the two-state behavior of Mad2. Structure *16*, 1616-1625.

Mapelli, M., and Musacchio, A. (2007). MAD contortions: conformational dimerization boosts spindle checkpoint signaling. Curr Opin Struct Biol *17*, 716-725.

Overlack, K., Primorac, I., Vleugel, M., Krenn, V., Maffini, S., Hoffmann, I., Kops, G.J., and Musacchio, A. (2015). A molecular basis for the differential roles of Bub1 and BubR1 in the spindle assembly checkpoint. eLife *4*, e05269.

Qi, W., Tang, Z., and Yu, H. (2006). Phosphorylation- and polo-box-dependent binding of Plk1 to Bub1 is required for the kinetochore localization of Plk1. Mol Biol Cell *17*, 3705-3716.

Qi, W., and Yu, H. (2007). KEN-box-dependent degradation of the Bub1 spindle checkpoint kinase by the anaphase-promoting complex/cyclosome. J Biol Chem *282*, 3672-3679.

Reddy, S.K., Rape, M., Margansky, W.A., and Kirschner, M.W. (2007). Ubiquitination by the anaphase-promoting complex drives spindle checkpoint inactivation. Nature *446*, 921-925.

Ricke, R.M., Jeganathan, K.B., Malureanu, L., Harrison, A.M., and van Deursen, J.M. (2012). Bub1 kinase activity drives error correction and mitotic checkpoint control but not tumor suppression. J Cell Biol *199*, 931-949.

Sacristan, C., and Kops, G.J. (2015). Joined at the hip: kinetochores, microtubules, and spindle assembly checkpoint signaling. Trends Cell Biol *25*, 21-28.

Santaguida, S., Vernieri, C., Villa, F., Ciliberto, A., and Musacchio, A. (2011). Evidence that Aurora B is implicated in spindle checkpoint signalling independently of error correction. EMBO J *30*, 1508-1519.

Saurin, A.T., van der Waal, M.S., Medema, R.H., Lens, S.M., and Kops, G.J. (2011). Aurora B potentiates Mps1 activation to ensure rapid checkpoint establishment at the onset of mitosis. Nat Commun *2*, 316.

Sivakumar, S., and Gorbsky, G.J. (2015). Spatiotemporal regulation of the anaphase-promoting complex in mitosis. Nat Rev Mol Cell Biol *16*, 82-94.

Sudakin, V., Chan, G.K., and Yen, T.J. (2001). Checkpoint inhibition of the APC/C in HeLa cells is mediated by a complex of BUBR1, BUB3, CDC20, and MAD2. J Cell Biol *154*, 925-936.

Suijkerbuijk, S.J., Vleugel, M., Teixeira, A., and Kops, G.J. (2012). Integration of kinase and phosphatase activities by BUBR1 ensures formation of stable kinetochore-microtubule attachments. Dev Cell *23*, 745-755.

Sumara, I., Gimenez-Abian, J.F., Gerlich, D., Hirota, T., Kraft, C., de la Torre, C., Ellenberg, J., and Peters, J.M. (2004). Roles of polo-like kinase 1 in the assembly of functional mitotic spindles. Curr Biol *14*, 1712-1722.

Tang, Z., Bharadwaj, R., Li, B., and Yu, H. (2001). Mad2-independent inhibition of APC^{Cdc20} by the mitotic checkpoint protein BubR1. Dev Cell *1*, 227-237.

Tang, Z., Shu, H., Oncel, D., Chen, S., and Yu, H. (2004). Phosphorylation of Cdc20 by Bub1 provides a catalytic mechanism for APC/C inhibition by the spindle checkpoint. Mol Cell *16*, 387-397.

Tang, Z., and Yu, H. (2004). Functional analysis of the spindle-checkpoint proteins using an in vitro ubiquitination assay. Methods Mol Biol *281*, 227-242.

Tian, W., Li, B., Warrington, R., Tomchick, D.R., Yu, H., and Luo, X. (2012). Structural analysis of human Cdc20 supports multisite degron recognition by APC/C. Proc Natl Acad Sci U S A *109*, 18419-18424.

Varetti, G., Guida, C., Santaguida, S., Chiroli, E., and Musacchio, A. (2011). Homeostatic control of mitotic arrest. Mol Cell *44*, 710-720.

Wang, K., Sturt-Gillespie, B., Hittle, J.C., Macdonald, D., Chan, G.K., Yen, T.J., and Liu, S.T.

(2014). Thyroid Hormone Receptor Interacting Protein 13 (TRIP13) AAA-ATPase is a Novel Mitotic Checkpoint Silencing Protein. J Biol Chem *289*, 23928-23937.

Westhorpe, F.G., Tighe, A., Lara-Gonzalez, P., and Taylor, S.S. (2011). p31^{comet}-mediated extraction of Mad2 from the MCC promotes efficient mitotic exit. J Cell Sci *124*, 3905-3916.

Williamson, A., Wickliffe, K.E., Mellone, B.G., Song, L., Karpen, G.H., and Rape, M. (2009). Identification of a physiological E2 module for the human anaphase-promoting complex. Proc Natl Acad Sci U S A *106*, 18213-18218.

Xia, G., Luo, X., Habu, T., Rizo, J., Matsumoto, T., and Yu, H. (2004). Conformation-specific binding of p31^{comet} antagonizes the function of Mad2 in the spindle checkpoint. EMBO J *23*, 3133-3143.

Yang, M., Li, B., Tomchick, D.R., Machius, M., Rizo, J., Yu, H., and Luo, X. (2007). p31^{comet} blocks Mad2 activation through structural mimicry. Cell *131*, 744-755.

Ye, Q., Rosenberg, S.C., Moeller, A., Speir, J.A., Su, T.Y., and Corbett, K.D. (2015). TRIP13 is a protein-remodeling AAA+ ATPase that catalyzes MAD2 conformation switching. Elife *4*.

Yu, H. (2007). Cdc20: a WD40 activator for a cell cycle degradation machine. Mol Cell *27*, 3-16.

CHAPTER FIVE

PERSPECTIVES AND FUTURE DIRECTIONS

First identified in yeast, Bub1 is a highly conserved spindle checkpoint protein that has multiple functions. It recruits other checkpoint proteins to the kinetochore; it phosphorylates histone H2A to recruit centromeric cohesion protector Sgo1-PP2A complex and Aurora B; it phosphorylates Cdc20 to inhibit APC/C^{Cdc20}.

My work aimed at understanding the mechanism of the spindle checkpoint through understanding the function of Bub1, which is the central player in the checkpoint. It integrates the signal from upstream kinetochore-microtubule attachment and tension sensors Mps1 and Aurora B, and transduces the signal to downstream effectors like BubR1, Mad1-Mad2 complex, and Cdc20. Recent studies have revealed many details in this complicated signaling network.

On the unattached kinetochore, the KMN network constitutes the platform for spindle checkpoint signaling. Mps1 associates with Ndc80C with two independent motifs. This interaction can be regulated by Aurora B. Ndc80C-bound Mps1 lies very close to Knl1, so it can phosphorylate the MELT motifs of Knl1, which brings Bub1-Bub3 complex. Mps1 then also phosphorylates Bub1 in the middle region, which is essential for Bub1-Mad1 interaction. Mad1 forms a constitutive complex with Mad2. At the same time, Bub1 also recruits BubR1-Bub3 and Cdc20 through direct binding. The MCC components BubR1, Mad2 and Cdc20 are brought together by Bub1, which very likely promotes MCC formation.

I have shown that in human cells, the interaction between Bub1 and Mad1 not only requires phosphorylation by Mps1, but also requires phosphorylation by Cdk1 at Bub1 S459. The reason for this requirement is not understood but will be interesting to investigate.

I have also shown that Bub1 is not only a kinase itself, but also brings another kinase Plk1 to phosphorylate Cdc20 at S92. The phosphorylations by Bub1 and Plk1 possibly have redundant function to inhibit APC/C^{Cdc20}, which provides a mechanism to inhibit APC/C^{Cdc20} other than MCC formation. This mechanism is also catalytic, explaining the high sensitivity of the spindle checkpoint. However, how Cdc20 phosphorylation prevents it from activating APC/C is not clear, biochemical and structural studies will be needed to answer this question.

The Bub1-Mad1 interaction and the Bub1-Plk1 interaction are both regulated by Cdk1 phosphorylation. Interestingly, the phosphorylation on Bub1 S459 and Cdc20 S92 are reduced when checkpoint is off but Cdk1 is still active. It is possible that phosphatases are important regulators for these phosphorylation events, and are key for turning off the spindle checkpoint.

With deeper and deeper understanding of the spindle checkpoint, it is possible to reconstitute this system in vitro, which will be the final goal for studies about the checkpoint. It will be exciting to see this complicated signaling network to be constructed piece by piece in a test tube.